Master thesis in inorganic chemistry

Synthesis and Functionalization of Periodic Mesoporous Silica

Bjørn Tore Lønstad
Kjemisk institutt
Universitetet i Bergen
2008

Føreord

Dette arbeidet blei starta hausten 2006 ved Kjemisk institutt, Universitetet i Bergen.

Største takk går til min rettleiar Reiner Anwander for å ha teke imot meg som mastergradsstudent. Han har vore ei god støtte for teoretiske utgreiingar og har gjeve meg inspirasjon for å finne vidare mål i forsøka. Eg har teke kurs med han der han òg har vist seg som ein framifrå forelesar for både skulekjemi og ved presentasjonar av nye forskningsresultat. Vidare vil eg takke Thomas Deschner som har lært meg det praktiske på laboratoriet og som alltid er tilgjengeleg for spørsmål og diskusjonar.

Takk til Hanne-Marthe Sommerfeldt, Hjørdis Skår og andre medstudentar ved kjemisk institutt for fem års studie med faglege og ufaglege diskusjonar, hjelp, støtte og nye tolkninger av verda vi lev i.

Takk til Yucang Liang, Alan Crozier, Erwan Le Roux og andre medlem og gjestestudentar i forskningsgruppa for å skape eit godt kollegium og sosialt samvere.

Takk til Inger Johanne Fjellanger for å ha målt element analyse for meg, Anne Frøystein for hjelp til atomabsorpsjonsspektroskopi og alt teknisk personale som vedlikeheld instrumentparken ved instituttet.

Takk til familie og gode venner som har vist interesse for kjemi, men også vekt interessa mi for andre emne og tankeplan.

Bergen 1. oktober 2008

_____
Bjørn Tore Lønstad

Abstract

Different periodic mesoporous silica materials have been synthesized in order to investigate the topic of size-selective heterogeneous catalysis. SBA-1, SBA-2, SBA-16, and MCM-41 were synthesized. The cagelike SBA-1 and the channel-like MCM-41 have been modified by post-synthesis methods involving grafting of $HN(SiHMe_2)_2$, $HN(SiMe_2Ph)_2$, and $HN(SiMePh_2)_2$ to tailor the surface for subsequent metalation reactions. The three disilazanes showed different reactivity to the two different topologies involving also of SBA-1 pore blocking. $\{Mg[N(SiHMe_2)_2]_2\}_2$ was synthesized and grafted onto the surface. The immobilized magnesium complex gave pore characteristics similar to those of the largest disilazane. $Ti(NMe_2)_4$ was chosen as a "small" transition metal complex and gave materials with around 10 weight % titanium. *R*-1,1'-binaphthol was used to exchange the amido ligands of the grafted titanium complex, but gave only the expected exchange on MCM-41 and not on SBA-1 which may be due to the small cage window of this material. $Ti(NMe_2)_3[N(SiHMe_2)_2]$ was synthesized and grafted on the surface for use as a spectroscopic probe in FT-IR spectroscopy. Metalorganic complexes were characterized by ^{1}H and ^{13}C NMR spectroscopy, DRIFT or FT-IR spectroscopy, and elemental analysis. Materials were characterized by powder X-ray diffraction, nitrogen physisorption, DRIFT or FT-IR spectroscopy and elemental analysis.

Table of contents

List of abbreviations

a_s	Specific BET surface area
bdsa	Bis(dimethylsilyl)amide
BET	Brunauer- Emmet- Teller
BINOL	*R*-1,1'-BINOLate
BJH	Barrett- Joyner- Halenda
btsa	Bis(trimethylsilyl)amide
cmc	Critical Micelle Concentration
$C_{18}NEt_3Br$	Triethyloctadecylammonium bromide
C_{16-3-1}	*N*-(3-trimethyl-ammoniumpropyl)hexadecylammonium dibromide
d_c	Pore diameter of cagelike materials
d_p	Pore diameter
DRIFT	Diffuse Reflectance Infrared Fourier-Transformed
Et	Ethyl
FID	Free Induction Decay
FT- IR	Fourier Transformed Infrared Spectroscopy
h	Hours
Hbdsa	1,1,3,3-Tetramethyldisilazane
H_2BINOL	*R*-1,1'-binaphthol
IUPAC	International Union of Pure and Applied Chemistry
ITQ	Instituto de Tecnología Química
KIT	Korean Institute of Technology
LCT	Liquid Crystal Templating
MAO	Methylalumoxane
MCM	Mobil Composition of Matter
Me	Methyl
MHz	Megahertz
MSF	Mesoporous Silica Film
MOF	Metal Organic Framework
NMR	Nuclear Magnetic Resonance
PMO	Periodic Mesoporous Organosilica
PMS	Periodic Mesoporous Silica
PNS	Periodic Nanoporous Silica
rt	Room temperature
SBA	Santa Barbara University
SOMC	Surface Organometallic Chemistry
THF	TetraHydroFurane
TEOS	Tetraethyl orthosilicate
Vp	Pore volume
PXRD	Powder X- Ray Diffraction

1 Introduction

1.1 From zeolites to periodic mesoporous silica

Periodic mesoporous silica (PMS) have been extensively explored over the last two decades because of the potential these robust materials have in areas such as hybrid materials, catalysis and as a possible replacement for zeolites. Zeolites (Greek, zein, "to boil"; lithos, "a stone") were discovered in the middle of the 18th century,[1] have been largely used by industry since the 1950s as catalysts for cracking petrochemicals and later for fine chemical synthesis.[2] As heterogeneous catalysts, zeolites have many advantages compared to homogeneous catalysts: The zeolites are easily separated and recovered from the reaction and hence can be reused. They are also thermally stable and inert to most chemical environments. The microporosity gives the zeolites large specific surface areas which maximizes the contact between the substrate and the catalyst. One important chemical feature of the zeolites is the highly acidic sites which may hold a proton (solid Brønsted acid) or a metal ion. The major drawback with zeolites is the limiting pore diameter of ~1.5 nm which prevents larger molecules from entering the pores and hence accessing the catalytic centers. In order to obtain mesoporosity in zeolites one can enlarge the pores by pillars or by dealumination which rearrange the structure.[3] The mesoporous materials MCM-36[4] (*M*obil *c*omposition of *m*atter) and ITQ-2[5] (Instituto de Tecnología Química) can be prepared by two different methods respectively from the MCM-22 zeolites (Scheme 1.1)
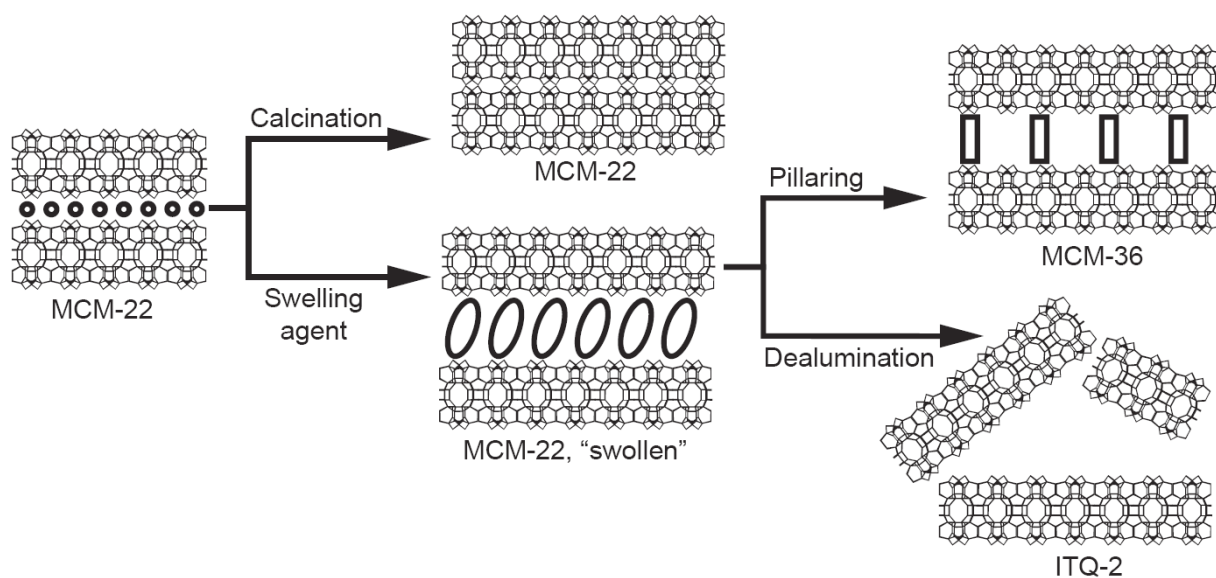
Scheme **1**.**1** Mesoporous materials made from MCM-22 zeolite.[3, 6]

The first report on such materials denoted as the M41S family were published by Mobil Oil researchers in 1992.[7] The materials contained pores with diameters in the range of 2-4 nm which are considered as mesoporous (d = 2-50 nm) according to IUPAC[8] (Figure 1.1). This family of new materials was a breakthrough in making ordered mesoporous materials.
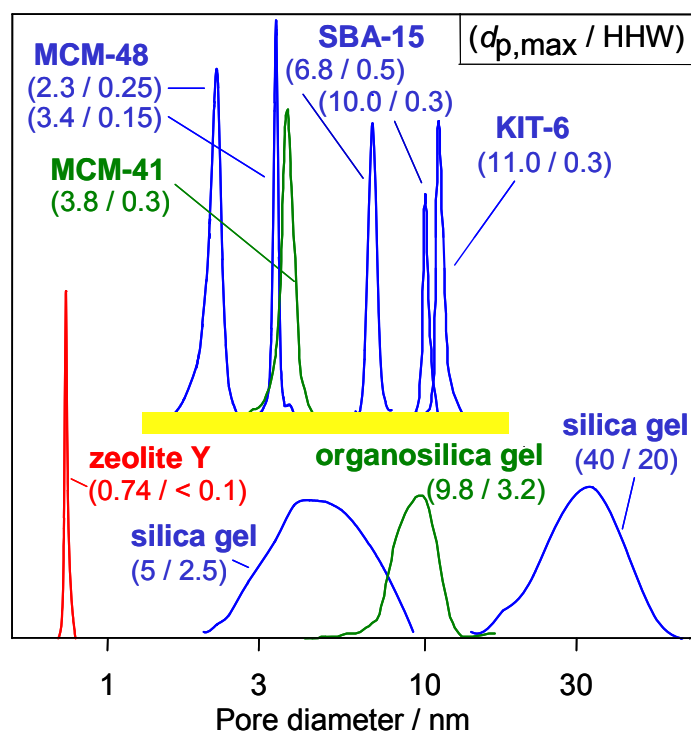
Figure **1**.1 The pore size distribution of some porous materials. The numbers denotes the maximum pore diameter and the width at half height for the distribution. (SBA: Santa Barbara, KIT: Korean Institute of Technology)

Mesoporous silica MCM- 41[7] belongs to the M41S family and is one of the most studied PMS materials. PMSs have many of the same properties as zeolites but larger pore diameters, however only the pore systems are ordered while the silica wall is amorphous. MCM-41 and SBA-15[9] both have 1-dimensional channel-like pore system with a desirable and uniform pore diameter, in addition they are also relatively easy to synthesize. Such materials have been used as exo-templates to make other structures in the nano-regime. For example nanothreads from palladium[10], platinum[11] and carbon[12] have been generated via nanocasting[13] in PMS. The lack of strong enough acid sites in PMS demands that the material is functionalized with other elements and functional groups. This can be done via one-pot synthesis where the desired group will be included in the framework of the material or via postsynthesis grafting at the surface by functionalizing silanol groups. Via the one-pot synthesis various metal complexes (e.g. $Ti(OC_2H_5)_4$[14], $VOSO_4$[15]) or organic groups from bridged dipodal alkoxysilanes[16] [$(RO)_3Si$-R'-$Si(OR)_3$] are reacted with a silica precursor in co-condensation. When organic groups are included in the framework the material is referred to as Periodic Mesoporous Organosilica (PMO). Organic groups can also be grafted onto the material to obtain functional groups like amines[17], thiols[18] and acids[19]. Efforts have also been put into immobilization of organometallic complexes, often in the course of making a homogeneous

catalyst heterogeneous.[2, 20] The steric environment around an immobilized catalytic center differs from the free movement of homogeneous catalysts in solution and can enhance the activity and selectivity of the catalyst. Shell developed and patented a silica based catalyst functionalized with titanium for epoxidizing olefins by mild organic hydroperoxides.[21] The zeolite TS-1 was very successful in several reactions because of the active site-isolated titanium atoms.[22] Also large complexes like Schiff's base have been reported to be trapped inside zeolites.[23] A MCM-41 hybrid material grafted with titanocene dichloride was given a lot of attention after it was presented in 1995.[24] The titanium centers were finely dispersed over the surface without any signs of clusters or Ti-O-Ti bonds. This site-isolation is very important to interpret the activity and performance at the metal center and for comparison with single complexes in solution.

SBA-1[25] (Santa Barbara) came to the world's knowledge in 1995. This new periodic mesoporous material features a more complicated and intrinsic pore system than the more famous MCM-41. Large mesocages are interconnected via smaller channels in a three dimensional fashion and implies size-selectivity to the native material. The cages have an internal diameter around 4 nm with entrance windows between 1-2 nm.[26] This way each cage may be considered as a "nanoreactor" with limited accessibility for different substrates. Zapilko et al.[27] showed this when they functionalized a SBA-1 material with $AlEt_3$ and used it for Meerwein-Ponndorf-Verley reduction of benzaldehyde and 1-pyrenecarboxaldehyde. To control the size-selectivity monosilazanes ($Me_2N(SiR_3)_2$) with a hydrocarbon tail were used to decrease the pore diameter of the channels leading into the material. In another work[28] by the same group a SBA-1 material was selectively grafted on the outside and inside by a magnesium and titanium complex, respectively. In the future PMSs may be used for advanced drug delivery or as super selective catalysts ("mesozymes") inspired from enzymes.

2 Theory

2.1 Periodic Mesoporous Silica

As the name suggest the pore diameter in periodic mesoporous silica is in the meso (Greek mésos = middle) range of 2-50 nm. The PMS materials (Table 2.1 holds a short overview) may be divided into two main groups according to their internal arrangement of channels. The first group which shows a channel-like pore system was the first to be discovered and has been in the center of research for a long time. This pore system exists in e.g. MCM-41, MCM-48 and SBA-15. In MCM-41 and SBA-15 the pores are 1-dimensional channels which are arranged parallel to each other in a hexagonal fashion. MCM-48 has a more complicated structure where the 1-dimensional channels are branched in a 3-dimmensional system. The channels have a uniform inner diameter. The second group includes materials like SBA-1, SBA-2, SBA-16 and KIT-5. These materials have larger cages connected via smaller openings and channels in a 3-dimensional system. PMSs have a high specific surface area > 1000 m^2/g and also a high specific pore volume > 0.5 cm^3/g. The materials are thermally robust and relatively inert to chemical environments (the morphology stays intact).

Table **2**.**1** Overview of some periodic mesoporous silicas

| Material	Channel system	Mesophase	Space group
MCM-41[7, 29], SBA-15[9], SBA-3[25]	1D unbranched	Hexagonal	*P6mm*
MCM-48[7, 29]	3D branched	Cubic	*Ia3d*
SBA-1[30]	Cagelike	Cubic	*Pm3n*
SBA-2[31]	Cagelike	Hexagonal	*P6₃/mmc*
KIT-5[32]	Cagelike	Cubic	*Fm3m*
SBA-16[9]	Cagelike	Hexagonal	*Im3m*
MCM-50[7, 29]		Lamellar	

2.1.1 SBA-1

The SBA-1 material falls into the second category of periodic mesoporous silica since it has a cagelike pore system with the space group *Pm3n*. The intrinsic pore system of SBA-1 has been characterized by electron crystallography and by mathematical models (Figure **2**.**1**) The material consists of two different mesocages A and B where A is ellipsoidal and B has a

spherical shape and is smaller than A. The B cage is surrounded by 12 A cages and the structure follows an A_3B system. Since the size is highly depended on the synthesis procedure of the material one can not state the exact pore diameter although 40 Å is typical. The cages connect to each other via three different windows. The window between the flat sides of two A-cages is the largest. The two other windows are between the A and B cages and between the tips of two A cages. The largest window (A-A) has been estimated by Sakamoto et al.[26] to be 15 × 22 Å while the (A-B) window is not larger than 2 Å. According to Anderson et al.[33] all the window sizes are less than 13 Å.
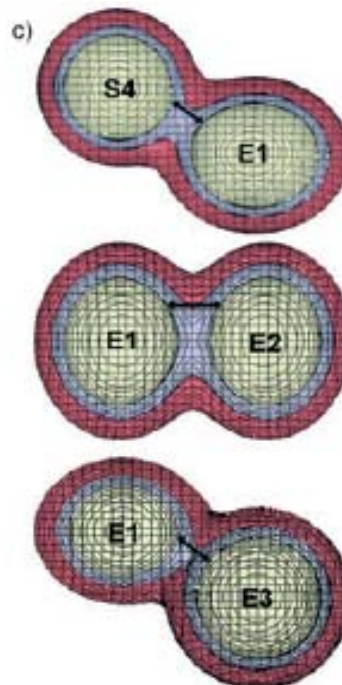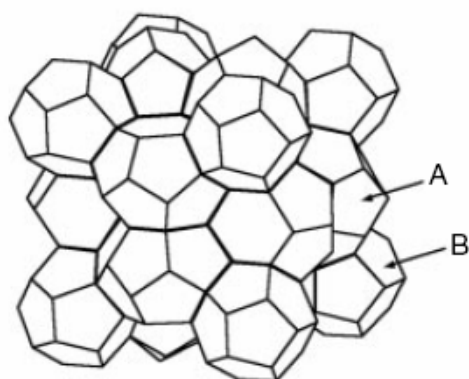
a)

b)

c)
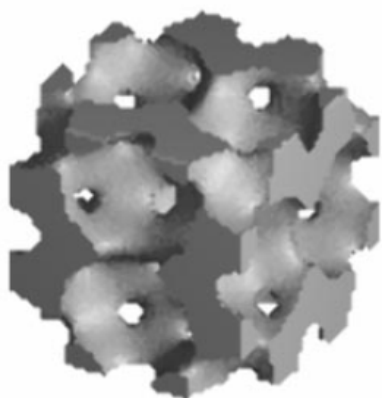
Figure **2**.**1** a) Structure and b) schematic drawing of SBA-1[26] c) Illustration of the window sizes in SBA-1**[33]**

Models of the SBA-1 suggest that it is close to a minimal surface which has a zero-mean curvature at all points.[33] This means that every point at the surface is the two principal curvatures equal in opposite signs.

Synthesis of periodic mesoporous silica

The synthesis of periodic mesoporous silica include the following ingredients: A silica source, an acid or base, a structure directing agent (SDA) to form the mesophase, water and sometimes another auxiliary component. A routine procedure would be first to homogenize the solvents together with acid/base and the SDA at the desired temperature. The silica source is then added and the reaction is stirred for a certain time. Some syntheses require a static treatment at elevated temperature before the material is washed, dried and calcined to combust the SDA inside the pores. The silica source may be Cab-O-Sil (SiO_2), sodium silicate or the commonly tetraethoxysilane (TEOS) as it only releases ethanol during the reaction which easily diffuses out of the pores. The SDA is usually an ionic surfactant with a long aliphatic tail. In high concentration of these surfactants agglomerates are formed of various shapes called micelles and thus create the mesophase needed. In basic solutions fatty acids act as anionic SDA and in acid solutions ammonium ions with one long alkyl chain act as a cationic SDA. The packing of these two surfactants can be described by the surfactant packing parameter *g*:

$$g = \frac{V}{a_0 \cdot l}$$

where *V* is the volume of the hydrocarbon chain, a_0 is the effective surface area of the head group and *l* is the length of the hydrocarbon chain. The packing parameter gives an idea of how the surfactants will arrange in water. At large values of a_0 will the head group occupy more space at the surface of the micelle and force the surrounding head groups to create a shape with higher curvature which leads to a spherical shape. At lower values of a_0 will the curvature be lower and one can observe long rod-like micelles and lamellar structures or bilayers.
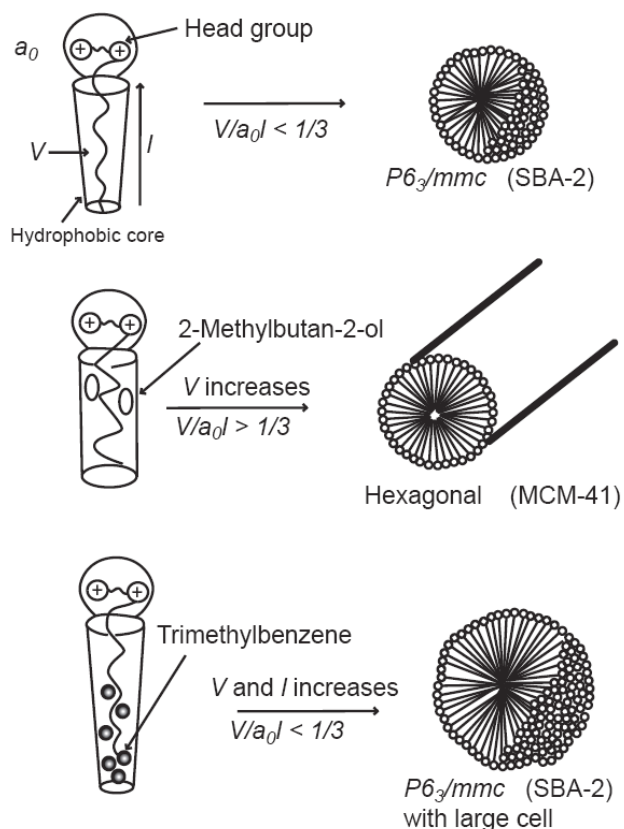
Figure **2**.2 Control of the mesophase by the surfactant.[31]

The effective surface area can be controlled by gemini surfactants (see Figure 2.2; Table 2.2) with a dicationic head group and a spacer in between. The volume and length of the hydrophobic part of the micelle can be adjusted with additives[31] such as 2-methylbutan-2-ol and trimethylbenzene.

Table **2**.2 Arrangement of surfactants in water using the surfactant packing parameter g.

g	**Mesophase**	**Example of material**
1/3	Cubic (*Pm3n*)	SBA-1
1/3 – 1/2	Cubic (*Fm3m*)	KIT-5
1/2	Hexagonal (*P6mm*)	MCM-41
1/2 – 2/3	Cubic (*Ia3d*)	MCM-48
1	Lamellar	MCM-50

Co-block polymers may also be surface active when one of the monomers is hydrophilic and the other one hydrophobic. This will make the polymer to curl up into a ball in water where the hydrophobic block in the core is surrounded by the hydrophilic block. The composition, temperature and reaction time can be changed in order to obtain the optimal material with respect to pore diameter or particle morphology.

2.2 Shape and size-selectivity in PMS

The typical pore diameters in periodic mesoporous silica make the material interesting as a host material for large species like organic molecules, nano particles, biomolecules, polymers and supramolecular aggregates.[34] The materials having channel-like pores are excellent hosts as they have a constant tunable pore diameter. The process of nanocasting where the silica material is used as a template for other materials has been already mentioned in section 1.1. One example on how size and pore geometry affect the rate of reaction and selectivity is epoxidation.[35] It has been proposed that larger pore sizes increase the rates of reaction so that SBA-2 gives a lower rate than a analogous hybrid material of MCM-41.[36] Also branched pore systems seem to perform better in catalytic reactions than unbranched ones (MCM-48 versus MCM-41).[37] Both observations may be explained by the better diffusion of the substrates which lead to higher rates of reaction. In an acetalization reaction of cyclohexanone (Scheme **2.1**) in MCM-41 materials, Iwamoto et al. found that the pore diameter influenced the rate constant.[38] Without any ambiguous explanation the pore diameter of 1.9 nm seemed to be the optimal size for the reaction even when the substrate was exchanged with pentanal.
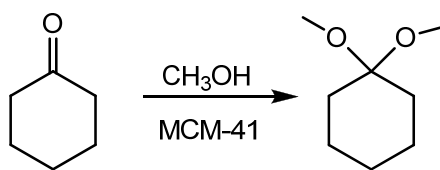
Scheme **2.1** Acetalization of cyclohexanone in MCM-41 containing tuned pore diameter.

2.3 Characterization of periodic mesoporous silica

Within this thesis the materials have been characterized via powder X-ray diffraction (PXRD), nitrogen physisorption, elemental analysis (N, C, H), and Fourier Transform Infrared Spectroscopy (FT-IR). Other methods which are not concerned in this work are solid state MAS-NMR spectroscopy, extended X-ray absorption fine structure (EXAFS) and X-ray

absorption near edge spectroscopy (XANES). The two latter methods are related to heavy metals immobilized on the surface.

Powder X-ray diffraction

This method is used to find any structural order in a material. An X-ray beam in exact angles is directed into a smooth surface of sample. If the material has any long range periodicity the X-rays will at some angles be reflected and collected by the detector. The output data show the angle of the beam and the intensity of the reflected X-rays. In highly crystalline materials like zeolites several sharp reflections corresponding to the different planes are discovered at high angles θ. Because of the semi-crystalline nature of periodic mesoporous silica, the X-ray reflections occur only as weak and broad peaks at low angles θ. The pattern can still be used to determine the unit cell and identify the material (compare SBA-1 and MCM-41 in Figure **2.3**).
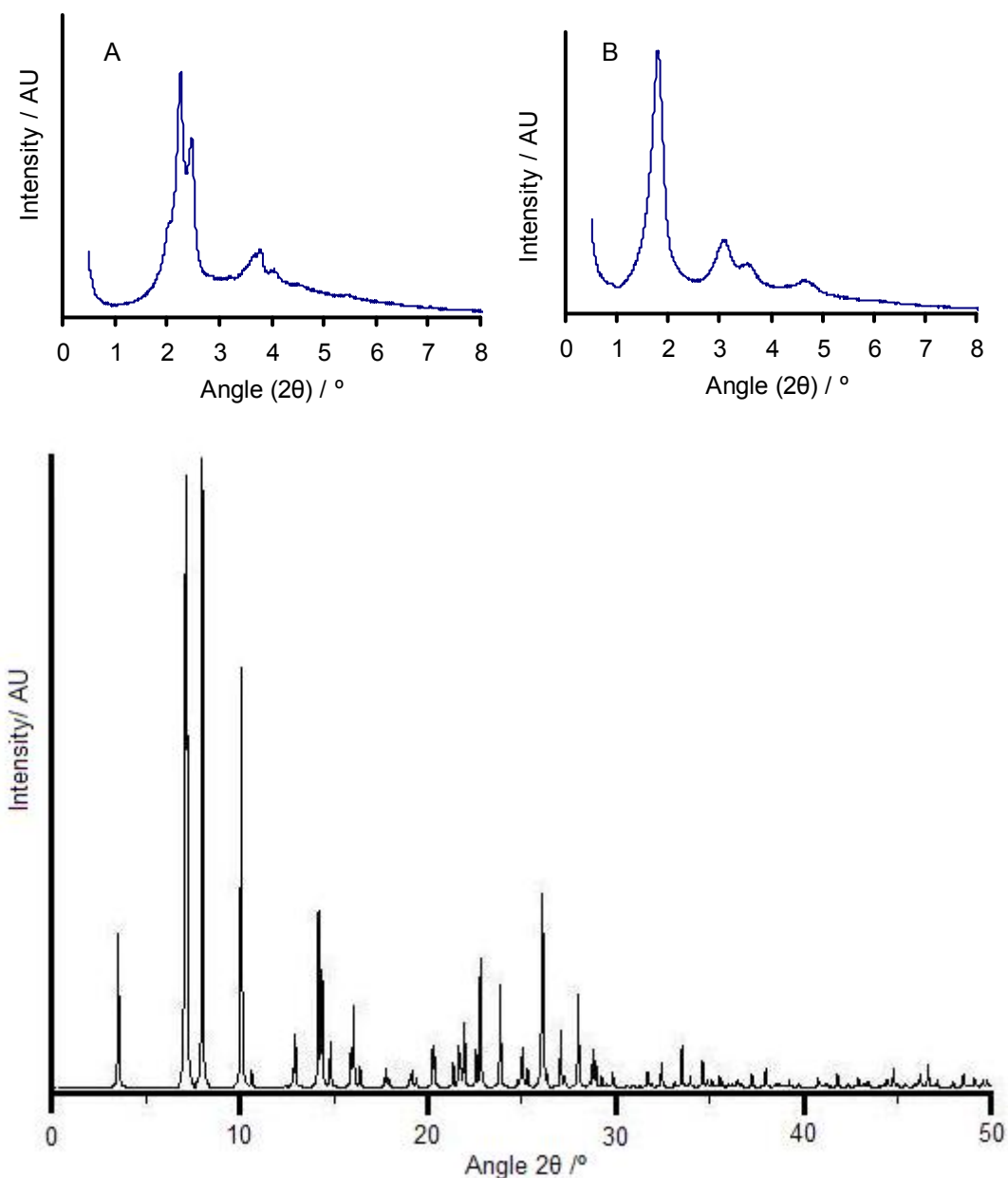
Figure **2.3** A) PXRD-pattern of SBA-1 and B) MCM-41. C) Simulated PXRD-pattern for zeolite MCM-22.

Nitrogen-physisorption

This method explores the porosity of the material. Nitrogen is filled into the sample at a constant temperature of 77 K at different pressures and the volume of nitrogen absorbed is measured. Theoretical models have been made to calculate the Brunauer-Emmett-Teller specific surface area (S_{BET})[39] and the Barrett-Joyner-Halenda (BJH)[40] pore size distribution which provides the pore volume (V_P) and pore diameter (d_p). Figure **2.4** shows typical isotherms of three different PMSs and the relevant equations.

11

BET surface area

$$\frac{p}{n^a\,(p^0-p)} = \frac{1}{n_m^a C} + \frac{(C\text{-}1)\,p}{n_m^a C\,p^0}$$

BJH pore size distribution

$$r_K = \frac{2\sigma^{lg}\,v^l}{RT\ln(p^0/p)}$$

$$d_p = 2(r_K + t_{ads})$$

$$t_{ads} = m\left(\frac{n}{\ln(p^0/p)}\right)^x$$
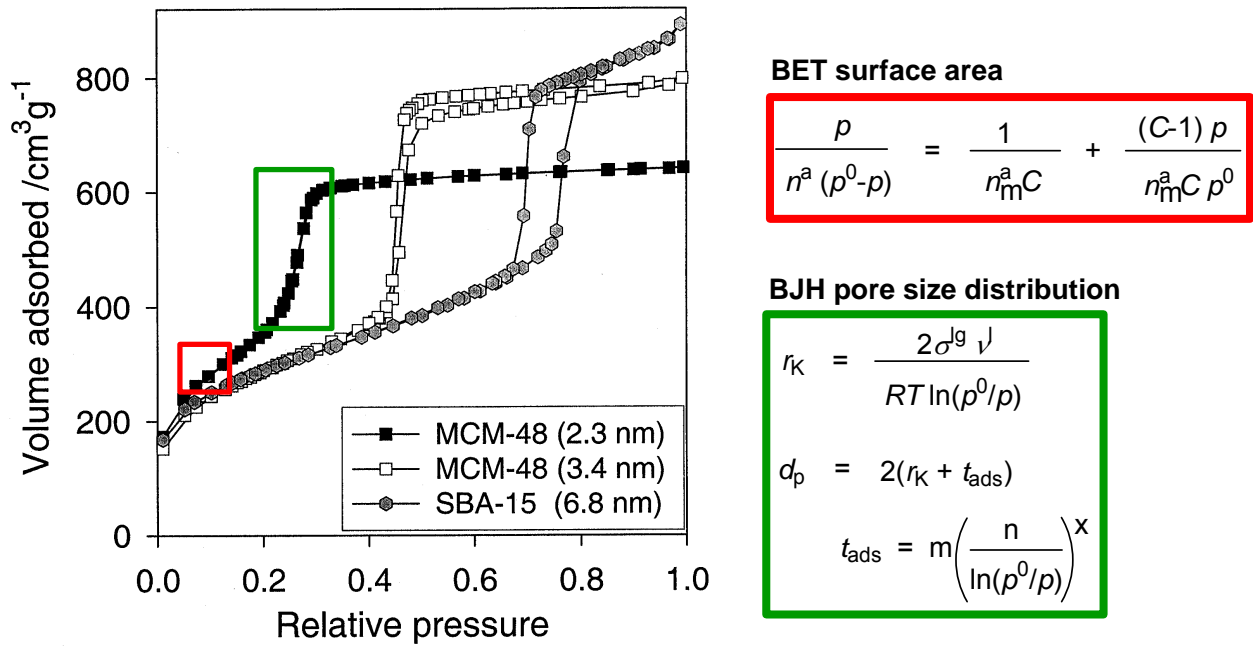
Figure **2.4** N$_2$-physisorption isotherm of MCM-48 and SBA-15. The red and green areas are used for the calculations.

The types of the isotherms are divided into six different categories according to IUPAC.[8] Type I is associated with microporous solids. Type III, V and VI are uncommon isotherms, but still obtained in special cases. Type II refers to a non-porous or macroporous material and Type IV isotherms are typical for mesopores. Hysteresis loops are seen in the isotherms of type IV and V. The adsorption and desorption branches do not follow the same pathway because of capillary condensation in the mesopores, i.e. there are differences in the mechanisms of adsorption and desorption of the nitrogen gas. A monolayer of nitrogen molecules builds up at low relative pressure until the inflection at point B (see Figure **2.5**) where a linear region starts due to multilayer formation on the surface. The different hysteresis corresponds to the different pore shapes: H1: spheres of approximately the same size, H2: 'ink bottle' pores, larger pores connected via smaller pores, H3: slit-shaped pores and H4: narrow slit-like pores.
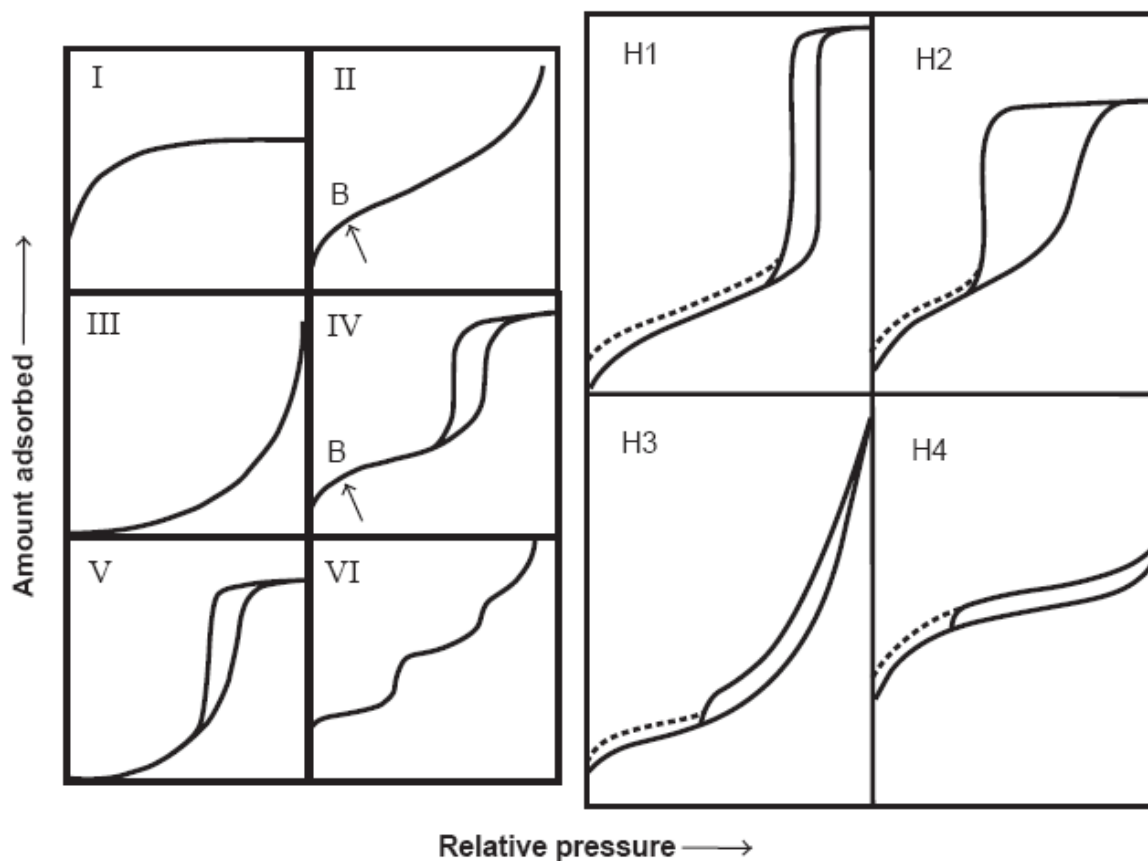
Figure **2.5** Different types of isothermes and hysteresis loops.[8]

Ravikovitch and Neimark[41] proposed a new method for the calculation of pore diameters for cagelike materials. The method is based on the geometry of the material and the pore volume obtained from powder X-ray crystallography and physisorption, respectively. The authors found that the pore diameter was up to 100% larger than reported by the BJH-method.

FT-IR spectroscopy

Infrared spectroscopy is an elegant technique to determine the surface species and kinetics of surface reactions. Typically one can follow the changes at the surface by examining characteristic vibrations which appears or disappears (e.g. O-H, Si-H). Particular diffuse reflectance Infrared Fourier transform (DRIFT) spectroscopy or in situ IR spectroscopy are preferred since these techniques avoid the use of any mineral oil (nujol), which would overlap important bands like C-H and C-C, and have the practical advantage to work under inert atmosphere.

2.4 Surface functionalization of periodic mesoporous silica

Surface organometallic chemistry (SOMC) represents a new approach to heterogeneous catalysis.[42, 43] Even though industry prefers heterogeneous catalysis it is difficult to establish the structure-activity relationship because of low homogeneity on the surface and low concentrations of the active sites. The SOMC method is based on a molecular approach in order to synthesize hetereogeneous catalysts. The method consists of controlled grafting of organometallic complexes directly onto a surface of an oxide through one or more ionic or covalent bonds to obtain isolated and well-defined active sites (Scheme **2**.**2**).
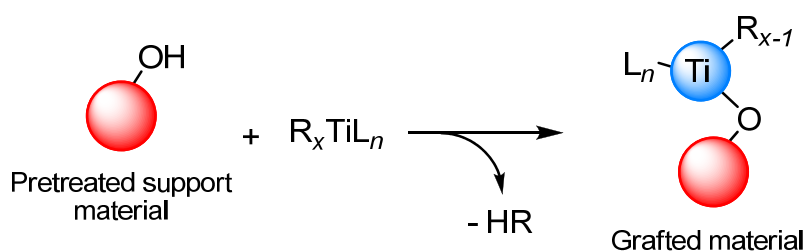
Scheme **2**.**2** General strategy to surface organotitanium chemistry. See Table 2.3 for possible derivatives of R and L.

A hybrid material with an immobilized zirconium(IV) alkyl complex (Figure **2**.**6**) displays a good example.[44, 45] This hybrid material was transformed into a reactive zirconium(IV) hydride via hydrogenolysis which was found to catalyze olefin hydrogenation, isomerization, and polymerization. Later the same hybrid material was further optimized and found to be active in the depolymerization of polyolefins.[46] The first example of SOMC@PMS, reported in 1994, was a heterobimetallic compound of tin and molybdenum grafted on MCM-41 (Figure **2**.**6**).[47]
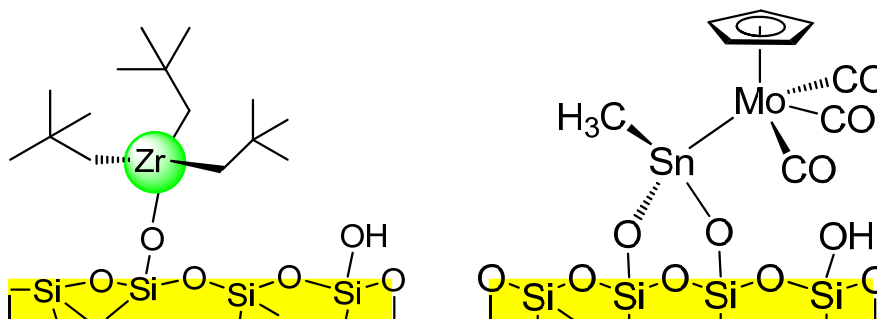
Figure **2**.**6** Examples of surface organometallic chemistry. $(\equiv SiO)Zr(CH_2C(CH_3)_3)_3$ (left)[44] and $MeSnMo(CO)_3(Cp)@MCM-41$ (right).[47]

A silica surface is known to have several different reactive surface sites. Siloxane bridges ($\equiv$Si-O-Si$\equiv$) being part of the continuous network and terminal silanol groups ($\equiv$Si-OH) are present (Figure **2**.**7**). Silanol groups can be arranged as isolated, geminal or vicinal functionalities.
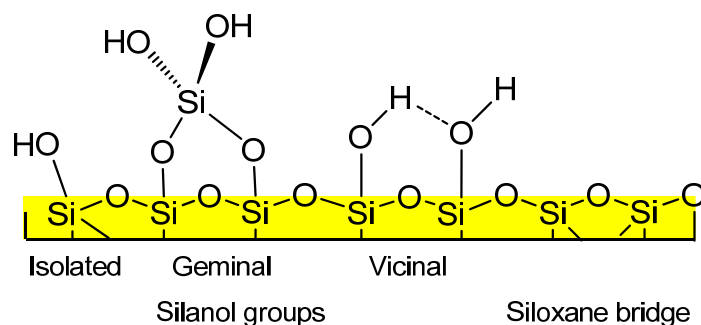

Figure **2**.**7** Various species on a silica surface.

Surface silanol groups condense when they are brought to elevated temperatures to form water which can be eliminated by vacuum. This dehydroxylation removes geminal and vicinal surface species in favor for siloxane bridges and is required to avoid grafting precursors to form clusters or other bulk species on the surface. After dehydroxylation between 200 and 300 ºC is the typical silanol population around 1.5-2.5 $SiOH/nm^2$.[47]

Silanol groups and organometallic precursors react mainly via rapid protonolysis reactions. The surface SiOH groups protonate basic ligands coordinated to the metal complex and create a Si-O-M bond while the ligand often exits the coordination sphere. In other words, the pK_a of the ligand must be higher than that of the SiOH group (pK_a = 6-7)[48] to observe an immobilization ("grafting") of the complex.

Being the utmost important metal in catalysis metalorganic complexes of titanium have been immobilized on several silica surfaces (Table 2.3). The titanium sources used are chlorides, alkyls, alkoxides, amides and titanocene derivatives. $TiCl_4$ reacts with Si-OH groups at high temperature to produce HCl which may degradate the silica structure. Alkoxides are inexpensive and easy to use but have a drawback because of incomplete surface silanol consumption and formation of clusters.[49] In a study on the grafting of non-porous silica it was found that $Ti(OiPr)_4$ only yielded dinuclear surface complexes, while the grafting of $Ti(NEt_2)_4$ gave mononuclear surface species.[50]
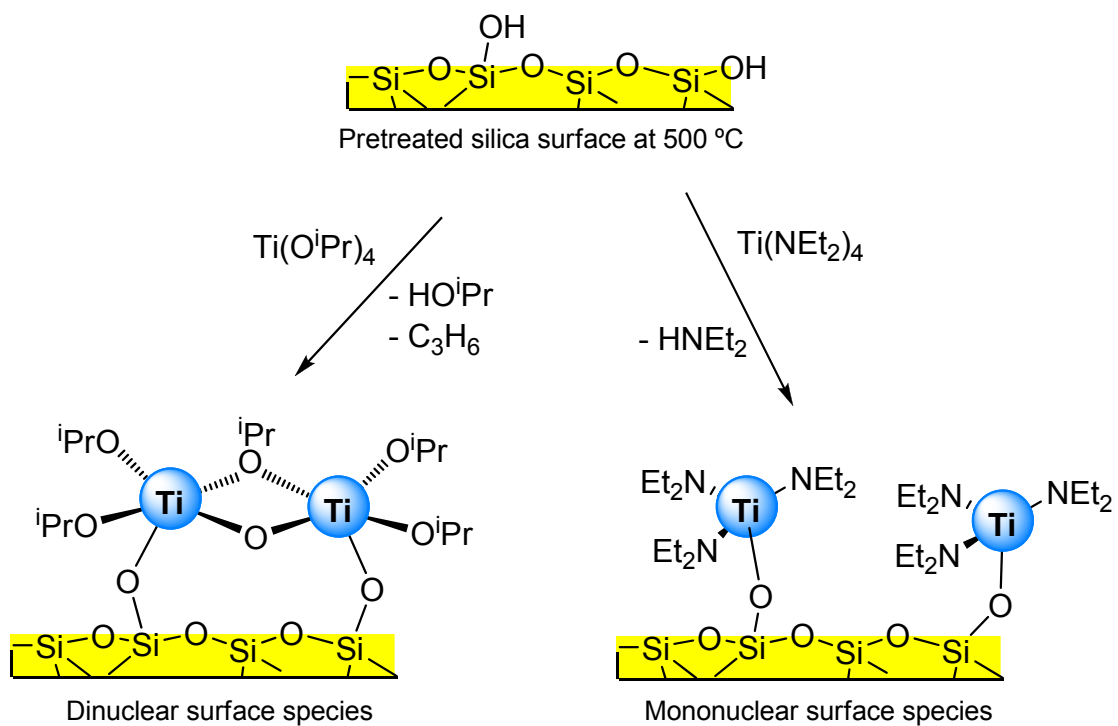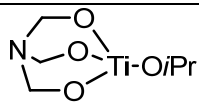
Scheme **2**.**3** Grafting of Ti(OiPr)$_4$ and Ti(NEt$_2$)$_4$ gives different agglomerated surface species.

Table 2.3 Overview of some titanium-grafted silica materials and their applications.

Metal source	Material	Application	Reference
TiCl$_4$	MCM-41, FSM-16	Oxidation of α-terpineol	[51]
TiCl$_4$	SBA-15	Epoxidation of cyclohexene	[52]
Ti(OiPr)$_4$	MCM-41	Hydrothermal stability	[53]
Ti(OiPr)$_4$	Silica	Epoxidation of cyclohexene	[50]
Ti(OiPr)$_4$	MCM-48, SBA-15	Dispersion of TiO$_2$ surface sites	[54]
Ti(OnBu)$_4$	MCM-41	Photocatalytic oxidation of phenol to CO$_2$	[55]
(triethanolaminato titanium isopropoxide: N(CH$_2$CH$_2$O)$_3$Ti-OiPr)	PNS^a	Epoxidation of 1-octene	[56]
Cp$_2$TiCl$_2$	MCM-41	Epoxidation of cyclohexene and α-pinene	[24]
Cp$_2$TiCl$_2$	MCM-41	Epoxidation of fatty acid methyl esters	[57,58]
Cp$_2$TiCl$_2$	SBA-15	Epoxidation of 1-octene	[59]
Cp$_2$TiCl$_2$/MAO	MSF	Ethylene polymerization	[60]
[(C$_5$H$_4$)$_2$SiMe$_2$]TiCl$_2$	MCM-41, MCM-48	Oxidation of cyclooctene	[61]
Ti(CH$_2$C(CH$_3$)$_3$)$_4$	Silica	Hydrogenolysis of light alkanes	[62]
Ti(NMe$_2$)$_4$	MCM-48	Epoxidation of cyclohexene	[63]
Ti(NEt$_2$)$_4$	Silica	Epoxidation of cyclohexene	[50]
Ti(NMe$_2$)$_4$	SBA-1	-	[28]

PNS = periodic nanoporous material. MSF = mesoporous silica film. MAO = methylalumoxane. Cp = C$_5$H$_5$ = cyclopentadienyl.

2.5 Objectives

This work is concerned about thesurface derivatization of periodic mesoporous silica with focus on the cagelike material SBA-1. The following surface reactions should be investigated

- surface silylation with disilazane reagents (HN(SiR$_3$)$_2$ R = H, alkyl, aryl)
- immobilization of magnesium silylamide and titanium amide complexes
- ligand exchange at surface-bonded titanium amide complexes with H$_2$BINOL

THEORY

Main emphasis should be put on whether cagelike materials can engage in size selective surface modifications. A PMS material with channel-like pore arrangement (MCM-41) has been for comparison.

3 Experimental section

3.1 Chemicals

Chemicals used in this thesis and their purity are found in **Table 3.1, Table 3.2**, and **Table 3.3**

Table 3.1 Reagents purchased or synthesised

Compound	Source	Purity	Purification
$C_{18}NEt_3Br$	Synthesized	-	See Chapter 2.2.3
HCl	Riedel	min. 37%	Used as received
H_2O	-	-	Destilled
Tetraethyl orthosilicate	Fluka	> 99%	Used as received
Octadecylbromide, $C_{18}H_{37}Br$	Fluka	> 97%	Used as received
Triethylamine	J.T. Barker		Used as received
C_{16-3-1}	Synthesized	-	See Chapter 2.2.3
$HN(SiHMe_2)_2$ (Hbdsa)	ABCR	> 97%	Used as received
$HN(SiMe_3)_2$ (Hbtsa)	ABCR	> 97%	Used as received
$HN(SiMe_2Ph)_2$	ABCR	> 97%	Used as received
$HN(SiMePh_2)_2$	ABCR	> 97%	Used as received
N,N-dimethylhexadecylamine, $C_{16}NMe_2$	Fluka	> 95%	Used as received
(3-bromopropyl)trimethylammonium bromide	Aldrich	> 97%	Used as received
Di-*n*-butylmagnesium solution	Aldrich	1.0 M in heptane	Used as received
Pluronic F127 $(EO_{106}PO_{70}EO_{106})^a$	Sigma	-	Used as received
$Ti(NMe_2)_4$	Aldrich	99.999 %	Used as received
$Zr(NMe_2)_4$	Aldrich	99.99+ %	Used as received
R-Binaphthol	Aldrich	99 %	Used as received
$Mg(bdsa)_2$	Synthesized	-	See Chapter 2.2.5
$Ti(NMe_2)_3(bdsa)$	Synthesized	-	See Chapter 2.2.5
$Mg(btsa)_2$	Synthesized	-	See Chapter 2.2.5
$Ti(NMe_2)_2(BINOL)$	Synthesized	-	See Chapter 2.2.5

[a]Poly(ethylene oxide)–poly(propene oxide)–poly(ethylene oxide) triblock copolymer.

Table 3.2 Solvents used in this work

Solvent	**Source**	**Purity**	**Purification**
Hexane	Aldrich	> 98.5 %	SPS
Toluene	Aldrich	> 99.7 %	SPS
Tetrahydrofuran	Aldrich	> 99.9 %	SPS
Acetonitrile	Riedel	> 99.5 %	Used as received
Tetramethylammonium hydroxide	Aldrich	25 % in H_2O	Used as received
Hydrofluoric acid	Merck	40 %	Used as received
Nitric acid	Fluka	65 %	Used as received
Diethylether	Riedel	Puriss (p.a.)	SPS

Table 3.3 Chemicals used for characterization

Compound	Purchase	Purity	Purification
Benzene-d_6	Aldrich	99.6 atom % D	Dried with Na
Potassium bromide	Aldrich	> 99%	Dried at 150 ºC
Mineral oil (Nujol)	Sigma	-	Dried over molecular sieves
Ti standard	Perkin Elmer	1.000 μg/mL	Used as received

Solvents to be used in the glovebox were purified with a MBraun SPS (solvent purification system) using Grubbs columns.

C_6D_6 was degassed, dried with Na, filtered and stored in a glovebox.

KBr powder was dried at 150 ºC for several days, degassed and stored in the glovebox.

Mineral oil (Nujol) was degassed and stored under molecular sieves in a glovebox.

3.2 Methods and experiments

3.2.1   General information

NMR spectroscopy

^{1}H and ^{13}C NMR spectra were recorded on a Bruker BioSpin DPX400 (^{1}H: 400.13 MHz; ^{13}C: 100.61 MHz), and a Bruker AV600 (^{1}H: 600.13 MHz; ^{13}C: 100.61 MHz) at 298 K. When recording ^{13}C spectra proton decoupling was used. Deuterated benzene was used as a solvent and as internal standard. Shifts are reported in parts per million relative to TMS. Coupling constants are given in Hz. Spectra were manipulated with MestReNova[64] (version 5.2.1-3586). Signals are assigned with the following abbreviations: s, singlet; d, doublet; t, triplet; dd, doublet of doublets.

FT-IR spectroscopy

IR spectra were obtained on different instruments. All spectra were obtained at ambient temperature. All samples were prepared inside a glovebox. A Nicolet Impact 410 FTIR spectrometer were used for measuring materials and solids as Nujol mull, sandwiched between KBr disks; liquid samples were measured as neat liquid. DRIFT (Diffuse Reflectance Infrared Fourier-Transform) spectra were recorded on a Nicolet Protégé 460 spectrometer for which the samples were mixed with KBr, finely grinded and packed into a sample holder. The sample holder was placed in a DRIFT cell and sealed. The measurement chamber was purged with nitrogen before the spectra were collected. Numbers are reported in wavenumber (cm^{-1}). For the intensity of the absorption bands the following abbreviations have been used: w, weak; m, middle; s, strong; vs, very strong, b, broad signal.

Elemental analysis

An Elementar Vario El III was used for the determination of carbon, nitrogen and hydrogen content. Air- and water sensitive samples were double packed inside the glovebox into tin ships. The ships were placed in glass tubes, sealed with parafilm, and stored there until the measurement took place. Measurements were kindly performed by Inger Johanne Fjellanger.

Atom absorption spectroscopy (AAS)

The titanium content determination was determined on a Perkin-Elmer Aanalyst 300. The materials to be characterized were dissolved in hydrofluoric acid overnight. The samples were left in air to evaporate, then dissolved in concentrated nitric acid and let to evaporate again.

The residue was dissolved and diluted with 2 *M* nitric acid before it was measured on the instrument using a mixture of air, acetylene and N_2O as combustion gases.

Porosimetry

A Micromeritics ASAP 2020 volumetric adsorption apparatus was used to examine the porous materials. Samples of 100 mg were degassed for at least 4 hours at 250 ºC (parent materials) and at 25 ºC (hybrid materials). Nitrogen was used as the sorption gas for relative pressures between 0.01 and 0.99 at 77 K. The $a_{S\ BET}$ (BET specific surface area) was calculated from the adsorption isotherm in the relative pressure range from 0.04 to 0.2.[8, 39] The pore size distributions were calculated using the Barret-Joyner-Halenda (BJH) method.[40] For SBA-1 materials a method proposed by Neimark[41] has been used to calculate the cage pore diameter.

Powder X-ray diffraction

Diffraction patterns of the materials were obtained on a Bruker D8 ADVANCE instrument. The following step/scan mode was used: Step width = 0.00825; accumulation time = 2 s/step; range (2θ) = 0.50-10.00º. Monochromatic CuKα radiation (λ = 1.5418 Å) was used as the X-ray source.

Glovebox techniques

Due to the high sensitivity to water and air, the synthesis of the metalorganic complexes was done using high vacuum, Schlenk techniques and glovebox techniques (MBraun MB150B-G; <1 ppm O_2, <1 ppm H_2O)

3.2.2 Synthesis of surfactants

Synthesis of triethyloctadecylammonium bromide, $C_{18}NEt_3Br$[65]

Octadecylbromide (25.32 g, 75.94 mmol) was dissolved in with 200 ml acetonitrile. Triethylamine (11.52 g, 113.91 mmol) was added and the reaction mixture refluxed for 24 hours. The mother liquid was cooled down to ambient temperature before the crude product was filtrated and washed with hexane. This white solid was recrystallized in hexane and methanol. After filtration, the white powder was dried in air at ambient temperature. **Elemental analysis** (wt %) calculated for $C_{24}H_{52}BrN$ (434.58 gmol^{-1}): C 66.33, H 12.06, N 3.22. Found: C 65.22, H 12.65, N 3.05.

Synthesis of *N*-(3-trimethyl-ammoniumpropyl)hexadecylammonium dibromide, C$_{16\text{-}3\text{-}1}$ [66]

(3-Bromopropyl)-trimethylammonium bromide (12.5 g, 47.89 mmol) was dissolved in 150 mL as a mixture of acetonitril and nitromethane (1:2). *N,N*-dimethylhexadecylamine (15.48 g, 57.44 mmol) was added and the reaction was heated up to 50 ºC and then refluxed for 24 hours. The mother liquid was cooled down and filtrated. The obtained white solid was washed with hexane. The product was purified by recrystallization in ethyl acetate and a few drops of methanol before it was dried in air. **Elemental analysis** (wt %) calculated for C$_{23}$H$_{52}$Br$_2$N$_2$ (516.48 gmol^{-1}): C 53.49, H 10.15, N 5.42. Found: C 51.30, H 10.60, N 4.99.

3.2.3   Synthesis of periodic mesoporous silica

Synthesis of PMS SBA-1 [30]

Surfactant C$_{18}$NEt$_3$Br (5.71 g, 13.10 mmol), distilled water (598.53 g, 33.25 mol) and concentrated hydrochloric acid (37%, 362.90 g, 3.68 mol) were mixed in a PET bottle. This mixture was stirred for one hour to produce a homogeneous solution. The solution temperature was set to 0 ºC and then TEOS (13.68 g, 65.67 mmol) cooled to 0 ºC, was added slowly to the solution. After the reaction was stirred 4 hours at 0 ºC, the bottle was closed and heated under static conditions at 100 ºC for 1 hour. The white precipitate was filtrated without any washing and dried in air overnight. After complete dryness the as-synthesised product (1 and **2**) was calcined at 540 ºC (air, 5 h) and dehydrated in vacuo (270 ºC, 10^{-4} Torr, 4 h). Final molar composition: 1 C$_{18}$NEt$_3$Br : 5 TEOS : 281 HCl : 2538 H$_2$O. XRD-reflections in 2θ: **1**: 2.17; 2.36; 2.58, **2**: 2.08; 2.27; 2.49. See Table 3.4 for nitrogen physisorption data.

Synthesis of PMS SBA-1 Large Pores (LP)

The synthesis of SBA-1 LP resembles the SBA-1 synthesis with the following modifications. The mixture was treated at 100 ºC for 72 hours to give material (**6**). XRD-reflections in 2θ: 1.93; 2.12; 2.33.

Synthesis of PMS SBA-2 [31]

Surfactant C$_{16\text{-}3\text{-}1}$ (1.00 g, 2.47 mmol), water (140.66 g, 7.81 mol) and tetramethylammonium hydroxide, TMAOH (25% in water, 10.00 g, 27.44 mmol) was homogenized in a PET bottle at ambient temperature for 30 minutes. TEOS (11.43 g, 54.87 mmol) was then added slowly dropwise. The solution was stirred for 2 hours. The product was filtrated and left to dry in air.

The white material (**5**) was calcined at 540 ºC (air, 5 h) and dehydrated in vacuo (270 ºC, 10^{-4} Torr, 4 h). Final molar composition: 0.05 C_{16-3-1} : 0.5 TMAOH : 142 H_2O : 1 TEOS. XRD-reflections in 2θ: 2.24; 3.63; 4.23; 5.70.

Synthesis of PMS MCM-41[7]

Surfactants C_{16-3-1} (5.51 g, 10.39 mmol) and CTMABr (4.27 g, 11.71 mmol) were dissolved in water (280.76 g, 15.6 mol) and tetramethylammonium hydroxide, TMAOH (25% in water, 23.65 g, 64.67 mol). After having obtained a complete homogeneous mixture (30 minutes), TEOS (27.04 g, 129.78 mmol) was added slowly drop by drop. The reaction mixture was stirred for 40 minutes. The obtained mixture was filtrated and washed with water then mixed with 350 ml water and treated in an oven at 100 ºC for 6 days. The obtained mesoporous silica was filtrated, washed with water and dried in air. The material (**3** and **4**) was calcined at 540 ºC and dehydrated in vacuo (270 ºC, 10^{-4} Torr, 4 h). Final molar composition: 0.08 C_{16-3-1} : 0.09 CTMABr : 0.5 TMAOH : 120 H_2O : 1 TEOS. XRD-reflections in 2θ: **3**: 1.84; 3.28; 3.64; 4.83.

MCM-41 materials were provided by Thomas Deschner and André Bienfait.

Synthesis of PMS SBA-16[67]

Copolymer surfactant Pluronic F127 ($EO_{106}PO_{70}EO_{106}$, 3.0 g) was dissolved in hydrochloric acid (37%, 22.1 g, 223.8 mmol) and distilled water (117.0 g, 6.5 mol), then the solution was heated and kept at 35 ºC. TEOS (11.7 g, 56.16 mmol) was added slowly dropwise and the reaction mixture was stirred at 35 ºC for 24 hours and then treated at 100 ºC for 24 hours. The material was filtrated without any washing and dried overnight. The obtained material (**7**) was calcined at 540 ºC (air, 5 h) and dehydrated in vacuo (270 ºC, 10^{-4} Torr, 4 h). Final molar composition: 0.004 Pluronic F127 : 1 TEOS : 4 HCl : 116 H_2O. XRD-reflections in 2θ: 0.88; 1.46.

Table 3.4 Physisorption data of the materials synthesized

Material	$a_{S, BET}$ / m^2g^{-1}	V_P / cm^3g^{-1}	$d_{p, Des}$ / nm	d_c / nm
SBA-1 **1**	1240	0.68	2.2	4.4
SBA-1 **2**	1350	0.83	2.3	4.7
MCM-41 **3**	1060	1.13	3.4	-
MCM-41 **4**	1170	1.25	3.3	-

SBA-2 **5**	990	0.64	2.5	-
SBA-1 LP **6**	1050	1.11	3.7	5.1
SBA-16 **7**	640	0.85	2.9	-

3.2.4 Synthesis of metalorganic complexes

Synthesis of {Mg[N(SiHMe$_2$)$_2$]$_2$}$_2$

The magnesium complex was synthesized following a slightly modified procedure.[28] 1,1,3,3-Tetramethyldisilazane (1.07 g, 8.02 mmol) was dissolved in hexane. A solution of dibutylmagnesium (1 *M* in heptane, 4.0 mL, 4.0 mmol) was added dropwise. Gas evolution of butane was observed. The reaction was stirred 4 hours at ambient temperature. The solvent was removed in vacuo. The remaining white solid was solved in hexane, filtrated and recrystallized at −35 ºC. Crystals were obtained after a few days, but were not characterized by single crystal X-ray diffraction. The hexane solution was removed by a Pasteur pipette and the white crystals were dried in vacuo several hours to give 90% yield (3.6 mmol). **Elemental analysis** (wt %) calculated for $C_8H_{28}MgN_2Si_4$ (288.97 gmol^{-1}): C 33.25, H 9.77, N 6.96. Found: C 35.20, H 11.79, N 8.57. **^{1}H NMR (400.13 MHz C$_6$D$_6$):** δ = 5.06 (2H, septet, ^3J(H,H) = 0.8 Hz, Si*H*), 4.96 (2H, septet, ^3J(H,H) = 0.8 Hz, Si*H*), 0.39(12H, dd, *J*(H,H) = 2.7, 1.0, SiC*H$_3$*), 0.37(12H, dd, *J*(H,H) = 3.1, 1.0). **^{13}C NMR (100.61 MHz C$_6$D$_6$):** δ = 3.97, 2.50. **DRIFT(cm^{-1}):** 2948 m, 2890 w, 2081 m, 2046 wb, 1256 m, 1057 m, 961 m, 891 vs, 839 s, 777 m, 486 w.

Synthesis of Ti(NMe$_2$)$_3$[N(SiHMe$_2$)$_2$]

The complex was synthesized following a slightly modified procedure.[65] 1,1,3,3-Tetramethyldisilazane (601 mg, 4.51 mmol) was dissolved in toluene. Tetrakis(dimethylamido)titanium(IV) (498 mg, 2.22 mmol) was added drop by drop. The colour changed from bright yellow (Ti(NMe$_2$)$_4$) to dark yellow. The reaction was stirred for 48 hours at ambient temperature. Afterwards the solvent and remaining precursors were removed under vacuum for several hours. The product was obtained as a dark green solid wax in 90 % yield (4.06 mmol). **Elemental analysis** (wt %) calculated for $C_{10}H_{32}N_4Si_2Ti$ (312.43 gmol^{-1}): C 38.44, H 10.32, N 17.93. Found: C 38.24, H 13.89, N 16.59. **^{1}H NMR (400.13 MHz C$_6$D$_6$):** δ = 5.03 (2H, sept, ^3J(H,H) = 3.2 Hz, NSi*H*), 3.08 (18 H, s, TiN*Me*), 0.35 (12H, d, ^3J(H,H) = 3.2 Hz, NSi*Me*). **^{13}C NMR (100.61 MHz C$_6$D$_6$):** δ = 45.38, 3.11. **DRIFT(cm^{-1}):**

2956 m, 2854 s, 2812 m, 2771 s, 2089 m, 1416 w, 1250 m, 1148 w, 947 ws, 901 m, 843 m, 591 w.

Synthesis of Ti(NMe$_2$)$_2$(BINOL) [68]

R-Binaphthol (H$_2$BINOL, 286.3 mg, 1.00 mmol) was dissolved in diethyl ether to give a 1 *M* solution. To this solution Ti(NMe$_2$)$_4$ (224.2 mg, 1.00 mmol) was added in one portion also as a 1 *M* solution in Et$_2$O. The reaction took place overnight and the solvent was removed in vacuo. The orange/red solid was separated in hexane soluble and toluene soluble parts. No crystals were obtained. The yield based on the hexane soluble part was 7 % (0.07 mmol). **Elemental analysis** (wt %) calculated for C$_{24}$H$_{24}$N$_2$O$_2$Ti (420.33 gmol^{-1}): C 68.58, H 4.76, N 6.66. Found: C 69.32, H 6.17, N 5.14. **^{1}H NMR (600.13 MHz, C$_6$D$_6$)**: δ 7.91 (2H, d, *J* = 7.8 Hz), 7.69 (2H, d, *J* = 8.8 Hz), 7.48 (2H, d, *J* = 8.5 Hz), 7.31 (2H, t, *J* = 7.8 Hz), 7.09 (2H, t, *J* = 8.0 Hz), 6.89 (2H, d, *J* = 8.7 Hz), 3.01 (12H, s).**^{13}C NMR (100.61 MHz C$_6$D$_6$):** Due to low concentration no signals were obtained after 10000 scans. **DRIFT(cm^{-1}):** 3050 w, 3000 w, 2895 w, 2858 m, 2770 w, 1613 m, 1590 m, 1506 m, 1465 s, 1335 vs, 1237 vs, 951 vs, 820 s, 745 s, 615 s, 594 s.

Reaction between Ti(NMe$_2$)$_4$ and {Mg[N(SiMe$_3$)$_2$]$_2$}$_2$

The magnesium complex (57.7 mg, 0.20 mmol) was dissolved in hexane. Ti(NMe$_2$)$_4$ (53.6 mg, 0.24 mmol) was added dropwise and the reaction was stirred overnight. The colour changed from yellow to dark orange/ red. The solvent was removed and the red brownish powder was dried under vacuum. Crystals were not obtained from a hexane solution at −35 ºC. **^{1}H NMR (400.13 MHz C$_6$D$_6$):** δ = 5.13 (1H, sept, *J* = 3.1), 3.18 (14H, s), 0.44 (9H, t, *J* = 3.2). **^{13}C NMR (100.61 MHz, C$_6$D$_6$):** δ = 100.64, 45.28, 3.10.

Synthesis of Zr(NMe$_2$)$_3$[N(SiHMe$_2$)$_2$]

Tetrakis(dimethylamido)zirconium (251.2 mg, 0.94 mmol) was solved in hexane and added to a solution of 1,1,3,3,-tetramethyldisilazane (252.8, 1.90 mmol) in hexane. The reaction was stirred overnight. The solvent was removed under vacuum and the remaining white solid was dissolved in hexane and filtrated. This solution did not produce crystals after two weeks at −35 ºC and the spectroscopic data were non-conclusive. Sublimation of the solid ≤ 100 ºC was not successful.

3.2.5 Functionalization of PMS

General procedure

The parent material was suspended in hexane. The precursor to be grafted was dissolved in hexane where needed and added to the suspension. The reaction took place overnight at ambient temperature in a glovebox. The mother liquid was removed after centrifugation. The material was washed with hexane three times and then dried under vacuum. Where possible the grafting precursor was recovered from the mother liquid and the washing water.

Table 3.5 Overview of materials (# means any number.)

Entry	Material
1,2	SBA-1
3,4	MCM-41
5	SBA-2
6	SBA-1 LP
7	SBA-16
#a	$SiHMe_2$@PMS
#b	$SiMe_2Ph$@PMS
#c	$SiMePh_2$@PMS
#d	$Mg[N(SiHMe_2)_2]$@PMS
#e	$Ti(NMe_2)_x$@PMS
#eB	$Ti(NMe_2)_x(BINOL)$@PMS
#f	$Ti(NMe_2)_x[N(SiHMe_2)_2]$@PMS
#g	$Zr(NMe_2)_x$@PMS

Surface silylation – determination of silanol groups

Following the general procedure dehydrated material (100.0 mg) was reacted with 1,1,3,3-tetramethyldisilazane (200 mg, 1.50 mmol). See Table 3.6 for numbers.

Surface silylation – modification of the surface

SBA-1 **1** (200 mg) was reacted with 1,3-diphenyl-1,1,3,3-tetramethyldisilazane (350 mg, 1.23 mmol). Following the general procedure, where the reaction time was extended to 20 hours, a white hybrid material, $SiMe_2Ph$@SBA-1 **1b** (242 mg) was obtained.

EXPERIMENTAL

SBA-1 **2** (305 mg) was reacted with 1,3-dimethyl-1,1,3,3-tetraphenyldisilazane (674 mg, 1.65 mmol). Following the general procedure with 20 hours reaction time a white material SiMePh$_2$@SBA-1 **2c** (324 mg) was obtained.

MCM-41 **4** (401 mg) was reacted with 1,3-dimethyl-1,1,3,3-tetraphenyldisilazane (1.031 g, 2.51 mmol). Following the general procedure with 20 hours reaction time a white material SiMePh$_2$@MCM-41 **4c** (347 mg) was obtained. 0.883 g of the silylation agent was recovered from the reaction.

Grafting of Mg(bdsa)$_2$

SBA-1 **2** (500 mg) was reacted with Mg(bdsa)$_2$ (523 mg, 1.81 mmol). The reaction followed the same steps as the general procedure except the reaction time which was 24 hours. A white powder (**2d**) was obtained (mass not recorded). The magnesium complex was recovered: 475 mg, 1.65 mmol.

Table 3.6 Hybrid materials properties part 1

Material	Physisorption data				Elemental analysis		
	$a_{S, BET}$ / m^2g^{-1}	V_P / cm^3g^{-1}	$d_{p, Des}$ / nm	d_c / nm	C / wt %	H / wt %	N / wt %
1a	b	b	b	b	7.39	2.35	0.08
1b	510	0.24	< 1.1	3.7	14.75	1.76	0.06
2a	b	b	b	b	7.24	1.77	0.10
2c	1030	0.54	2.2	4.4	11.44	1.28	0.43
2d	1200	0.71	2.2	4.6	3.03	1.51	0.28
4a	b	b	b	a	7.53	1.71	6.14
4c	90	0.09	3.3	a	10.60	1.76	0.40

^{a} This calculation only applies to SBA-1 ^{b} No data available

Grafting of Ti(NMe$_2$)$_4$

Several materials, were reacted with tetrakis(dimethylamido)titanium. The mother liquid turned orange upon addition of the titanium complex. Following the general procedure a yellow material, **#e**, was obtained. See Table 3.7 for numbers.

Table 3.7 Reaction conditions for the grafting of Ti(NMe$_2$)$_4$

Material (mg)	Ti(NMe$_2$)$_4$ mg / mmol	Reaction time	Recovered Ti(NMe$_2$)$_4$ mg / mmol	Product (mg)
SBA-1 **1** (216)	280 / 1.25	Overnight	[a]	**1e** (214)
SiMe$_2$Ph@SBA-1 **1b** (206)	270 / 1.20	4 days	[a]	**1be** ([a])
MCM-41 **3** (420)	550 / 2.45	24 hours	[a]	**3e** ([a])
SBA-1 **2** (200)	327 / 1.46	48 hours	95 / 0.42	**2e** (288)
SBA-1 **2** (410)	669 / 2.98	48 hours	150 / 0.67	**2e2** (557)
SiMePh$_2$@SBA-1 **2c** (159)	142 / 0.63	24 hours	[a]	**2ce** (183)
Mg(bdsa)$_x$@SBA-1 **2d** (453)	448 / 2.00	24 hours	223 / 1.00	**2de** ([a])
SiMePh$_2$@MCM-41 **4c** (200)	158 / 0.70	24 hours	79 / 10.17	**4ce** (245)

[a] Not recorded

Ligand exchange on surface

H$_2$BINOL was dissolved in toluene with some drops of THF. The material was suspended in toluene and added to the first solution. The reaction stirred overnight at ambient temperature while the colour changed from yellow to dark orange. The material was washed three times with toluene/THF and two times with hexane. A slightly darker yellow material was dried under vacuum. Numbers are given in Table 3.8.

Table 3.8 Reaction conditions for ligand exchange on surface

Material (mg)	H$_2$BINOL (mg / mmol)	Reaction time	Product (mg)
SBA-1 **2e2** (254)	259 / 0.92	48 hours	**2e2B** (273)
MCM41 **3e** (150)	150 / 0.52	Overnight	**3eB** ([a])

[a] Not recorded

Grafting of Ti(NMe$_2$)$_3$[N(SiHMe$_2$)$_2$]

The material and the titanium complex were reacted following the general procedure except for the reaction time as noted in Table 3.9. Materials Ti(NMe$_2$)$_x$[N(SiHMe$_2$)$_2$]@PMS **#f**, displayed a dark green colour.

Table 3.9 Reaction conditions for the grafting of Ti(NMe$_2$)$_3$[N(SiHMe$_2$)$_2$]

Material (mg)	Ti(NMe$_2$)$_3$(bdsa) (mg / mmol)	Reaction time	Recovered (mg / mmol)	Product (mg)
2 (152)	223 / 0.71	24 hours	120 / 0.38	**2f** (201)
2 (405)	615 / 1.97	5 days	400 / 1.28	**2f2** (547)
4 (155)	218 / 0.70	Overnight	76 / 0.24	**4f** (205)

Grafting of Zr(NMe$_2$)$_4$

SBA-1 **2** (209 mg) was reacted with tetrakis(dimethylamido)zirconium (384 mg). Following the general procedure except the reaction time was 48 hours material **2g** (318 mg) was obtained.

Table 3.10 Hybrid materials properties part 2

Material	Physisorption				Elemental analysis			
	$a_{S, BET}$ / m^{2}g^{-1}	V_P / cm^{3}g^{-1}	$d_{p, Des}$ / nm	d_c / nm	C / wt %	H / wt %	N / wt %	Ti / wt %
1e	1090	0.50	2.0	4.2	5.18	1.17	2.44	[a]
1be	420	0.21	< 1.1	3.7	16.46	2.15	0.66	[a]
2e	710	0.29	1.6	4.0	12.44	2.88	7.00	[a]
2e2	690	0.29	< 1.1	4.0	[a]	[a]	[a]	[a]
2e2B	670	0.28	< 1.1	3.9	[a]	[a]	[a]	[a]
2ce	650	0.28	< 1.1	3.9	15.48	2.97	5.97	10.25
2de	710	0.30	< 1.1	4.0	12.84	3.12	6.49	11.0
2f	900	0.47	< 1.1	4.3	12.43	2.93	4.98	4.56
2f2	740	0.34	< 1.1	4.1	[a]	[a]	[a]	[a]
2g	600	0.26	< 1.1	3.9	12.96	2.99	7.01	0
3e	640	0.60	2.9	[b]	12.18	2.85	6.80	12.1
3eB	370	0.20	2.1	[b]	29.14	2.66	2.60	5.87
4ce	610	0.53	2.8	[b]	15.84	2.83	5.70	8.21
4f	610	0.48	2.6	[b]	12.27	3.51	5.39	8.73

[a] Not recorded. [b] Applies only to cagelike materials

4 Results and discussion

4.1 Periodic mesoporous silica

Surfactants

$C_{18}NEt_3Br$ and C_{16-3-1} were synthesized and characterised by elemental analysis (Table 4.1 and Table 4.2). $C_{18}NEt_3Br$ was used in the synthesis of SBA-1 while C_{16-3-1} was used in synthesis of SBA-2 and in several attempts to make MCM-41.

Table 4.1 Elemental analysis of $C_{18}NEt_3Br$

	wt% C	wt% H	wt% N
Required	66.33	12.06	3.22
Found	65.22	12.65	3.05

Table 4.2 Elemental analysis of C_{16-3-1}

	wt% C	wt% H	wt% N
Required	53.49	10.15	5.42
Found	51.30	10.60	4.99

With three ethyl groups in the hydrophilic end the $C_{18}NEt_3^+$ has a larger head group area than the corresponding fatty acid $C_{17}H_{35}COOH$. C_{16-3-1} (Figure 4.1) has two cationic nitrogen separated with a $(CH_2)_3$ spacer. This makes the head group area larger and decreases the packing parameter.
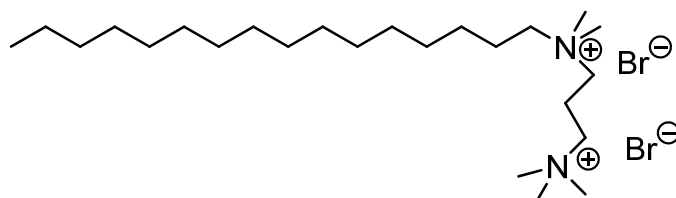
Figure 4.1 Structure of C_{16-3-1}

4.2 Materials

SBA-1

RESULTS AND DISCUSSION

The two SBA-1 materials, synthesized by a known literature procedure[30], showed the same X-ray diffraction pattern for a cubic material with the space group *Pm3n* as previously reported. Both materials were found to have a high specific surface area above 1200 m^2g^{-1}. The pore volumes were found to be 0.68 and 0.83 cm^3g^{-1}. The pore size diameters calculated from the BJH method were approximately 2.2 nm, but this value describes the cagelike pores and the interconnecting channels in one value. A method proposed by Neimark explains how to calculate the inner pore diameter of the cages by using the pore volume and the geometrical data obtained from powder X-ray diffraction analysis. By using Neimark's method the cagelike pores are calculated to have a diameter of 4.4 and 4.7 nm, nearly a doubling of the values obtained from the BJH method. Even though these physisorption measurements are inaccurate it is possible to compare the pore size values from the parent material and hybrid materials. The high values for the cagelike pore diameter does not tell us how large the windows into the material are, but as long as the reagent to be immobilized passes through the window one may tune the inner environment as desired. This method may be called "ship in a bottle" synthesis. The appendix shows the powder X-ray diffraction pattern (Figure 6.1 and Figure 6.2) and nitrogen physisorption (Figure 6.51 and Figure 6.52) for materials **1** and **2** respectively.

SBA-2

By using a divalent surfactant $C_{16}H_{33}NMe_2(CH_2)_3NMe_3^{2+}$ a SBA-2 material **5** with space group P6$_3$/mmc was obtained. The powder X-ray pattern is shown in Figure 6.55. This material shows a lower specific surface area (990 m^3g^{-1}) and a lower pore volume (0.64 m^3g^{-1}) than the SBA-1 materials, while the BJH pore size distribution shows a higher pore diameter (2.5 nm). See Figure 6.55 for physisorption isotherm and BJH pore size distribution.

MCM-41

Two MCM-41 materials, with space group P6mm, were synthesized by fellow group members following a slightly modified procedure described by Beck et al.[7] The surfactant $C_{18}H_{37}NEt_3^+$ was used in a molar composition to give a hexagonal mesophase which was confirmed by the powder X-ray diffraction pattern recorded for the materials **3** (Figure 6.3) and **4** (Figure 6.4). The materials have a specific surface area of 1060 (**3**) and 1170 m^3g^{-1} (**4**) which is about 200 m^3g^{-1} lower than the SBA-1 materials. The pore volumes are 1.13 (**3**) and 1.25 cm^3g^{-1} (**4**) which is higher than the SBA-1 materials. Since the BJH method is based on 1 dimensional tubes it is more reliable used on MCM-41 than on SBA-1. The pore diameters

obtained 3.4 (**3**) and 3.3 nm (**4**) are about 1 nm larger than for the SBA-1 materials. N_2-physisorption isotherms and BJH pore size distribution can be found in Figure 6.53 and Figure 6.54

SBA-1 LP (Large pores)

The SBA-1 LP material **6** is made by the analogues procedure as the common SBA-1 material, however, with longer crystallization time (hydrothermal treatment) is set to 72 hours compared to 4 hours. The powder X-ray diffraction pattern (Figure 6.6) reveals a highly crystalline material like the common SBA-1 material with reflections shifted to lower angles. The specific surface area (1050 m^3g^{-1}) is somewhat smaller than the common SBA-1 material and the MCM-41. The pore volume (0.85 cm^3g^{-1}) is lower than the MCM-41 materials and slightly higher than the common SBA-1. The SBA-1 LP shows a BJH pore diameter of 3.7 nm and 5.1 nm for the inner pore diameter. Isotherm and BJH pore size distribution is shown in Figure 6.56.

SBA-16

SBA-16 was synthesized by using a triblock polymer poly(ethylene oxide)$_{106}$-poly(propylene oxide)$_{70}$-poly(ethylene oxide)$_{106}$ as structure directing agent. This resulted in a crystalline material **7**, with space group *Im3m*, shown by powder X-ray diffraction pattern in Figure 6.7. The specific surface area (640 m^2g^{-1}) is significantly lower than the other materials in this work. The pore volume (0.85 cm^3g^{-1}) and the pore size (2.9 nm) lies between the pore volume of SBA-1 materials and MCM-41 materials. See Figure 6.57 for physisorption isotherm and BJH pore size distribution.

4.3 Metalorganic precursors

4.3.1 {Mg[N(SiHMe$_2$)$_2$]$_2$}$_2$

The synthesis of {Mg[N(SiHMe$_2$)$_2$]$_2$}$_2$ (Scheme 4.1) was done after literature procedures.[28] By reacting n-butyl magnesium with 2 equivalents of Hbdsa gas formation was observed. The complex gave large crystals after recrystallization in hexane at −35 °C.
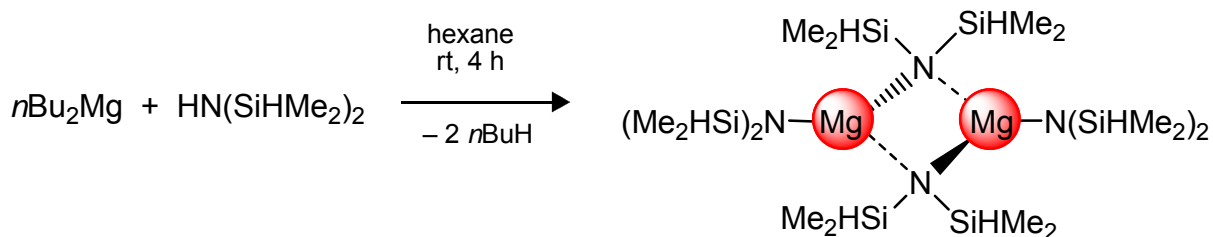
Scheme 4.1 Synthesis of $\{Mg[N(SiHMe_2)_2]_2\}_2$

The ^1H NMR spectrum (Figure 6.13) shows a set of two peaks according to a dimer. One set is the terminal silylamide ligand and the other set is the bridging silylamide ligand. The signals for the Si-H at 5.06 and 4.96 ppm show two multiplets which may be interpreted as two septets caused by the coupling to 6 other protons. The signals at 0.39 man 0.37 corresponds to the methyl groups connected to the silicon. The signals occur as doublet of doublets where one can find the coupling constants to the Si-H proton. The second coupling constant 1.0 Hz exist in both peaks and indicate a coupling between the two methyl proton environments. The ^{13}C NMR spectrum (Figure 6.14) shows to distinct signals at 3.97 and 2.50 ppm according to the two different methyl environments in the complex. The DRIFT spectrum (Figure 6.25) shows two peaks around 2050 cm^{-1} corresponding to the Si-H stretch. Two new peaks at 1058 and 493 cm^{-1} appear while the N-H stretch at 3384 cm^{-1} and the vibration 1178 cm^{-1} have disappeared.

4.3.2   Ti(NMe$_2$)$_3$[N(SiHMe$_2$)$_2$]

Ti(NMe$_2$)$_3$(bdsa) (Scheme 4.2) was obtained by Ti(NMe$_2$)$_4$ with one equivalent of Hbdsa. The green wax obtained gave three peaks in the ^1H NMR spectrum. The Si-H proton resonance at 5.03 ppm is coupled to six other protons and shows a septet. A singlet at 3.08 ppm is in accordance with the eighteen protons in the methyl amido groups. A doublet which account for the Si-Me groups at 0.35 ppm shows the same coupling constants as found for the Si-H proton.
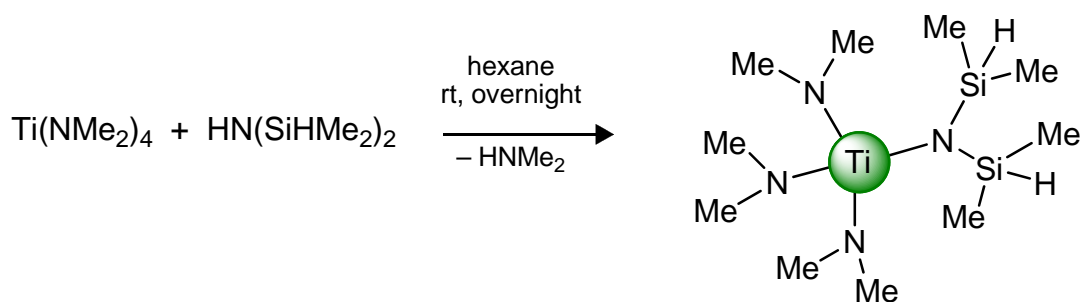
Scheme 4.2 Synthesis of Ti(NMe$_2$)$_3$[N(SiHMe$_2$)$_2$]

^{13}C NMR reveals two different peaks which fit the N-C and the Si-C environments as expected. The DRIFT spectrum (Figure 6.26) shows the Si-H stretch at 2090 cm^{-1} which is 30 cm^{-1} lower than the Si-H stretch in free Hbdsa. The H-N stretch at 3385 cm^{-1} is no longer observed.

4.3.3 Ti(NMe$_2$)$_3$(BINOL)

The reaction was carried out as shown in Scheme 4.3. Characterization showed that the complex existed in both hexane- and toluene soluble parts, even though the ^{1}H NMR spectrum (Figure 6.17) showed that the hexane soluble part was purer. The spectrum further reveals one singlet at 3.01 ppm corresponding to the N-Me groups and six other signals between 6.9 and 8.0 ppm. One notice that two of the signals (7.31 and 7.01 ppm) split into triplets while the other four signals split into doublets. The two triplets correspond to two protons coupled to two other protons in ortho position. The ^{13}C NMR spectra did not show any signals due to low concentration, but the NMR sample itself showed a nice yellow colour.
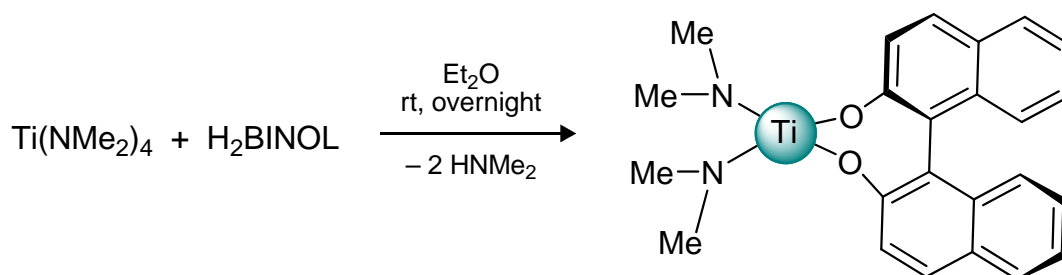
Scheme 4.3 Synthesis of Ti(NMe$_2$)$_2$(BINOL)

The DRIFT spectrum (Figure 6.27) showed a new peak at 3050 cm^{-1} according to the carbon hydrogen stretch vibration for aromatic compounds.

4.3.4 The reaction between Ti(NMe$_2$)$_4$ and {Mg[N(SiHMe$_2$)$_2$]$_2$}$_2$

This reaction was done in order to confirm that the two complexes would not interact with each other when immobilising them on a silica surface. The results from this reaction indicate that interaction may happen. The product was obtained as a brownish powder and not as an heterogeneous mixture of the liquid titanium complex and the white crystalline magnesium complex. The ^{1}H NMR spectrum shows three distinct signals 5.03, 3.08, 0.36 ppm (integral ratios: 1; 14-, 9) and are believed to be MgNSi*H*, TiN*Me* and MgNSi*Me* respectively. The ^{13}C NMR spectrum reveals three signals (ppm): 100.64 (unassigned), 45.28 (TiN*Me*), 3.10 (NSi*Me*). Without any other measurement data this discussion does not give any clear answer on what the product may be.

4.4 Hybrid materials

4.4.1   SiHMe$_2$@PMS

The reaction between Hbdsa and materials (Scheme 4.4) is done to get an estimate of accessible Si-OH groups on the surface.[69]
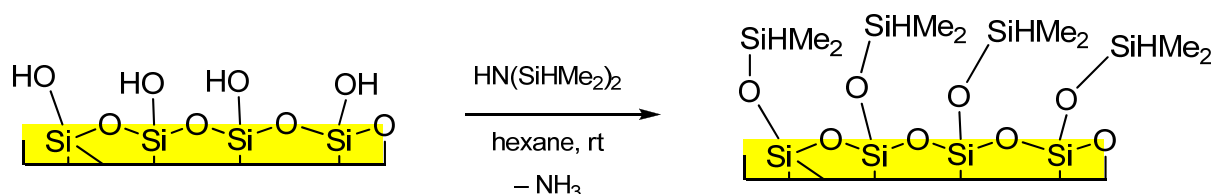
Scheme 4.4 Grafting of Hbdsa on PMS

Hbdsa is a small and reactive molecule to silanol groups and the by-product ammonia is easy to remove from the surface under vacuum. The modification of the surface may be observed form FT-IR spectra (Figure 4.2) via the O-H stretch vibration at around 3500 cm^{-1}. The Si-H stretch also shows up at around 2150 cm^{-1}. A complete consumption of the silanol groups confirmed by FT-IR proves that most silanol groups are accessible for Hbdsa. Calculated values of silanol population are given in Table 4.3.
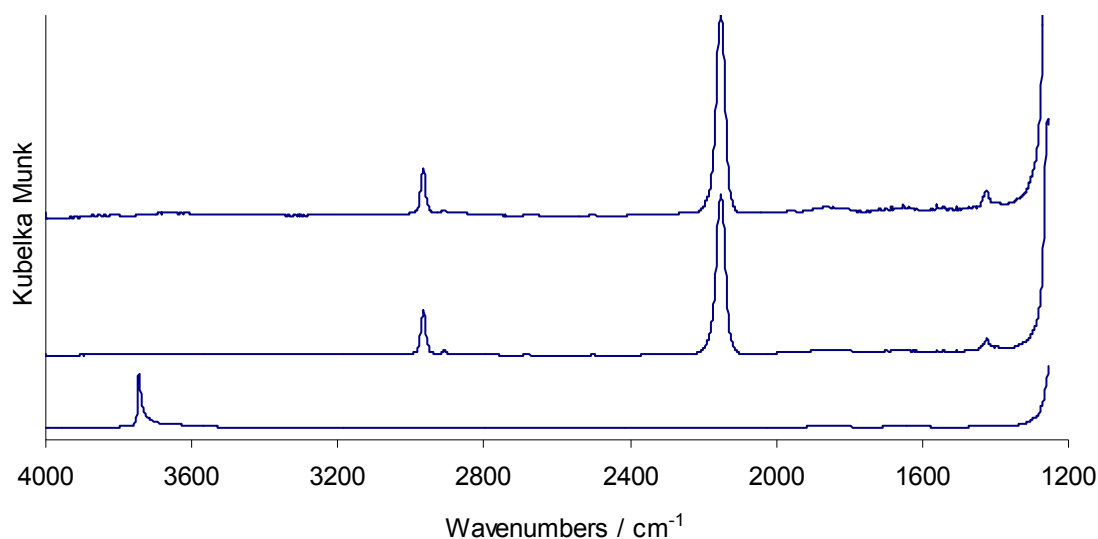
Figure 4.2 DRIFT spectra of silylated PMS. Bottom: SBA-1 2, middle SiHMe$_2$@SBA-1 2a, top SiHMe@MCM-14 4a

The carbon content determined from elemental analysis was used to calculate the amount of silanol groups given by the formula:

$$n(SiOH) = \frac{\%C}{100 \cdot 2M_c} \qquad \%C = \frac{wt\%C}{100 - (wt\%C + wt\%H + \frac{wt\%C}{2M_c})}$$

Table 4.3 Silanol group population

Entry	wt% C	wt% H	wt% N	Si-OH / mmol g
1a	7.57	2.30	< 0.1	3.75
2a	7.24	1.77	0.1	3.65
3a				3.47[a]
4a	7.53	1.71	0.1	3.83

[a]Provided by Thomas Deschner

4.4.2   Grafting of HN(SiMe₂Ph)₂ and Ti(NMe₂)₄ on SBA-1

SBA-1 material was modified with $HN(SiMe_2Ph)_2$ and $Ti(NMe_2)_4$ as proposed in Scheme 4.5. The FT-IR spectrum (Figure 4.3) shows the silanol stretching in two peaks where one accounts for silanol groups inaccessible by the disilazane. The second silanol peak which is moved to lower wavenumbers are believed to be silanol groups being in close interaction with the phenyl groups which are grafted to the surface. By grafting $Ti(NMe_2)_4$ the silanol stretch is not observed.
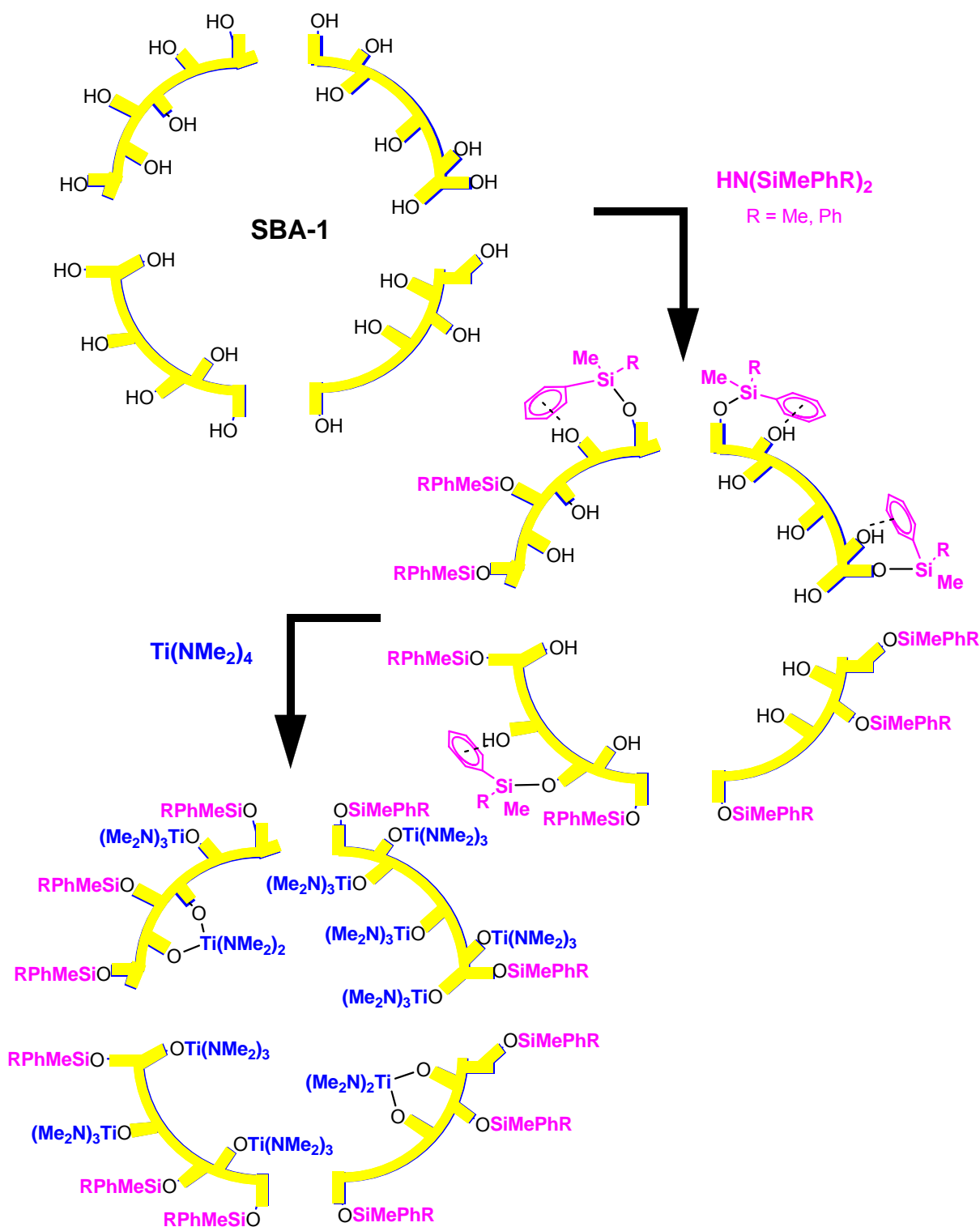
Scheme 4.5 Proposed hybrid materials after grafting with HN(Si(MePhR)$_2$ (R = Me, Ph) and Ti(NMe$_2$)$_4$.

From the physisorption data (Figure 4.4) one can see a dramatic drop in specific surface area which indicates that the windows into the cagelike pores are blocked by the surface silylation. Grafting the titanium complex does decrease the specific surface area slightly. The BJH pore

size distribution does show a maximum at lower than 1.1 nm and makes it useless in the discussion of pore diameters. The pore diameter calculated for the cagelike pores is decreasing from 4.4 nm (**1**) to 3.7 nm (**1b**). After the grafting of $Ti(NMe_2)_4$ there is no change in the cagelike pore diameter. The carbon content increase from 14.75 weight % (**1b**) to 16.46 weight % for the titanium grafted sample (**1be**) which suggest that some of the titanium complex has been immobilized.
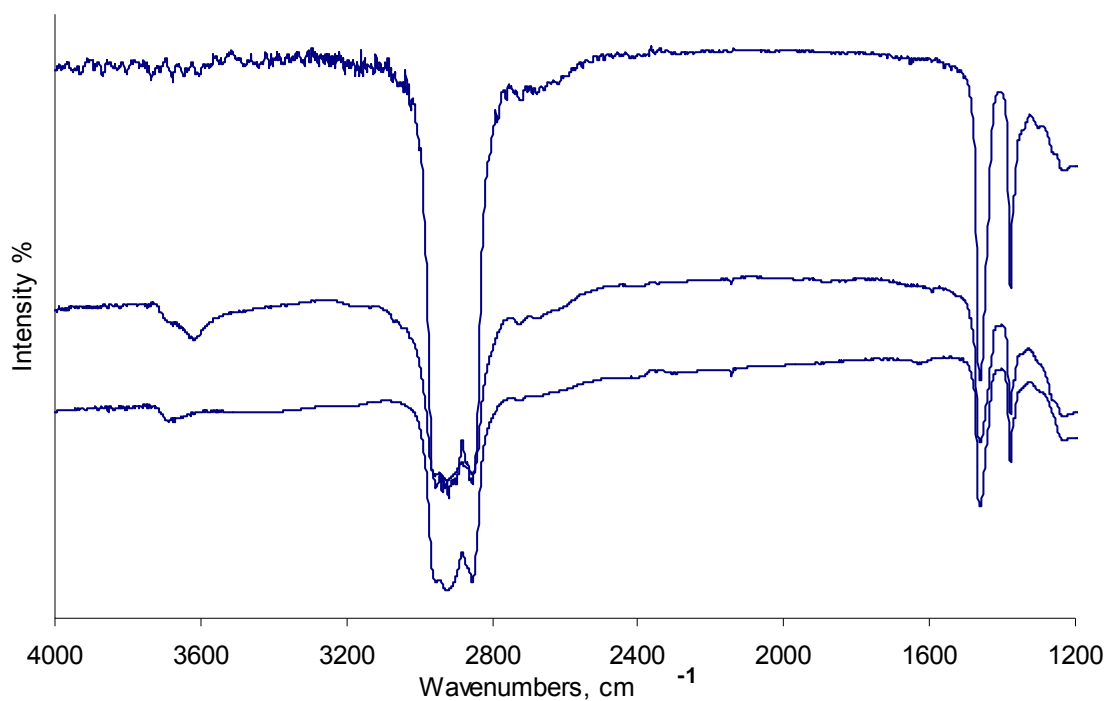
Figure 4.3 FT-IR spectra of SBA-1 1 bottom, $SiMe_2Ph@SBA$-1 1b middle, $Ti(NMe_2)_x@SiMe_2Ph@SBA$-1 1be top
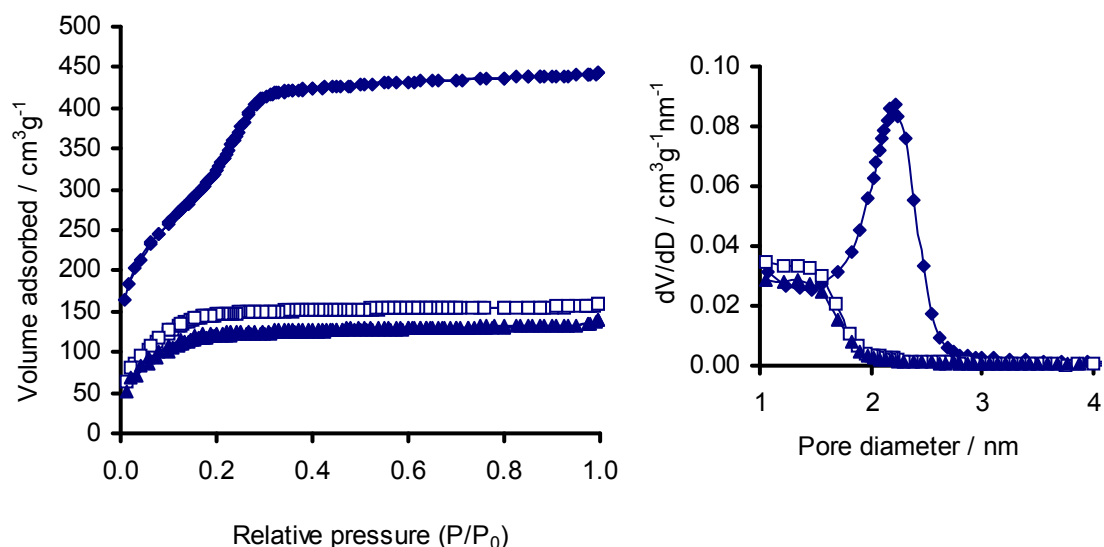
Figure 4.4 N$_2$ physisorption isotherm and BJH pore size distribution for 1(diamond) 1b(squares) 1be(triangles).

4.4.3   Grafting of HN(SiMePh$_2$)$_2$ and Ti(NMe$_2$)$_4$ on SBA-1

Material **2c** is SBA-1 reacted with a larger disilazane HN(SiMePh$_2$)$_2$ (Scheme 4.5). From the DRIFT spectra (Figure 4.5) one can see that there are still free silanol groups on the surface and the interaction between some silanol groups and the phenyl groups. In the absence of nujol one can also observe the C-H stretching from aromatic and aliphatic environments. The carbon content increases to 11.44 weight % through the first step and in total 15.48 weight % for the titanium grafted material.
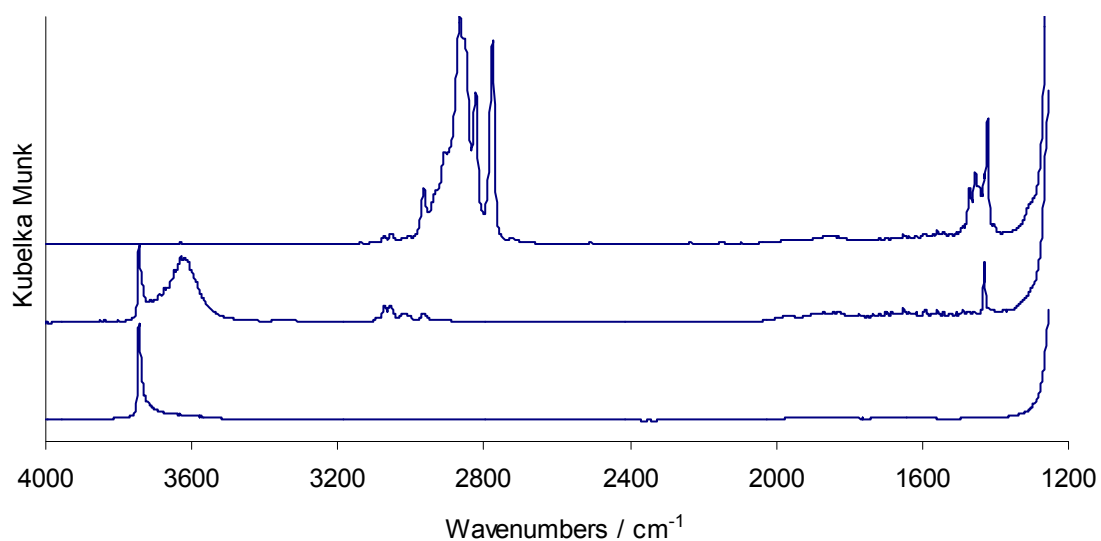
Figure 4.5 DRIFT spectra of SBA-1 2 bottom, SiMePh$_2$@SBA-1 2c middle, Ti(NMe$_2$)$_x$@SiMePh$_2$@SBA-1 2ce

Physisorption data (Figure 4.6) shows a significant decrease in the specific surface area through each grafting step. The cagelike pore size diameter decrease slightly from 4.7 to 4.4 nm through the first step and down to 3.9 nm after grafting of the titanium complex. No silanol groups are observed after the second step. The titanium content was found to be 10.3 weight %.
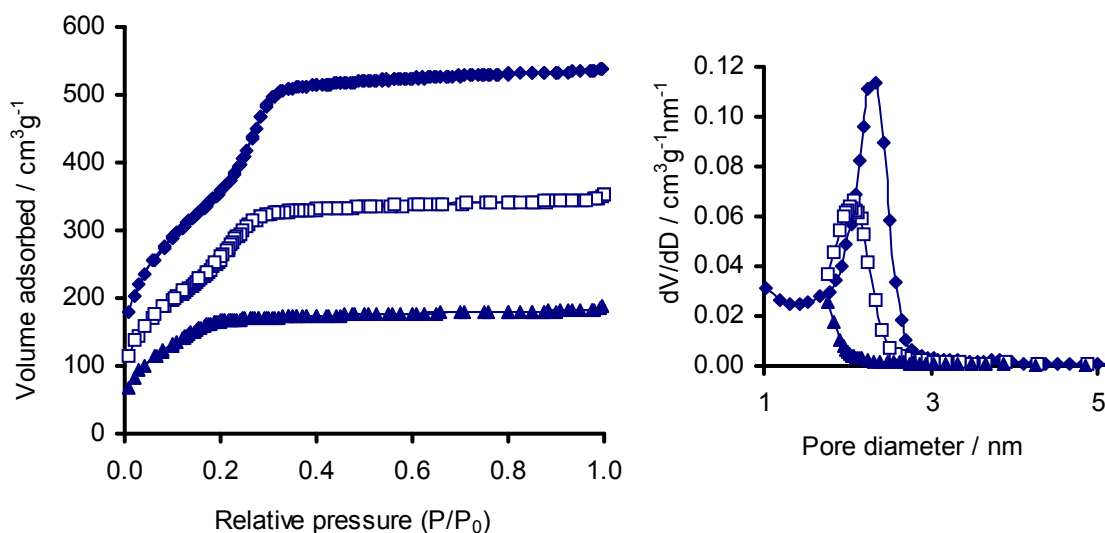
Figure 4.6 N_2 physisorption isotherm and BJH pore size distribution for 2(diamond) 2c(squares) 2ce(triangles).

4.4.4 Grafting of Mg(bdsa)$_2$ and Ti(NMe$_2$)$_4$ on SBA-1

Material **2de** is obtained by a two step grafting with Mg(bdsa)$_2$ and Ti(NMe$_2$)$_4$ (Scheme **4.6**). DRIFT spectrum (Figure 4.7) display silanol groups left after the first grafting step and a full consumption after the second step. A weak bond from the Si-H stretch in the magnesium complex appears at about 2150 cm^{-1}.

SBA-1

{Mg[N(SiHMe₂)₂]₂}₂

Scheme **4**.**6** Proposed hybrid materials after grafting with {Mg(bdsa)₂}₂ and Ti(NMe₂)₄.

Physisorption data (Figure 4.8) shows a smaller decrease in the specific surface area for the first step compared to the grafting of disilazane. The second grafting step on the other hand gives about the same surface area as the two materials (**1be** and **2ce**) treated with disilazane. The cagelike pore diameter decreases with only 0.1 nm after grafting the magnesium complex. Through the second grafting step this diameter decreases to 4.0 nm. The carbon content (3.03 wt%) increases little through the grafting of the magnesium complex, but goes

up to 12.84 weight % in total after the grafting of $Ti(NMe_2)_4$. The titanium content was found to be 11.0 %.
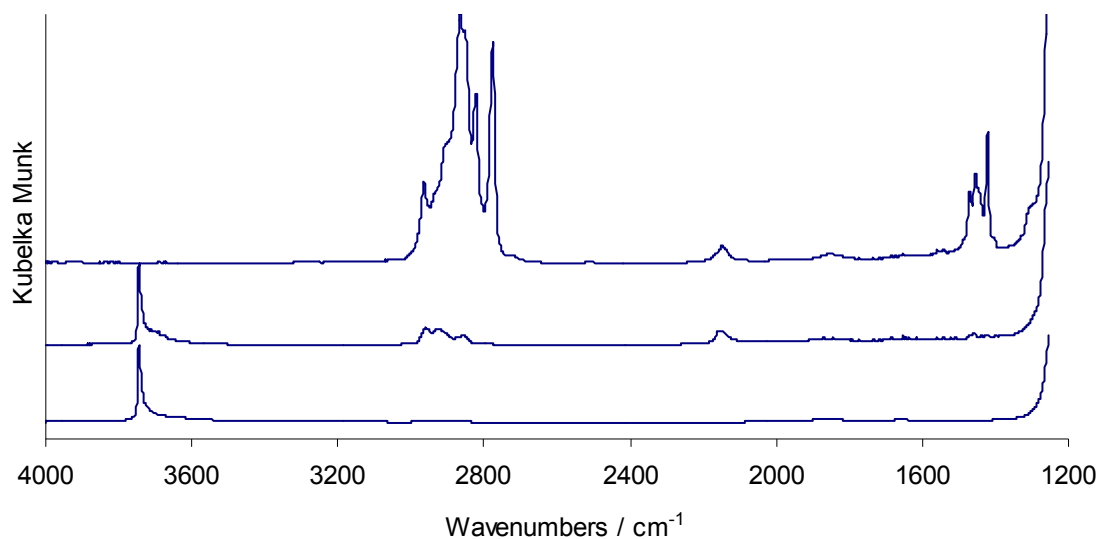
Figure 4.7 DRIFT spectra of SBA-1 2 bottom, $Mg(bdsa)_x$@SBA-1 2d, $Ti(NMe_2)_y$@$Mg(bdsa)_x$@SBA-1 2de
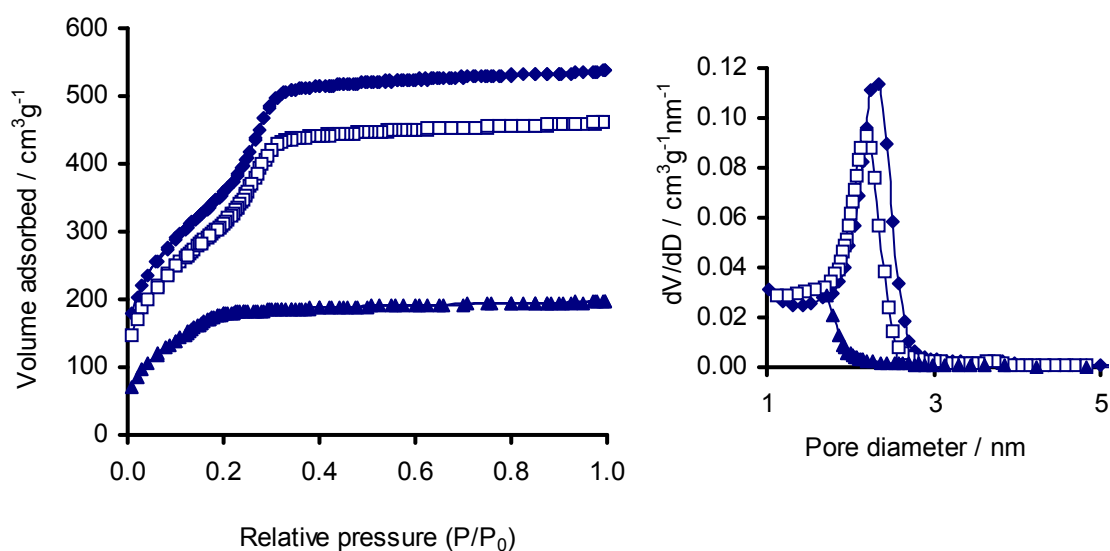
Figure 4.8 N_2 physisorption isotherm and BJH pore size distribution for 2(diamond) 2d(squares) 2de(triangles).

4.4.5 Grafting of $Ti(NMe_2)_4$, $Ti(NMe_2)_3bdsa$ on SBA-1 and ligand exchange on surface

Material **2e2B** is a SBA-1 material grafted with $Ti(NMe_2)_4$ which was treated with R-H_2BINOL to undergo a ligand exchange (Scheme 4.7). Grafting of the titanium complex

consumes all silanol groups as seen in the DRIFT spectrum (Figure 4.9), but there is little or no change in the spectrums before and after ligand exchange.
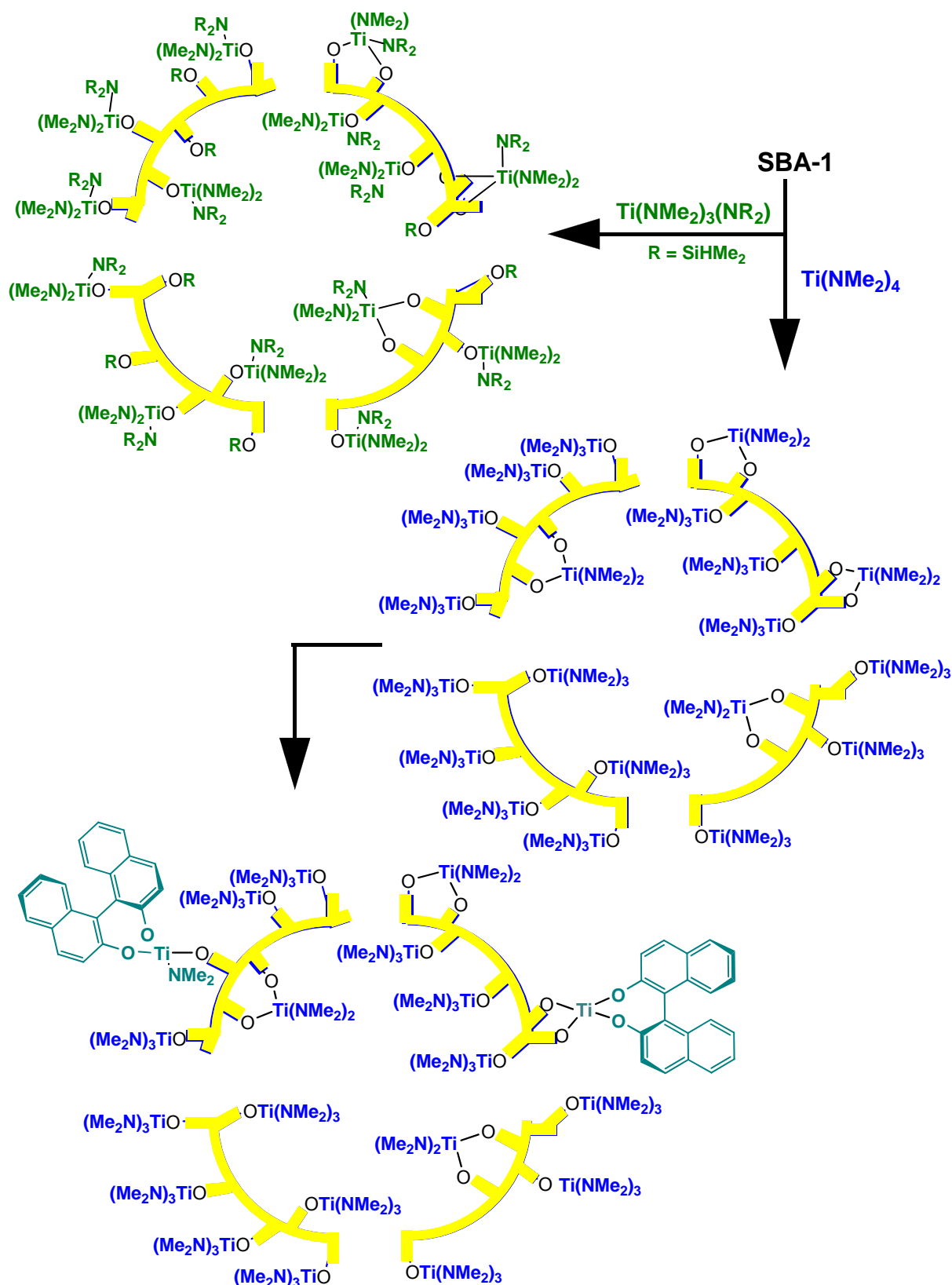
Scheme 4.7 Proposed hybrid materials after grafting with Ti(NMe$_2$)$_3$(bdsa) and Ti(NMe$_2$)$_4$ including ligand exchange with H$_2$BINOL.

The surface area decreases to a level which has already been seen in **2ce** and **2de** and the cagelike pore size diameter also decrease to a familiar value of 4.0 nm (Figure 4.10). After ligand exchange this value only decreases to 3.9 nm. The carbon content of the analogous grafter material **2e** is 12.44 weight %. Without the elemental analysis of **2e2B** there is no evidence for the ligand exchange taking place. The reason for this may be that the small windows in the material are too small for the H_2BINOL to enter. Material **2f2** is a SBA-1 grafted with a mixed amido/silyl amide titanium complex. The grafting has been done in order to bring in a spectroscopic probe (Si-H) into the material as can be seen in the DRIFT spectrum. Two broad signals appear at around 2200 to 2100 cm^{-1}.The physisorption data for **2f2** lies around the same values as for **2e**. An analogous material (**2f**) which did not consume all the silanol groups (Figure 6.41) had a titanium content of 4.6 weight %.
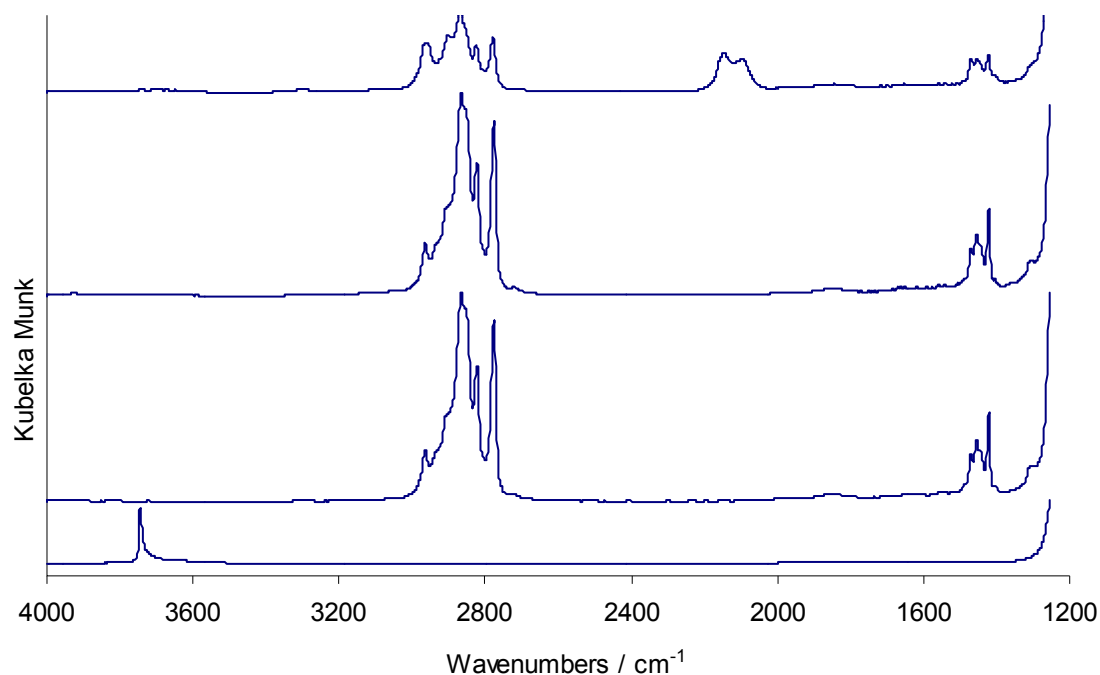
Figure 4.9 DRIFT spectra: From bottom to top: SBA-1 2, $Ti(NMe_2)_x$@SBA-1 2e2, $Ti(NMe_2)_x(BINOL)_y$@SBA-1 2e2B, $Ti(NMe_2)_x(bdsa)$@SBA-1 2f2
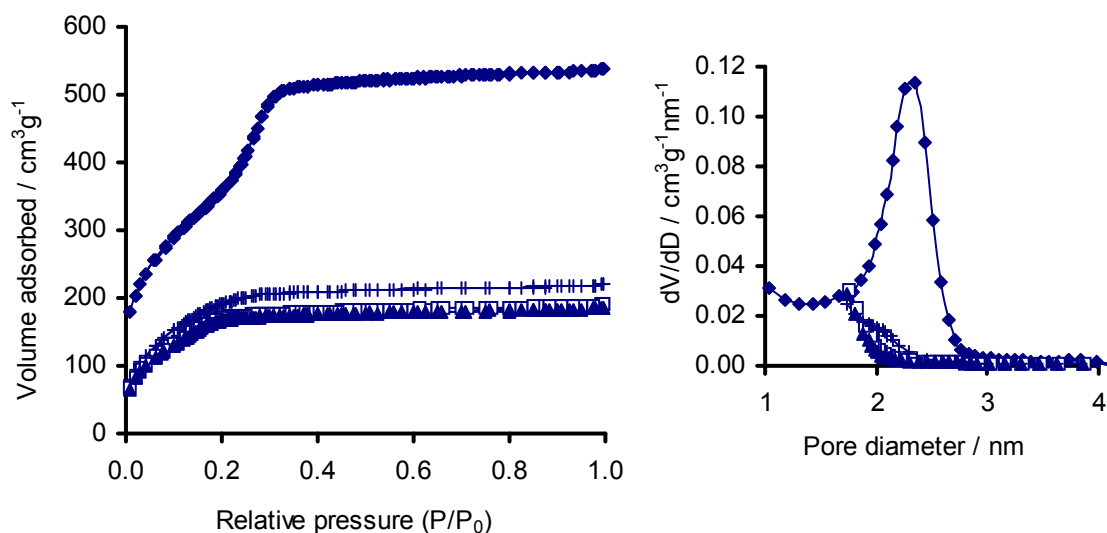
Figure 4.10 N_2 physisorption isotherm and BJH pore size distribution for 2(diamond) 2e2(squares) 2e2B(triangles) and 2f2(+)

4.4.6 Grafting of HN(SiMePh₂)₂ and Ti(NMe₂)₄ onto MCM-41

4ce is made from a MCM-41 material grafted with HN(SiMePh₂)₂ and Ti(NMe₂)₄ in two steps. (Scheme 4.8)
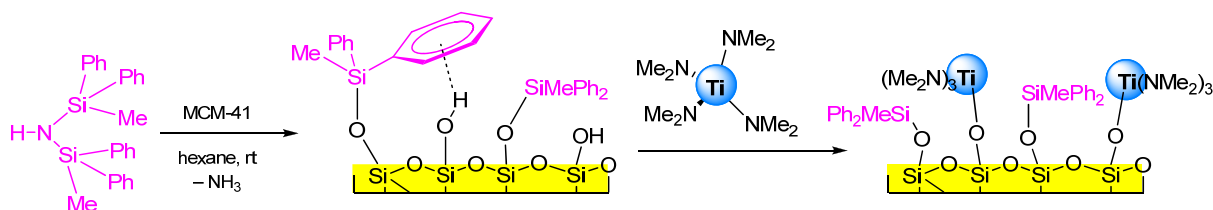
Scheme 4.8 Grafting of HN(SiMePh₂)₂ and Ti(NMe₂)₄ onto MCM-41.

The first step gives a large decrease in surface area (Figure 4.12) to 10 % of the parent material, while the second step shows a surface area (610 m^2g^{-1}) between the parent material **4** and **4c**. The pore diameter (3.3 nm) does not decrease after the first step, but decreases to 2.8 nm after the second step. This suggest that the diphenylsilyl groups on the surface in some way blocks the one dimensional tubes The carbon content (**4c**: 10.60 wt%; **4ce**: 15.84 wt%) increases through both steps and the titanium content was found to be 8.2 weight % for **4ce**. Material **4f** (Scheme 4.9) have a titanium content of 8.7 weight % and shows similar surface area and pore diameter values to **4ce**. The DRIFT spectra (Figure 4.11) of **4c** and **4ce** are similar to the ones already discussed; **4f** holds only one distinguished peak around 2150 cm^{-1} according to the Si-H bond.
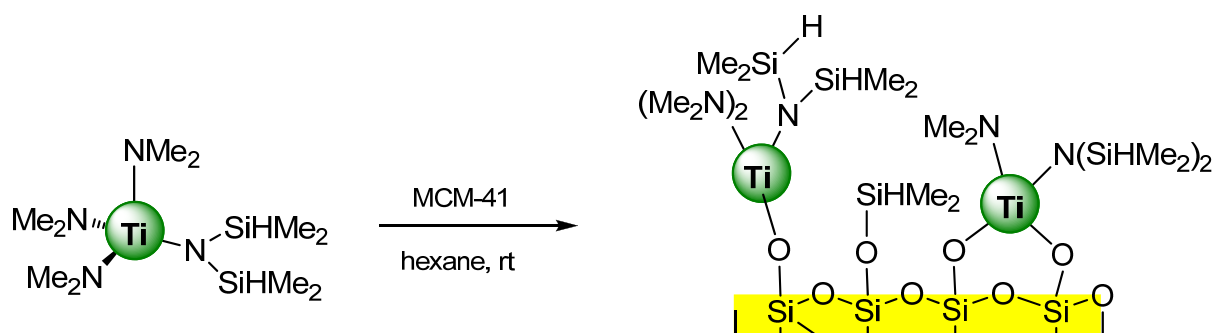
Scheme 4.9 Grafting of Ti(NMe$_2$)$_3$(bdsa) onto MCM-41
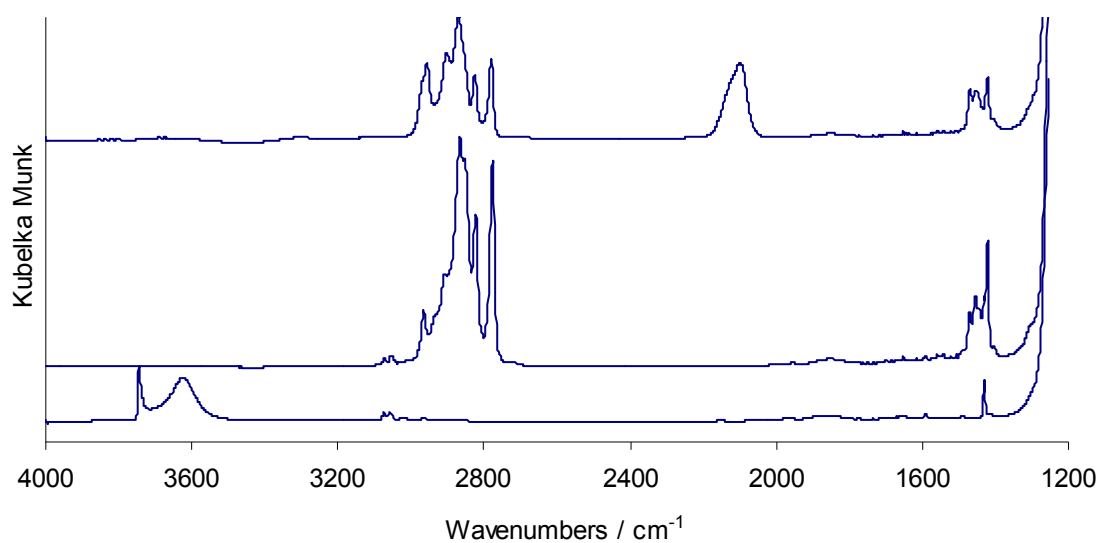
Figure 4.11 DRIFT spectra of SiMePh$_2$@MCM-41 4c bottom, Ti(NMe$_4$)$_x$@SiMePh$_2$@MCM-41 4ce middle, Ti(NMe$_2$)$_x$(bdsa)@MCM-41 4f top.
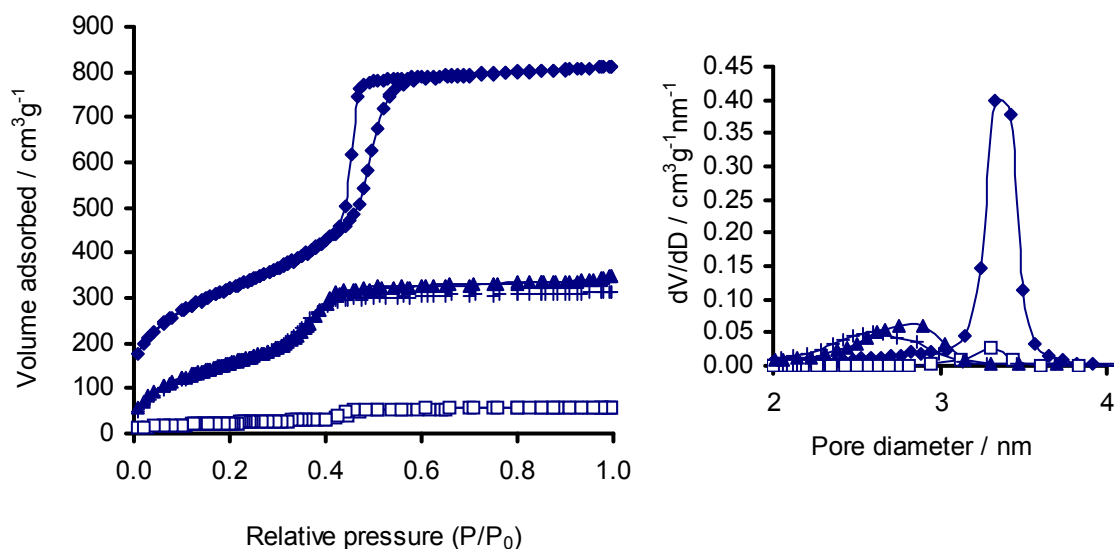
Figure 4.12 N$_2$ physisorption isotherm and BJH pore size distribution for 4(diamond), 4c(squares), 4ce(triangles), and 4f(+)

4.4.7   Grafting of Ti(NMe$_2$)$_4$ onto MCM-41 and ligand exchange on surface

Ti(NMe$_2$)$_4$ reacted easily with the silanol groups on MCM-41 to give **3e**. The hybrid material has a surface area (Figure 4.14) about 400 m^{2}g^{-1} than the parent material. The pore diameter decreased to 2.9 nm. The ligand exchange reaction shows a more promising result for the MCM-41 material compared to SBA-1 (Scheme 4.10).
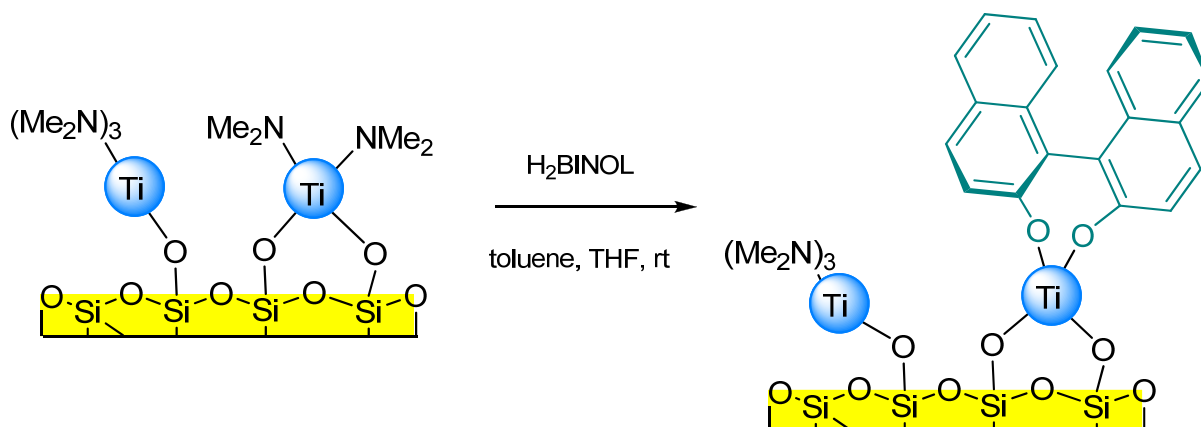
Scheme 4.10 Ligand exchange at grafted titanium complex at MCM-41

One can see the changes in surface area, pore diameter (2.1 nm) and in the DRIFT spectrum (Figure 4.13) where a distinct peak for an aromatic C-H stretch. The carbon content increased

from 12.18 wt% (**3e**) to 29.14 wt% (**3eB**). As expected the titanium content decreased from 12.1 wt% (**3e**) to 5.9 wt% (**3eB**).
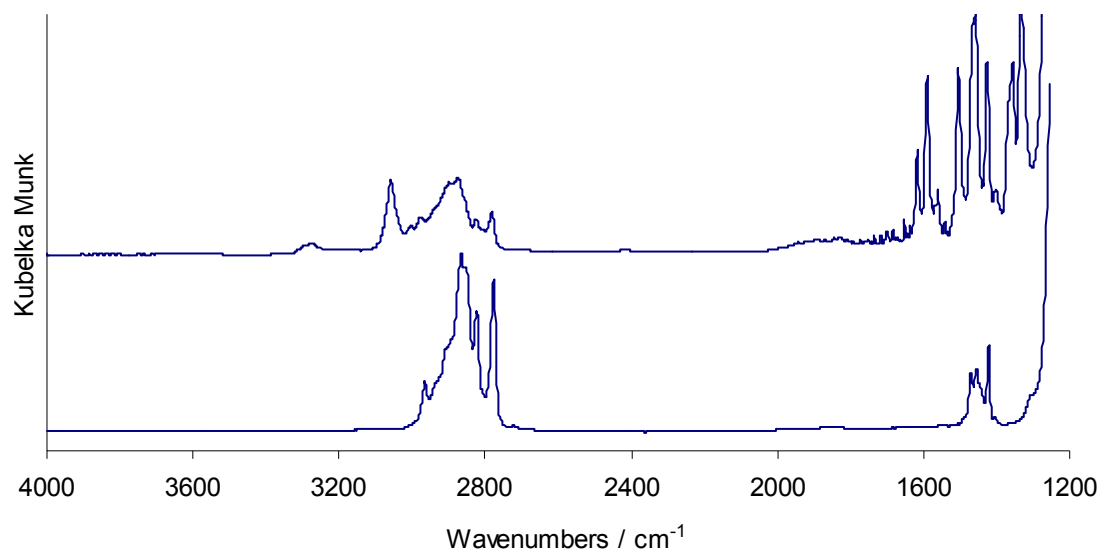
Figure 4.13 DRIFT spectra of Ti(NMe$_2$)$_x$@MCM-41 3e bottom and Ti(NMe$_2$)$_x$(BINOL)$_y$@MCM-41 3eB top
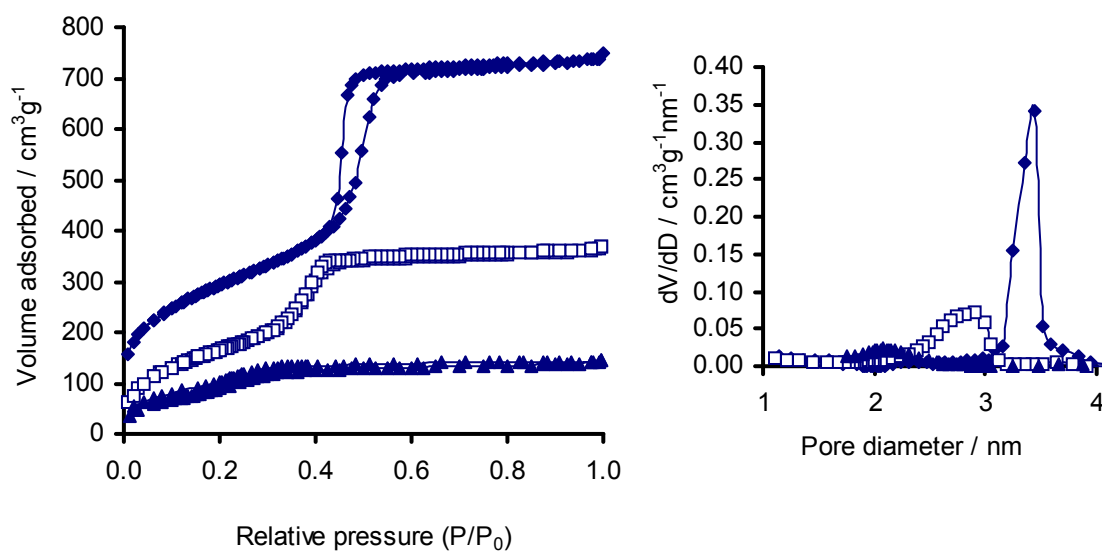
Figure 4.14 N$_2$ physisorption isotherm and BJH pore size distribution for 3(diamond), 3e(squares) and 3eB(triangles).

5 Conclusion and perspectives

It has been shown that disilazanes, $Mg(bdsa)_2$, $Ti(NMe_2)_4$ and $Ti(NMe_2)_3[N(SiHMe_2)_2]$ are sensitive to the pore structure when grafted onto periodic mesopourous silica. With the right knowledge it is possible to change the surface area and the pore size distribution. $\{Mg[N(SiHMe_2)_2]_2\}_2$ and $HN(SiMePh_2)_2$ are to large to enter the SBA-1 through the windows and occupy the outer surface area of the material. $Ti(NMe_2)_4$ is a small and reactive complex to graft inside SBA-1 in order to get a size selective catalyst. Surface modified MCM-41 may be a less size selective catalysis material since its pore diameters are equal at the entrance and inside the tube. The materials need to be characterized by several techniques in order to be more accurate on the surface species. DRIFT spectroscopy is a good way to reveal information in hybrid materials in comparison to the Nujul mull technique.

The surface species and proposed size selectivity should be proved by simple organic reactions or further surface derivatization. The oxidation of cyclohexene and a larger molecule with a double bond may prove whether the active site is mainly inside the pores of SBA-1. Another possibility is to see whether bulky alcohols would react in a ligand exchange at all the active sites or only partially because of small pore entrances to the cages which would leave some active sites inaccessible.

Attempts to get single X-ray crystals of organometalic complexes would be needed in order to know the different structures and properties by heart.

REFERENCES

1. J. L. Guth, P. Caullet, *J. Chim. Phys.* **1986**, *83*, 155.
2. A. Corma, H. Garcia, *Adv. Synth. Catal.* **2006**, *348*, 1391.
3. A. Corma, *Chem. Rev.* **1997**, *97*, 2373.
4. Y. J. He, G. S. Nivarthy, F. Eder, K. Seshan, J. A. Lercher, *Microporous Mesoporous Mater.* **1998**, *25*, 207.
5. A. Corma, V. Fornes, S. B. Pergher, T. L. M. Maesen, J. G. Buglass, *Nature* **1998**, *396*, 353.
6. A. Corma, V. Fornés, J. Martínez-Triguero, S. B. Pergher, *J. Catal.* **1999**, *186*, 57.
7. J. S. Beck, J. C. Vartuli, W. J. Roth, M. E. Leonowicz, C. T. Kresge, K. D. Schmitt, C. T. W. Chu, D. H. Olson, E. W. Sheppard, et al., *J. Am. Chem. Soc.* **1992**, *114*, 10834.
8. K. S. W. Sing, D. H. Everett, R. A. W. Haul, L. Moscou, R. A. Pierotti, J. Rouquerol, T. Siemieniewska, *Pure Appl. Chem.* **1985**, *57*, 603.
9. D. Zhao, Q. Huo, J. Feng, B. F. Chmelka, G. D. Stucky, *J. Am. Chem. Soc.* **1998**, *120*, 6024.
10. H. Kang, Y. Jun, J. I. Park, K. B. Lee, J. Cheon, *Chem. Mater.* **2000**, *12*, 3530.
11. Y. Sakamoto, A. Fukuoka, T. Higuchi, N. Shimomura, S. Inagaki, M. Ichikawa, *J. Phys. Chem. B* **2004**, *108*, 853.
12. B. Z. Tian, S. N. Che, Z. Liu, X. Y. Liu, W. B. Fan, T. Tatsumi, O. Terasaki, D. Y. Zhao, *Chem. Commun.* **2003**, 2726.
13. H. F. Yang, D. Y. Zhao, *J. Mater. Chem.* **2005**, *15*, 1217.
14. A. Corma, M. T. Navarro, J. P. Pariente, *J. Chem. Soc., Chem. Commun.* **1994**, 147.
15. K. M. Reddy, I. Moudrakovski, A. Sayari, *J. Chem. Soc., Chem. Commun.* **1994**, 1059.
16. F. Hoffmann, M. Cornelius, J. Morell, M. Fröba, *Angew. Chem. Int. Ed.* **2006**, *45*, 3216.
17. H. Yoshitake, T. Yokoi, T. Tatsumi, *Chem. Mater.* **2002**, *14*, 4603.
18. C. M. Crudden, M. Sateesh, R. Lewis, *J. Am. Chem. Soc.* **2005**, *127*, 10045.
19. M. Alvaro, A. Corma, D. Das, V. Fornes, H. Garcia, *Chem. Commun.* **2004**, 956.
20. A. Corma, H. Garcia, *Chem. Rev.* **2002**, *102*, 3837.
21. H. P. Wulff British Patent 1,249,079, 1971 (Shell).
22. P. Ratnasamy, D. Srinivas, H. Knozinger, Active sites and reactive intermediates in titanium silicate molecular sieves. In *Advances in Catalysis, Vol 48*, 2004; Vol. 48, pp 1.
23. C. Schuster, E. Mollmann, A. Tompos, W. F. Holderich, *Catal. Lett.* **2001**, *74*, 69.
24. T. Maschmeyer, F. Rey, G. Sankar, J. M. Thomas, *Nature* **1995**, *378*, 159.
25. Q. Huo, D. I. Margolese, G. D. Stucky, *Chem. Mater.* **1996**, *8*, 1147.
26. Y. Sakamoto, M. Kaneda, O. Terasaki, D. Y. Zhao, J. M. Kim, G. Stucky, H. J. Shin, R. Ryoo, *Nature* **2000**, *408*, 449.
27. C. Zapilko, Y. C. Liang, W. Nerdal, R. Anwander, *Chem. Eur. J.* **2007**, *13*, 3169.
28. C. Zapilko, Y. C. Liang, R. Anwander, *Chem. Mater.* **2007**, *19*, 3171.
29. C. T. Kresge, M. E. Leonowicz, W. J. Roth, J. C. Vartuli, J. S. Beck, *Nature* **1992**, *359*, 710.
30. M. J. Kim, R. Ryoo, *Chem. Mater.* **1999**, *11*, 487.
31. Q. Huo, R. Leon, P. M. Petroff, G. D. Stucky, *Science* **1995**, *268*, 1324.
32. F. Kleitz, D. Liu, G. M. Anilkumar, I. S. Park, L. A. Solovyov, A. N. Shmakov, R. Ryoo, *J. Phys. Chem. B* **2003**, *107*, 14296.
33. M. W. Anderson, C. C. Egger, G. J. T. Tiddy, J. L. Casci, K. A. Brakke, *Angew. Chem. Int. Ed.* **2005**, *44*, 3243.
34. M. Hartmann, *Chem. Mater.* **2005**, *17*, 4577.

REFERENCES

35.   M. P. Kapoor, A. Raj, S. Abdelhamid, J. Mietek, *Stud. Surf. Sci. Catal.* **2000**, *Vol 129*, 327.

36.   J. Pérez-Pariente, I. Díaz, F. Mohino, E. Sastre, *Appl. Catal. A* **2003**, *254*, 173.

37.   Carla D. Nunes, M. Pillinger, Anabela A. Valente, J. Rocha, André D. Lopes, Isabel S. Gonçalves, *Eur. J. Inorg. Chem.* **2003**, *2003*, 3870.

38.   M. Iwamoto, Y. Tanaka, N. Sawamura, S. Namba, *J. Am. Chem. Soc.* **2003**, *125*, 13032.

39.   S. Brunauer, P. H. Emmett, E. Teller, *J. Am. Chem. Soc.* **1938**, *60*, 309.

40.   E. P. Barrett, L. G. Joyner, P. P. Halenda, *J. Am. Chem. Soc.* **1951**, *73*, 373.

41.   P. I. Ravikovitch, A. V. Neimark, *Langmuir* **2002**, *18*, 1550.

42.   J. M. Basset, A. Choplin, *J. Mol. Catal.* **1993**, *21*, 95.

43.   R. Anwander, *Chem. Mater.* **2001**, *13*, 4419.

44.   Y. I. Ermakov, A. M. Lazutkin, E. A. Demin, Y. P. Grabovskii, V. A. Zakharov, *Kinet. Katal.* **1972**, *13*.

45.   J. Schwartz, M. D. Ward, *J. Mol. Catal.* **1980**, *8*, 465.

46.   S. L. Scott, J. M. Basset, G. P. Niccolai, C. C. Santini, J. P. Candy, C. Lecuyer, F. Quignard, A. Choplin, *New. J. Chem.* **1994**, *18*, 115.

47.   C. Huber, K. Moller, T. Bein, *J. Chem. Soc., Chem. Commun.* **1994**, 2619.

48.   N. Sahai, *Environ. Sci. Technol.* **2002**, *36*, 445.

49.   M. S. Morey, G. D. Stucky, S. Schwarz, M. Fröba, *J. Phys. Chem. B* **1999**, *103*, 2037.

50.   A. O. Bouh, G. L. Rice, S. L. Scott, *J. Am. Chem. Soc.* **1999**, *121*, 7201.

51.   B. J. Aronson, C. F. Blanford, A. Stein, *Chem. Mater.* **1997**, *9*, 2842.

52.   F. Chiker, J. P. Nogier, F. Launay, J. L. Bonardet, *Appl. Catal. A* **2004**, *259*, 153.

53.   S. B. McCullen, J. C. Vartuli U.S. Patent 5,156,829, 1992 (Mobil Oil Corporation).

54.   M. S. Morey, S. O'Brien, S. Schwarz, G. D. Stucky, *Chem. Mater.* **2000**, *12*, 898.

55.   S. Zheng, L. A. Gao, Q. H. Zhang, J. K. Guo, *J. Mater. Chem.* **2000**, *10*, 723.

56.   L. Barrio, J. M. Campos-Martín, M. P. de Frutos-Escrig, J. L. G. Fierro, *Microporous Mesoporous Mater.* **2008**, *113*, 542.

57.   M. Guidotti, N. Ravasio, R. Psaro, E. Gianotti, S. Coluccia, L. Marchese, *J. Mol. Catal. A: Chem.* **2006**, *250*, 218.

58.   M. Guidotti, R. Psaro, N. Ravasio, M. Sgobba, E. Gianotti, S. Grinberg, *Catal. Lett.* **2008**, *122*, 53.

59.   J. A. Melero, J. Iglesias, J. M. Arsuaga, J. Sainz-Pardo, P. de Frutos, S. Blazquez, *J. Mater. Chem.* **2007**, *17*, 377.

60.   K. Kageyama, J. Tamazawa, T. Aida, *Science* **1999**, *285*, 2113.

61.   P. Ferreira, Isabel S. Gonçalves, Fritz E. Kühn, M. Pillinger, J. Rocha, Ana M. Santos, A. Thursfield, *Eur. J. Inorg. Chem.* **2000**, 551.

62.   C. Rosier, G. P. Niccolai, J. M. Basset, *J. Am. Chem. Soc.* **1997**, *119*, 12408.

63.   M. Widenmeyer, S. Grasser, K. Köhler, R. Anwander, *Microporous Mesoporous Mater.* **2001**, *44-45*, 327.

64.   Mestrelab Research S.L. www.mestrec.com (23.01.2008)

65.   M. Widenmeyer. Ph.D. Thesis, Technischen Universität München, München, 2001.

66.   R. Zana, M. Benrraou, R. Rueff, *Langmuir* **1991**, *7*, 1072.

67.   T. W. Kim, R. Ryoo, M. Kruk, K. P. Gierszal, M. Jaroniec, S. Kamiya, O. Terasaki, *J. Phys. Chem. B* **2004**, *108*, 11480.

68.   L. Ackermann, R. G. Bergman, R. N. Loy, *J. Am. Chem. Soc.* **2003**, *125*, 11956.

69.   R. Anwander, I. Nagl, M. Widenmeyer, G. Engelhardt, O. Groeger, C. Palm, T. Roser, *J. Phys. Chem. B* **2000**, *104*, 3532.

6 Appendixes

6.1 X-ray diffraction pattern
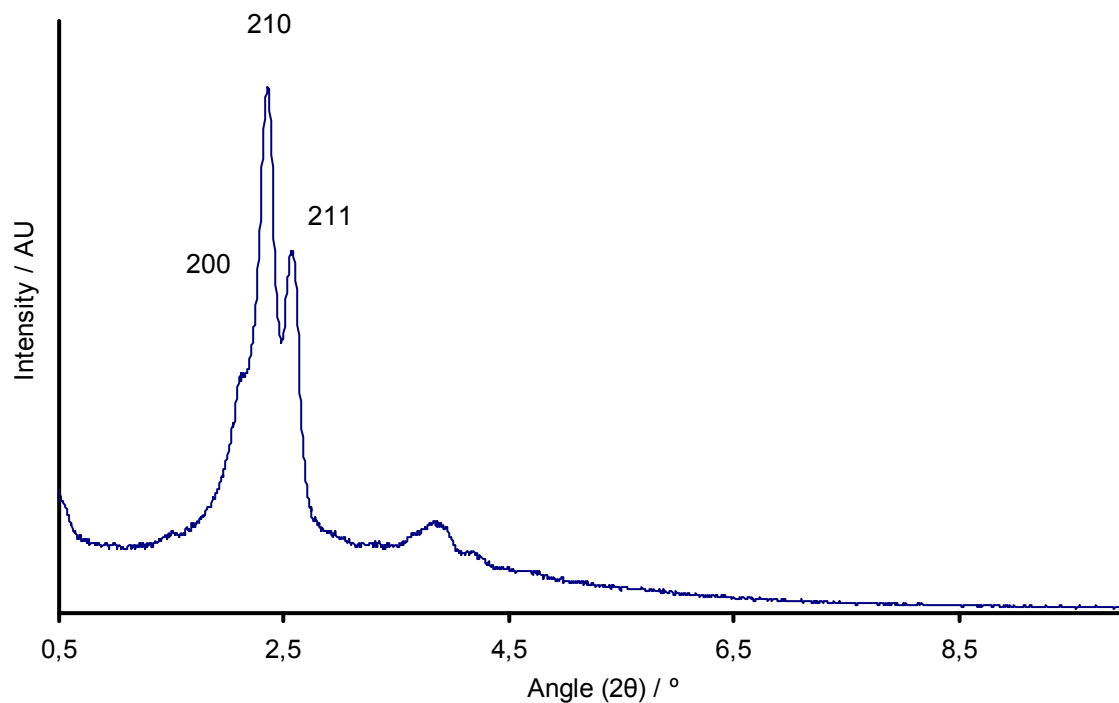
Figure 6.1 PXRD of SBA-1 1
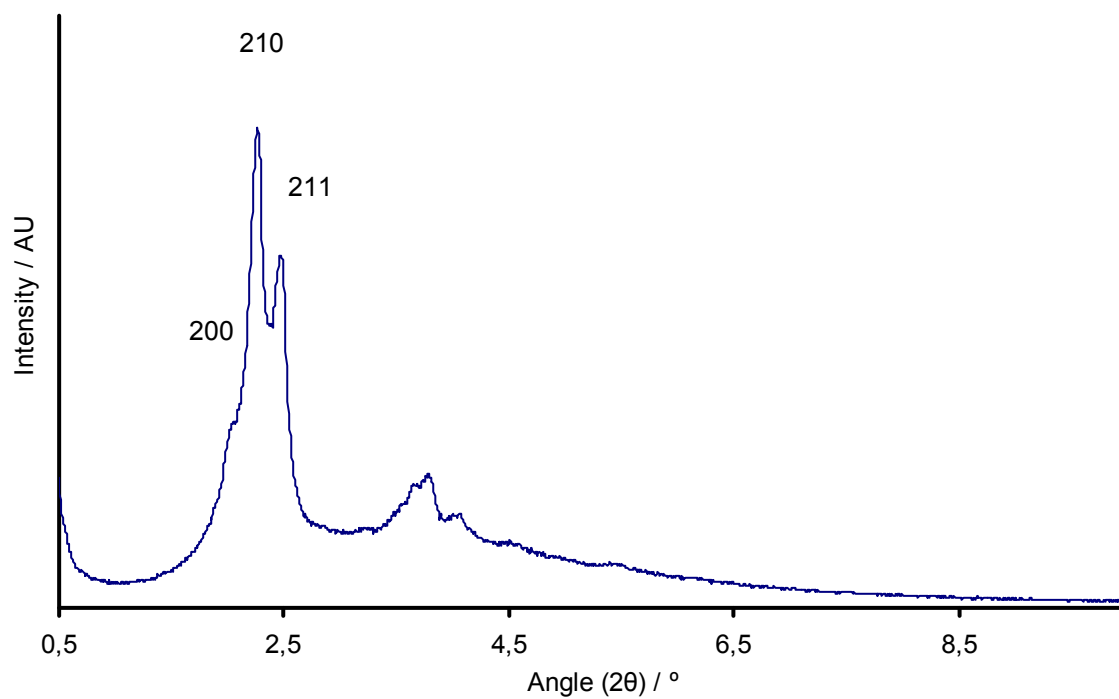
Figure 6.2 PXRD of SBA-1 2
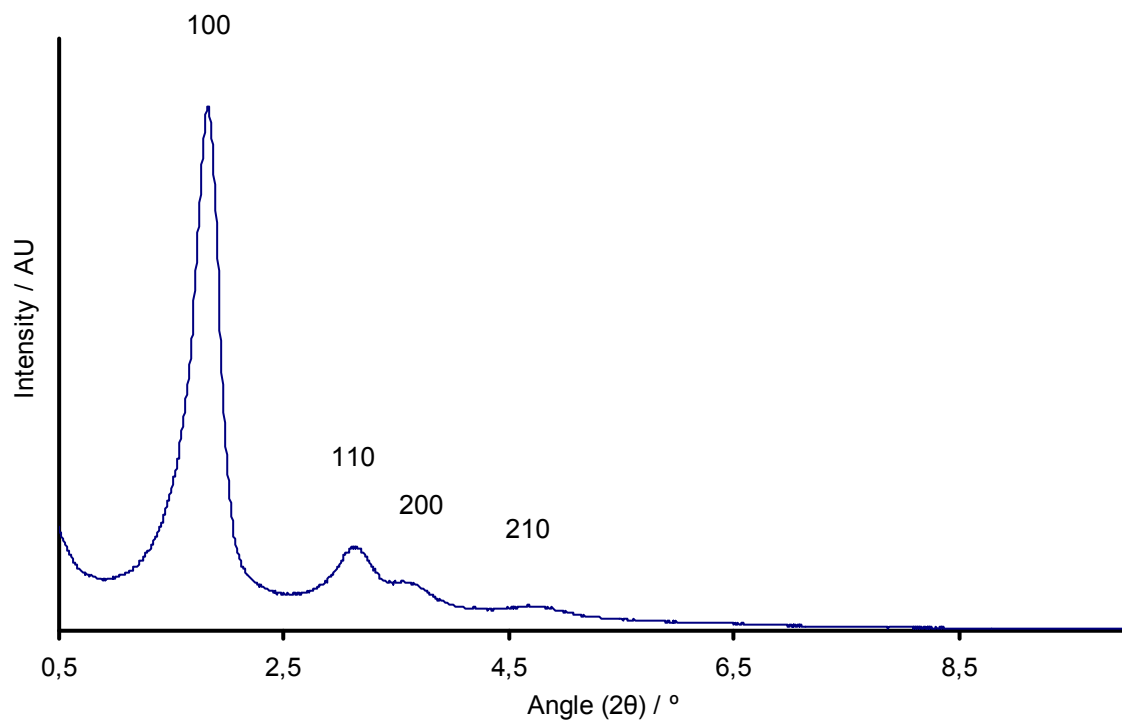
Figure 6.3 PXRD of MCM-41 3
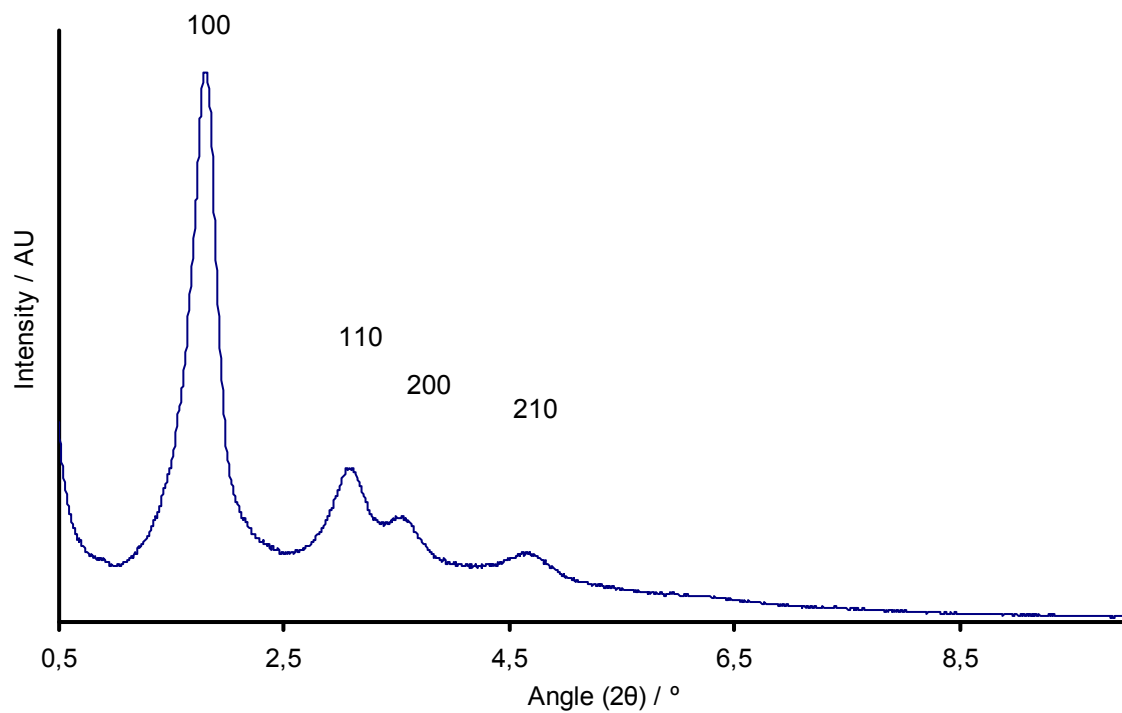
Figure 6.4 PXRD of MCM-41 4
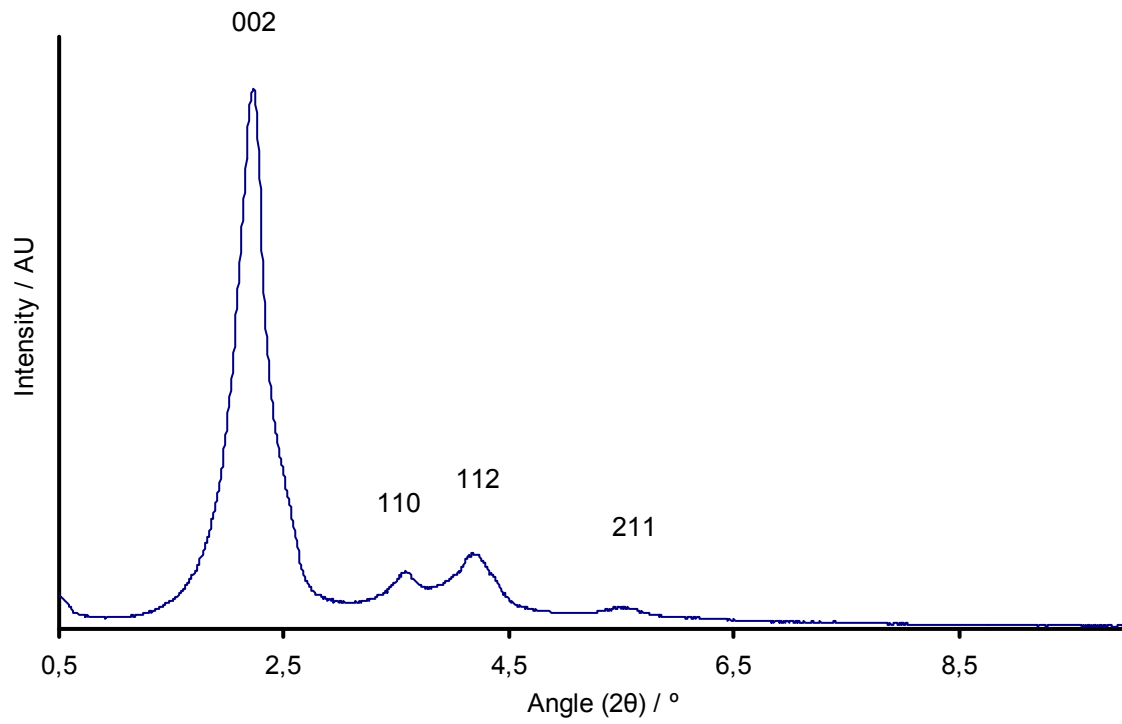
Figure 6.5 PXRD of SBA-2 5
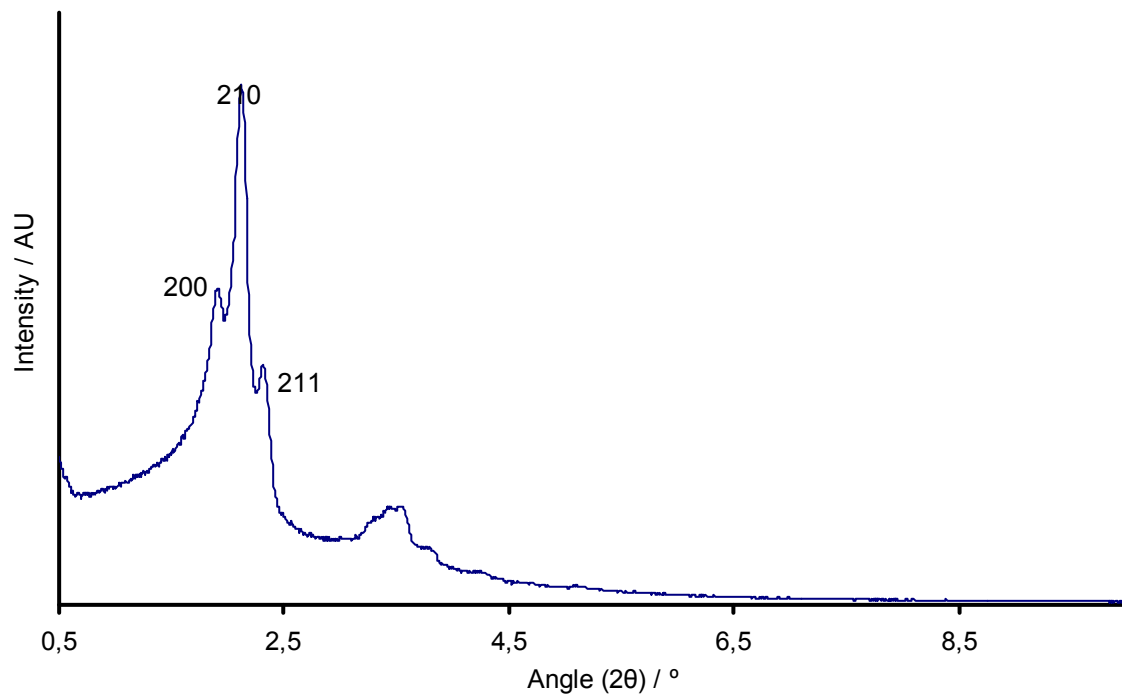
Figure 6.6 PXRD of SBA-1 LP 6
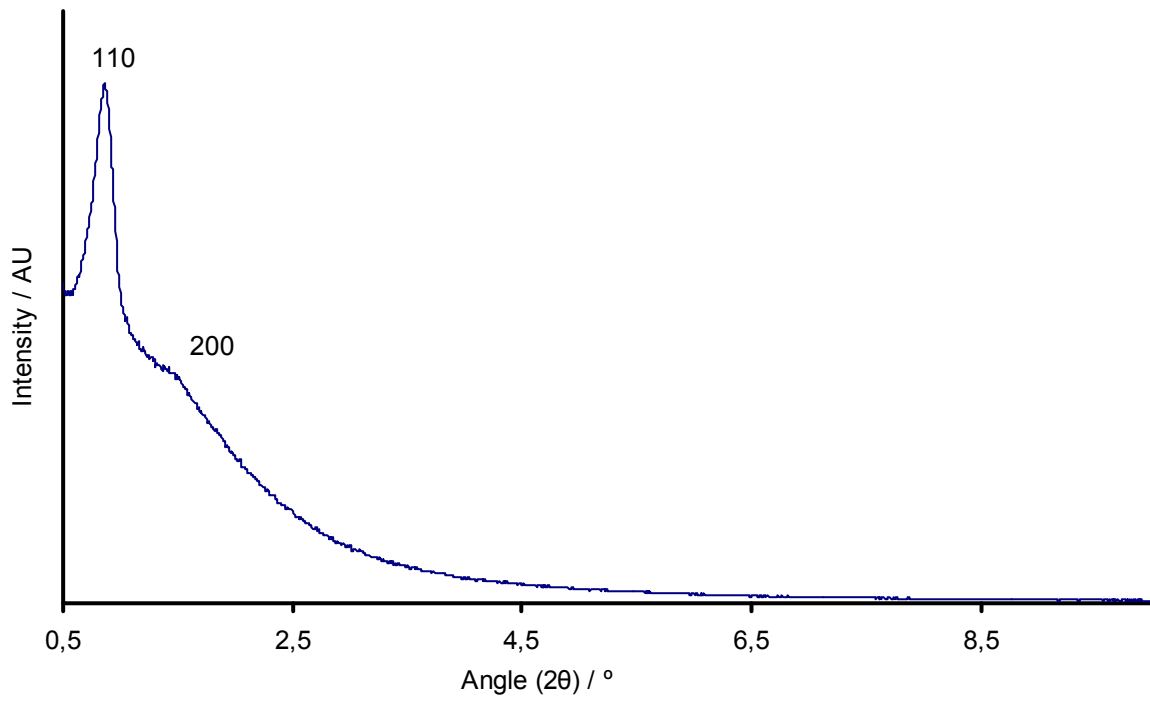
Figure 6.7 PXRD of SBA-16 7

6.2 NMR of precursors
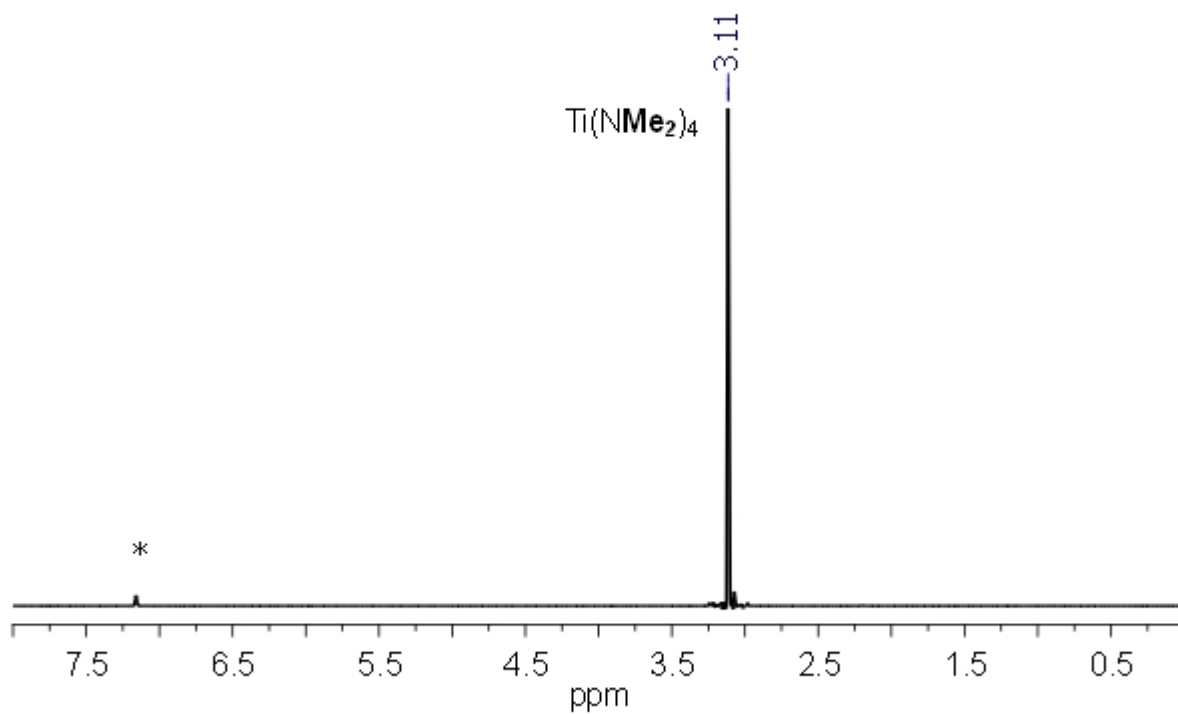
Figure 6.8 ^{1}H NMR spectrum of Ti(NMe$_2$)$_4$
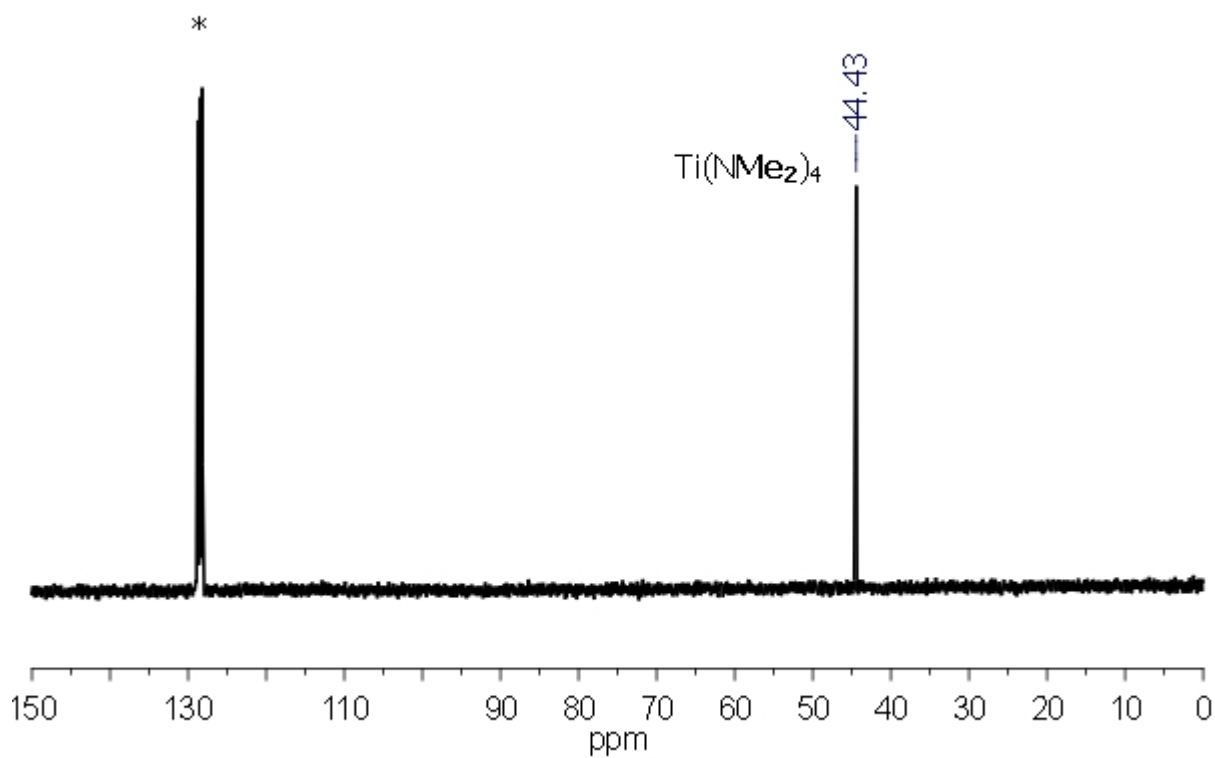
Figure 6.9 ^{13}C NMR spectrum of Ti(NMe$_2$)$_4$
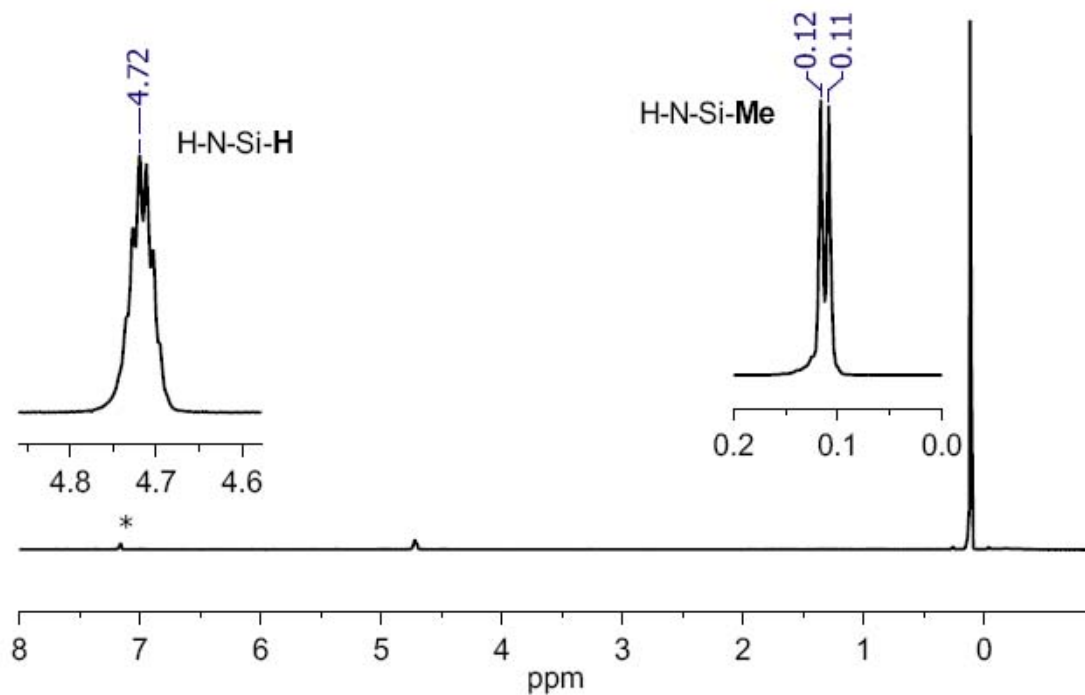
Figure 6.10 ^{1}H NMR spectrum of HN(SiHMe$_2$)$_2$
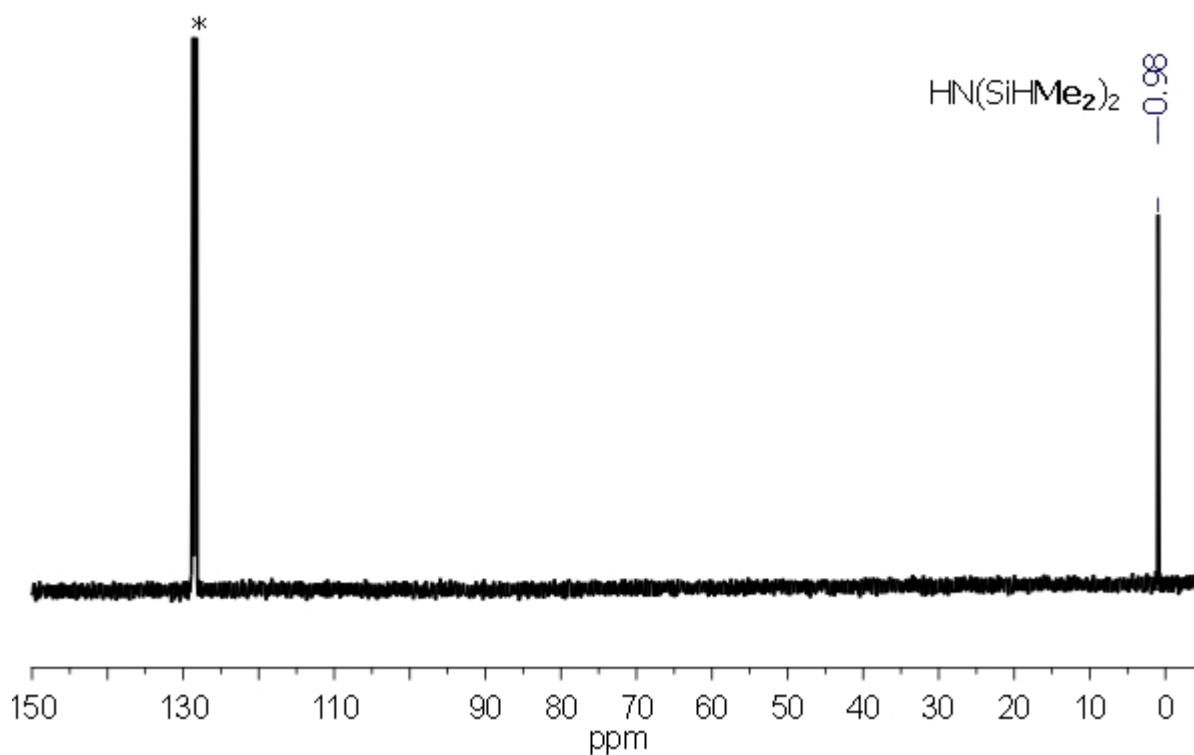
Figure 6.11 ^{13}C NMR spectrum of HN(SiHMe2)2
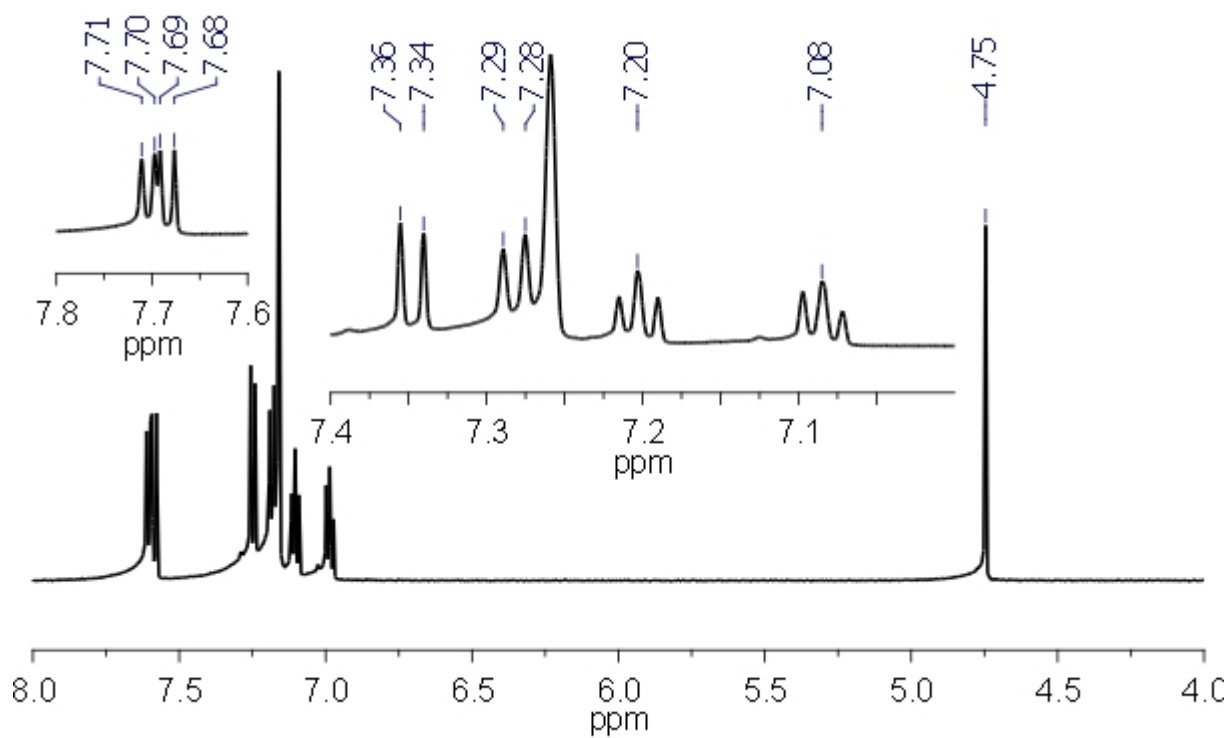
Figure 6.12 ^{1}H NMR spectrum of H_2BINOL

6.3 NMR of products
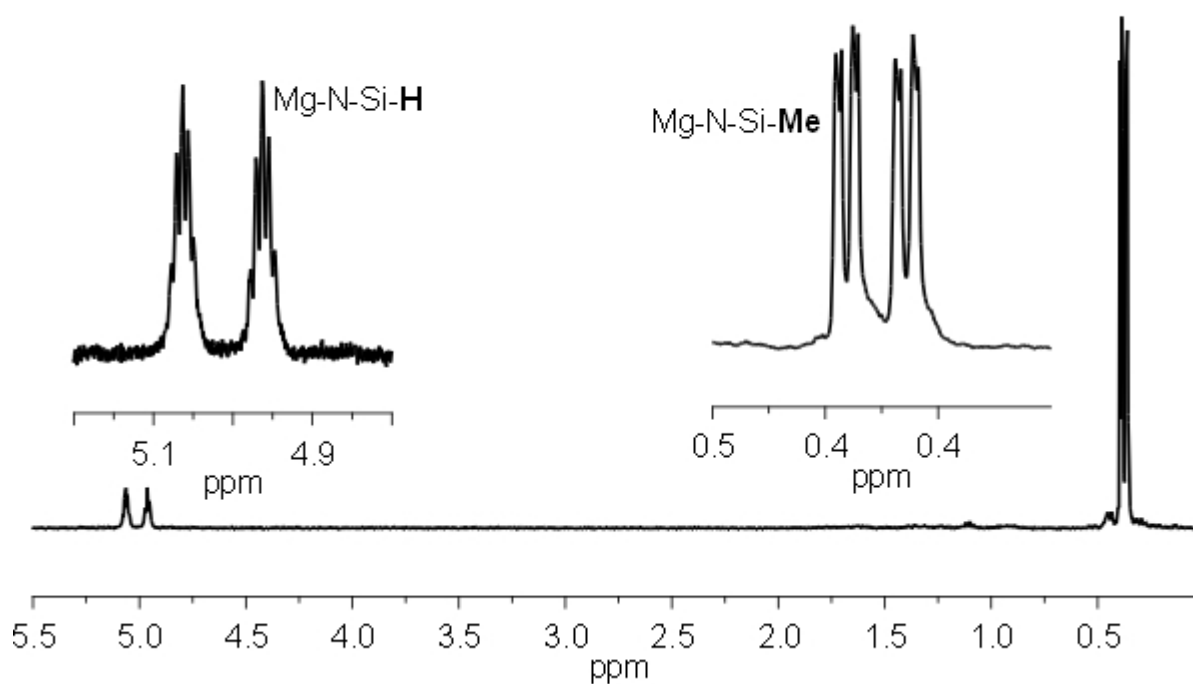
Figure 6.13 ^{1}H NMR spectrum of {Mg[N(SiHMe$_2$)$_2$]$_2$}$_2$
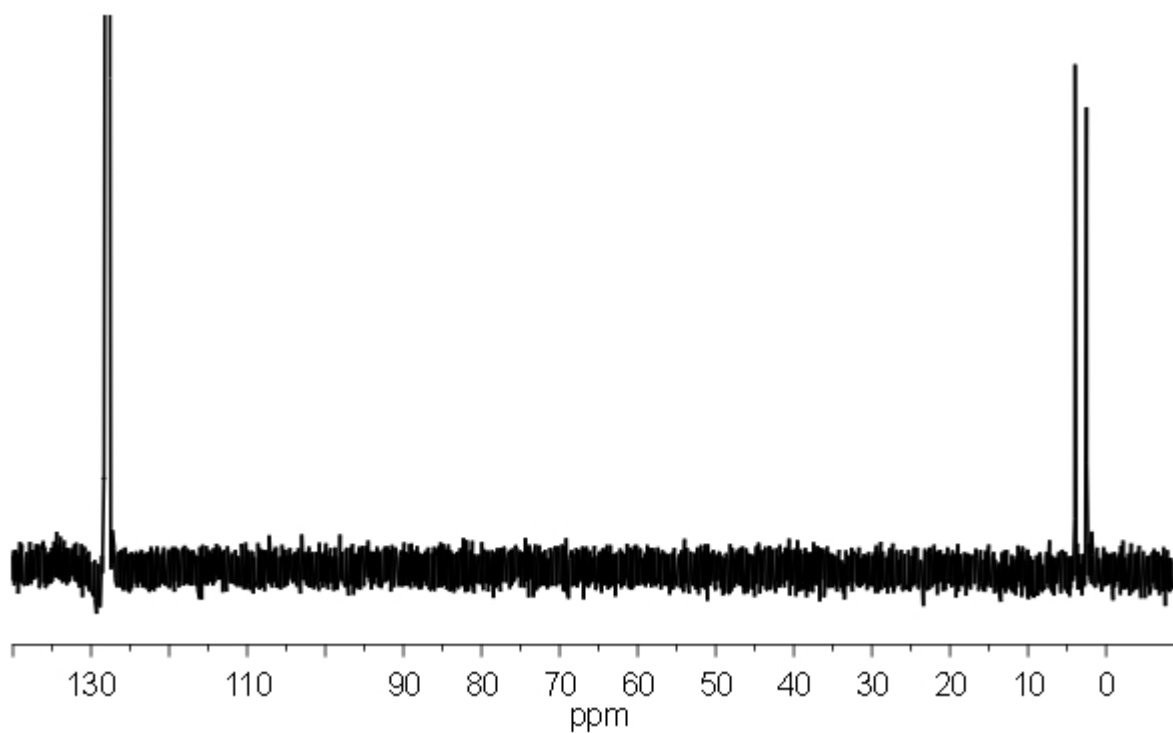
Figure 6.14 ^{13}C NMR spectrum of {Mg[N(SiHMe$_2$)$_2$]$_2$}$_2$
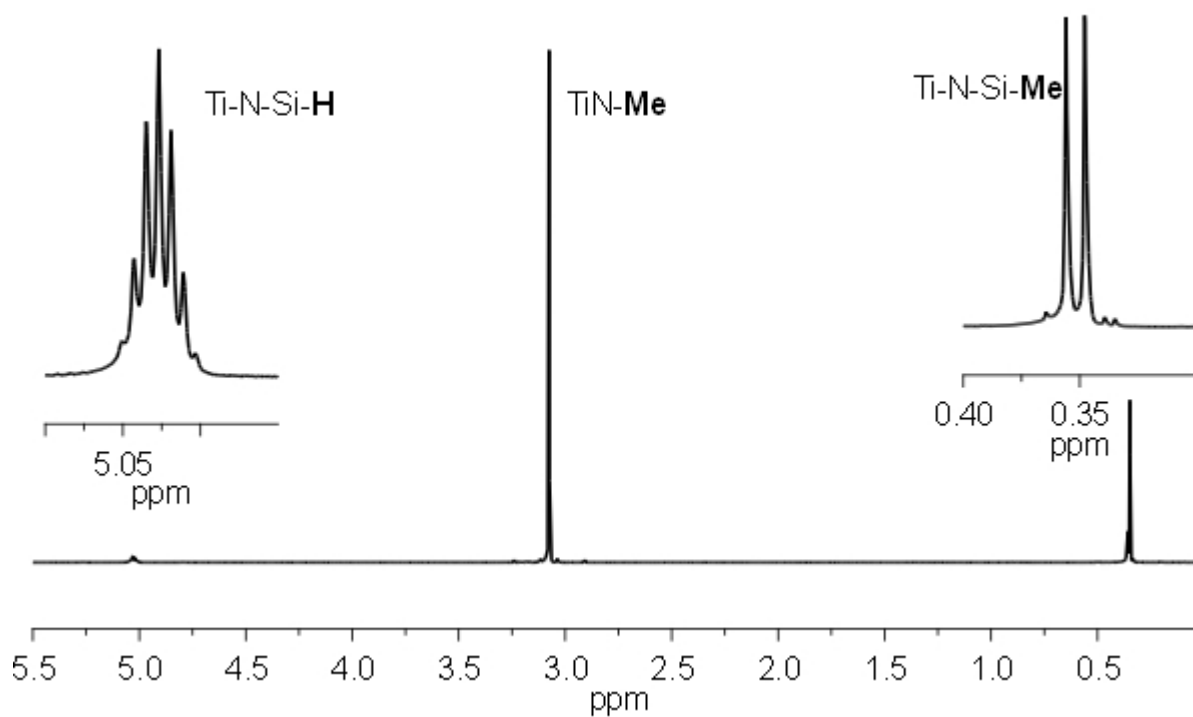
Figure 6.15 ^{1}H NMR spectrum of Ti(NMe$_2$)$_3$(bdsa)
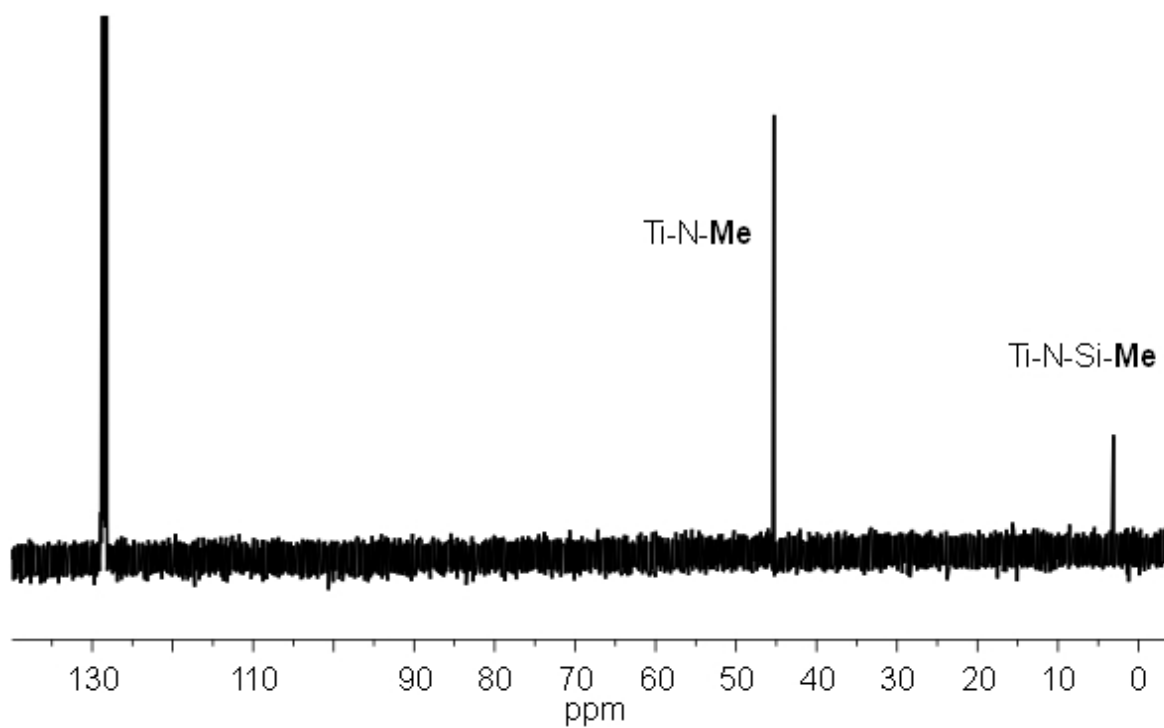
Figure 6.16 ^{13}C NMR spectrum of Ti(NMe$_2$)$_3$(bdsa)
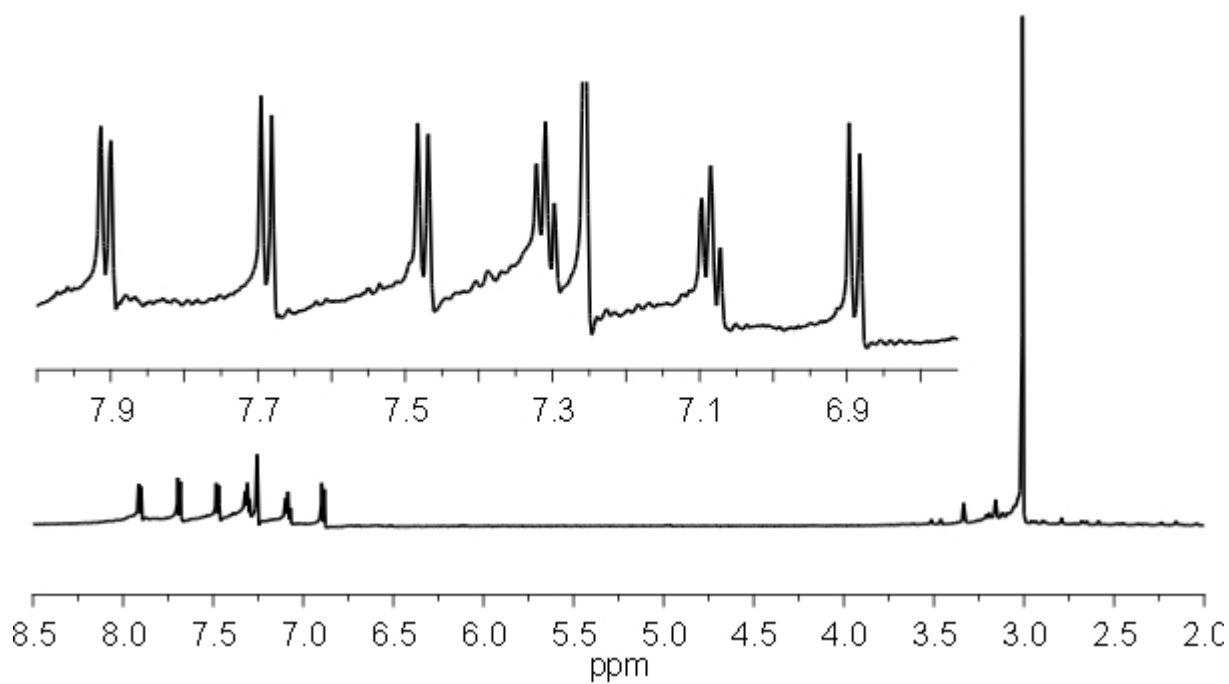
Figure 6.17 ^{1}H NMR spectrum of Ti(NMe$_2$)$_2$(BINOL)
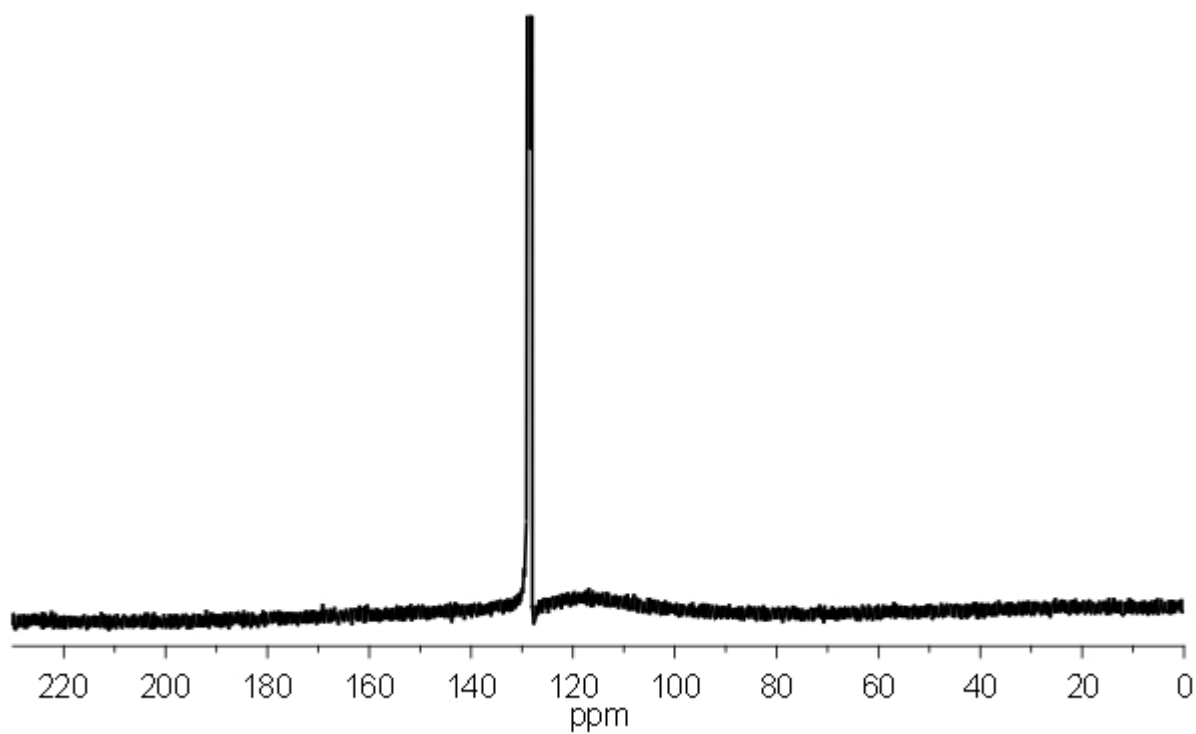
Figure 6.18 ^{13}C NMR spectrum of Ti(NMe$_2$)$_2$(BINOL)
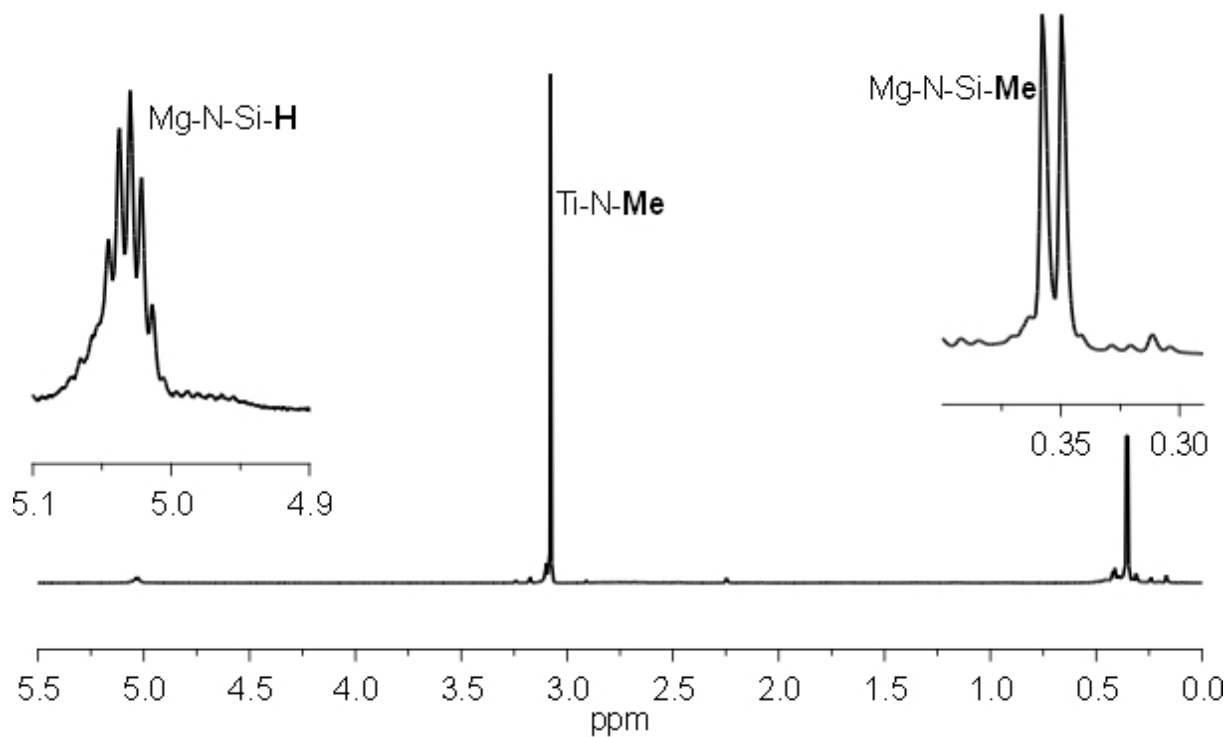
Figure 6.19 ^{1}H NMR spectrum form the reaction between {Mg[N(SiHMe$_2$)$_2$]$_2$}$_2$ and Ti(NMe$_2$)$_4$

Figure 6.20 ^{1}H NMR spectrum from the reaction between {Mg[N(SiHMe$_2$)$_2$]$_2$}$_2$ and Ti(NMe$_2$)$_4$

6.4 IR of precursors
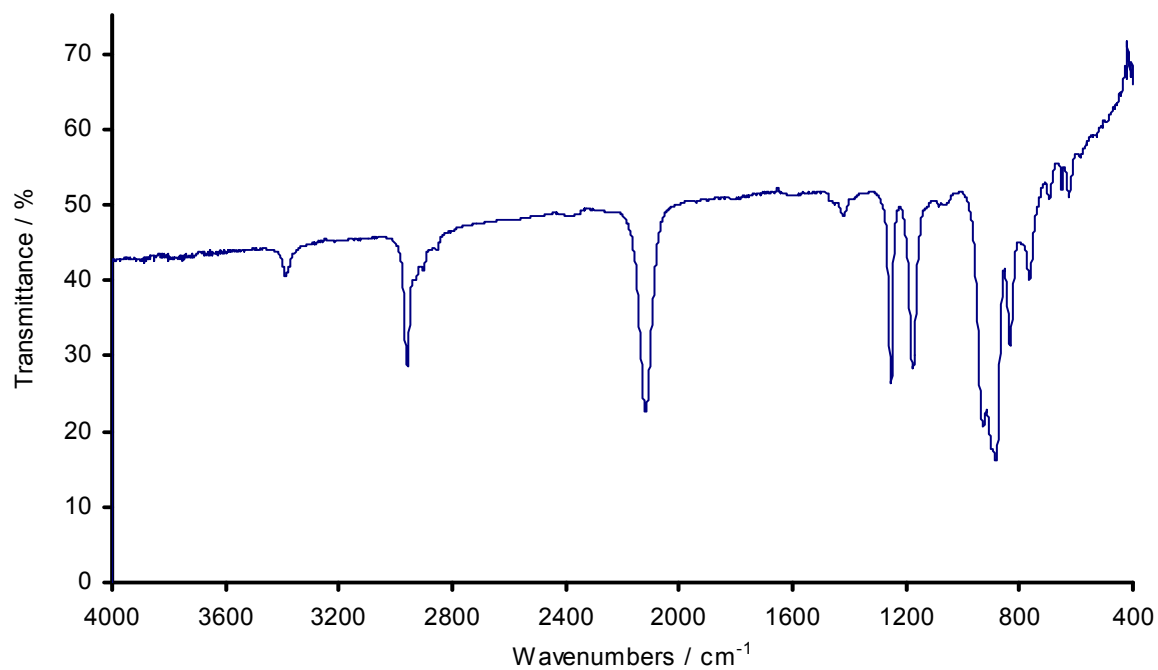
Wavenumber / cm^{-1}	Vibration
3385	N-H stretch
2854, 2922, 2897	C-H stretch, aliphatic
2120	Si-H stretch

Figure 6.21 FT-IR spectrum (neat) of 1,1,3,3-tetramethyldisilazane
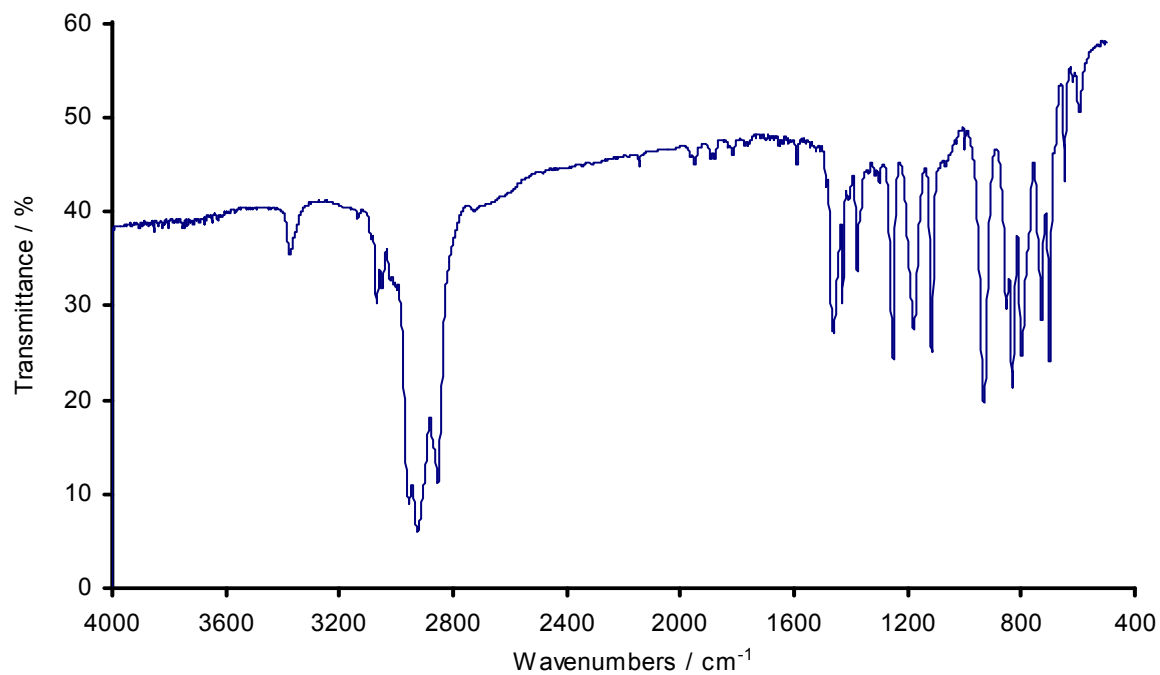
Wavenumber / cm^{-1}	Vibration
3370	N-H stretch
3073	C-H stretch, aromatic
2957, 2924, 2857	C-H stretch, aliphatic

Figure 6.4.2 FT-IR spectrum (neat) of 1,3-diphenyl-1,1,3,3-tetramethyldisilazane
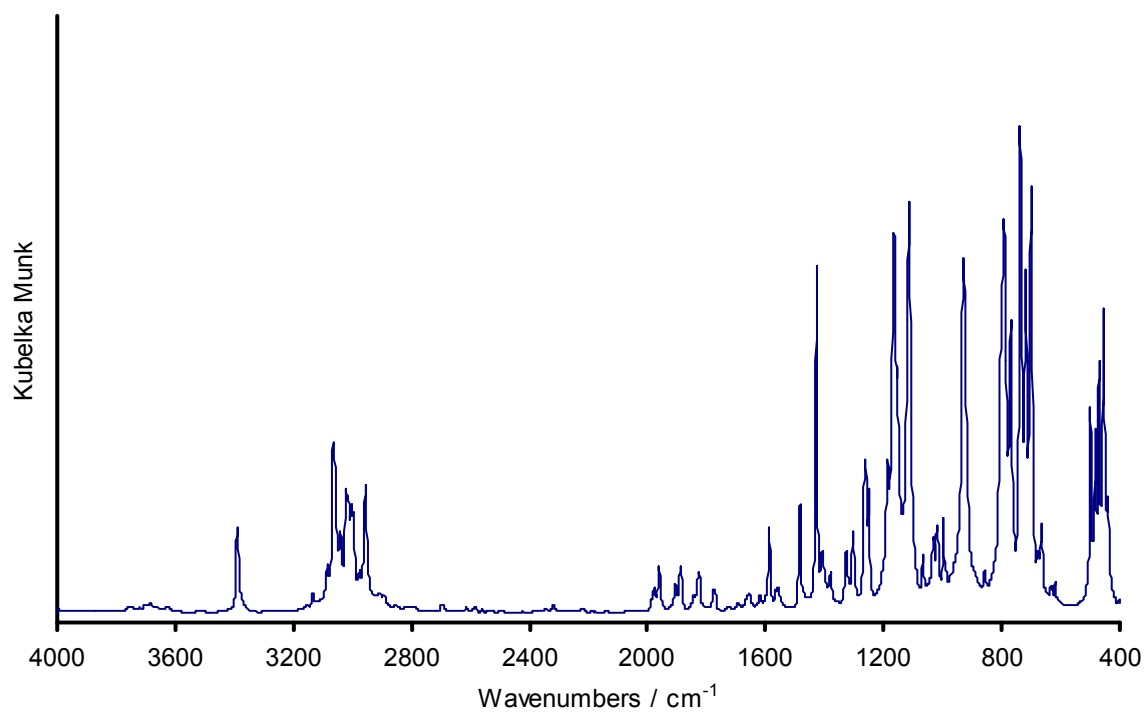
Wavenumber / cm^{-1}	Vibration
3390	N-H stretch
3058, 3019	C-H stretch, aromatic
2949	C-H stretch, aliphatic
1595, 1480	C=C stretch

Figure 6.22 DRIFT spectrum of 1,3-dimethyl-1,1,3,3-tetraphenyldisilazane
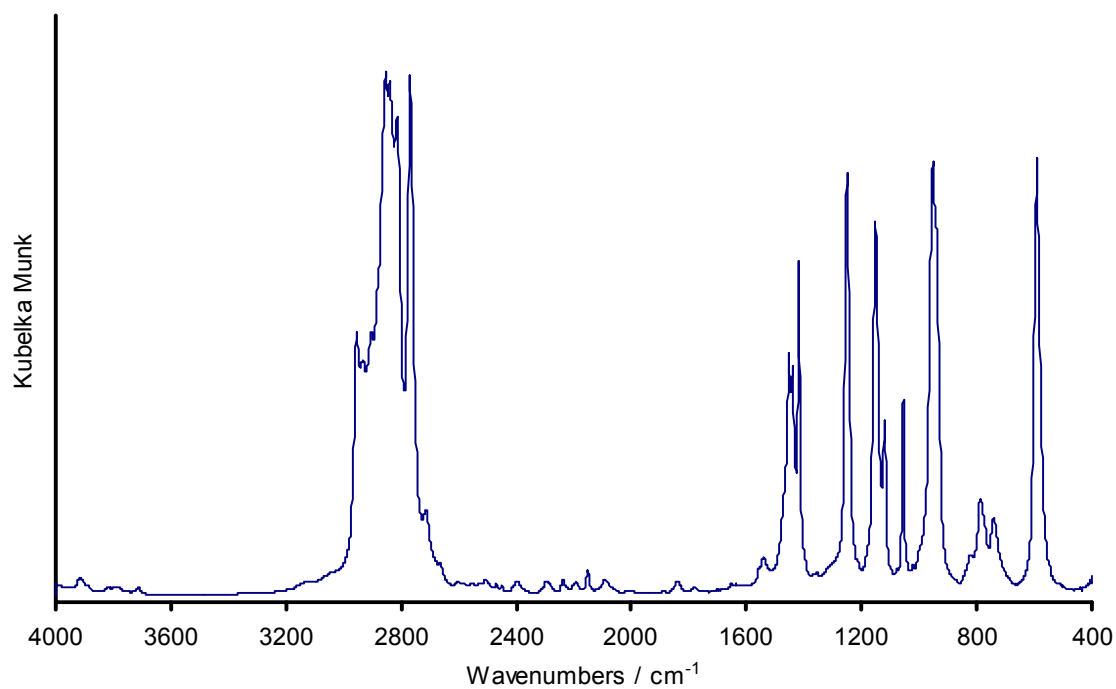
Wavenumber / cm^{-1}	Vibration
2955, 2845, 2765	C-H stretch, aliphatic

Figure 6.23 DRIFT spectrum of Ti(NMe$_2$)$_4$
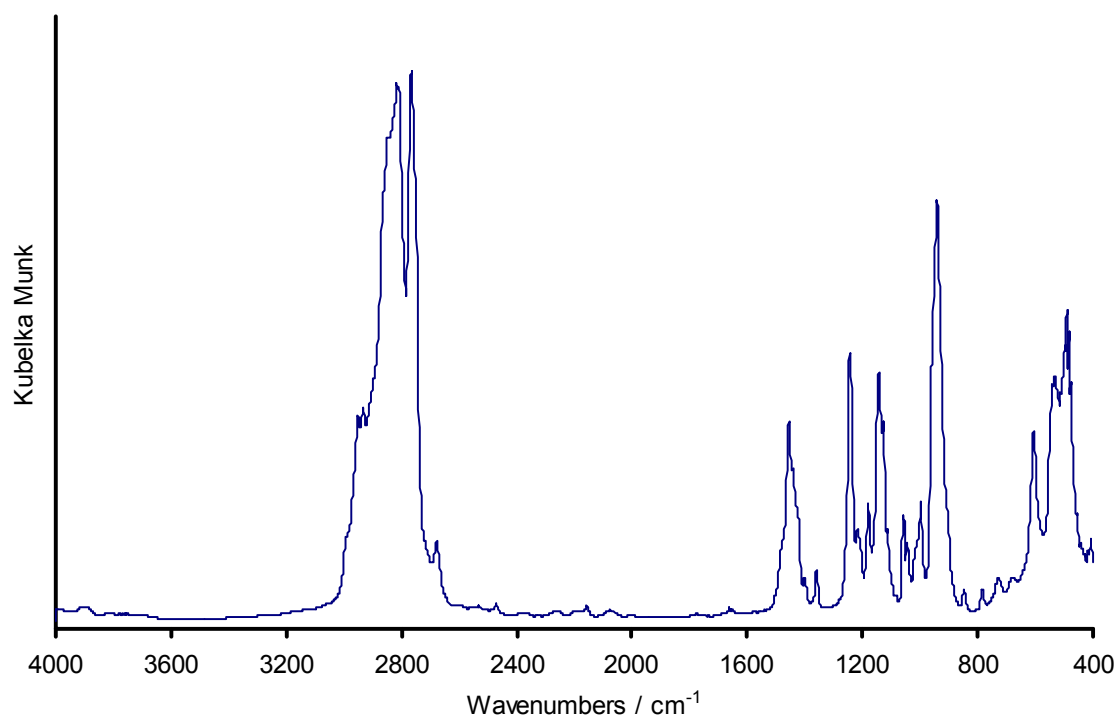
Wavenumber / cm^{-1}	Vibration
2959, 2805, 2775	C-H stretch, aliphatic

Figure 6.24 DRIFT spectrum of Zr(NMe$_2$)$_4$

6.5 FT-IR spectra of molecular products

Wavenumber / cm^{-1}	Vibration
2950, 2890	C-H stretch, aliphatic
ca. 2090-2000	Si-H stretch
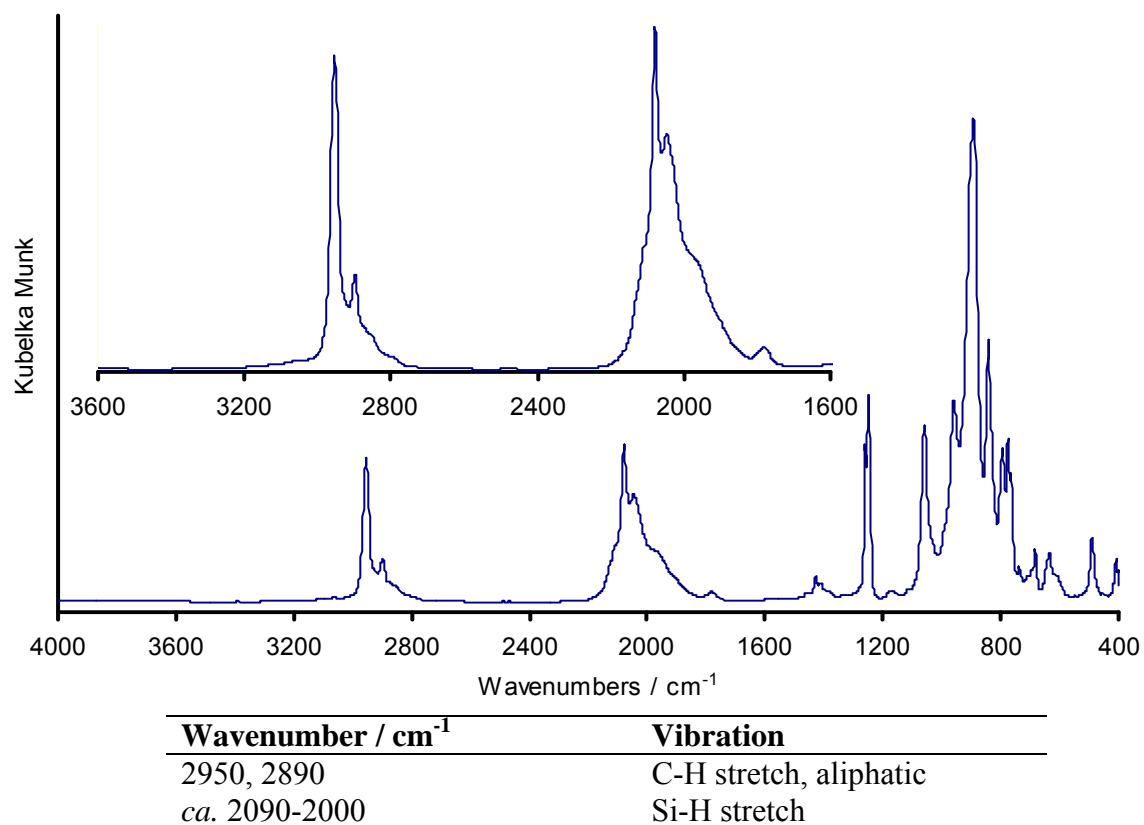
Figure 6.25 DRIFT spectrum of {Mg[N(SiHMe$_2$)$_2$]$_2$}$_2$

Wavenumber / cm^{-1}	Vibration
2955, 2855, 2770	C-H stretch, aliphatic
2090	Si-H stretch
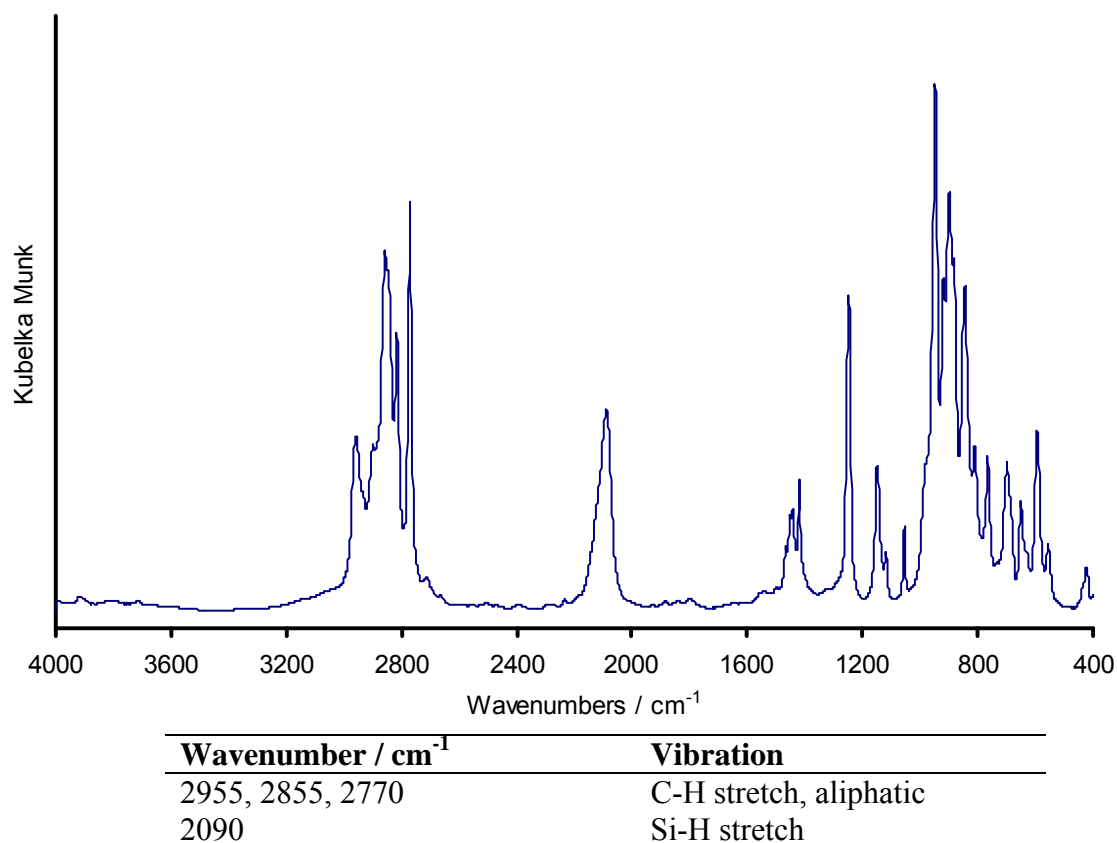
Figure 6.26 DRIFT spectrum of Ti(NMe$_2$)[N(SiHMe$_2$)$_2$]

Wavenumber / cm^{-1}	Vibration
3050	C-H stretch, aromatic
2895, 2860, 2765	C-H stretch, aliphatic
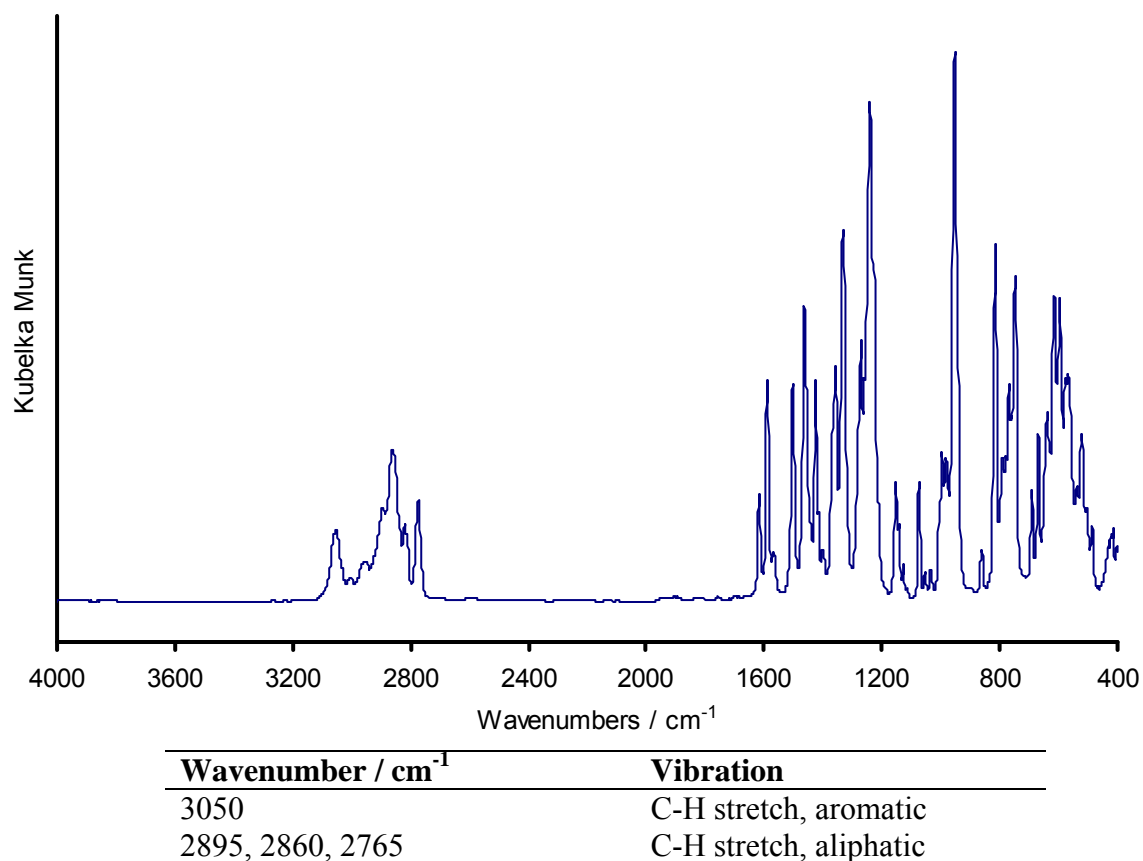
Figure 6.27 DRIFT spectrum of Ti(NMe$_2$)$_2$(BINOL)

6.6 FT-IR spectra of materials
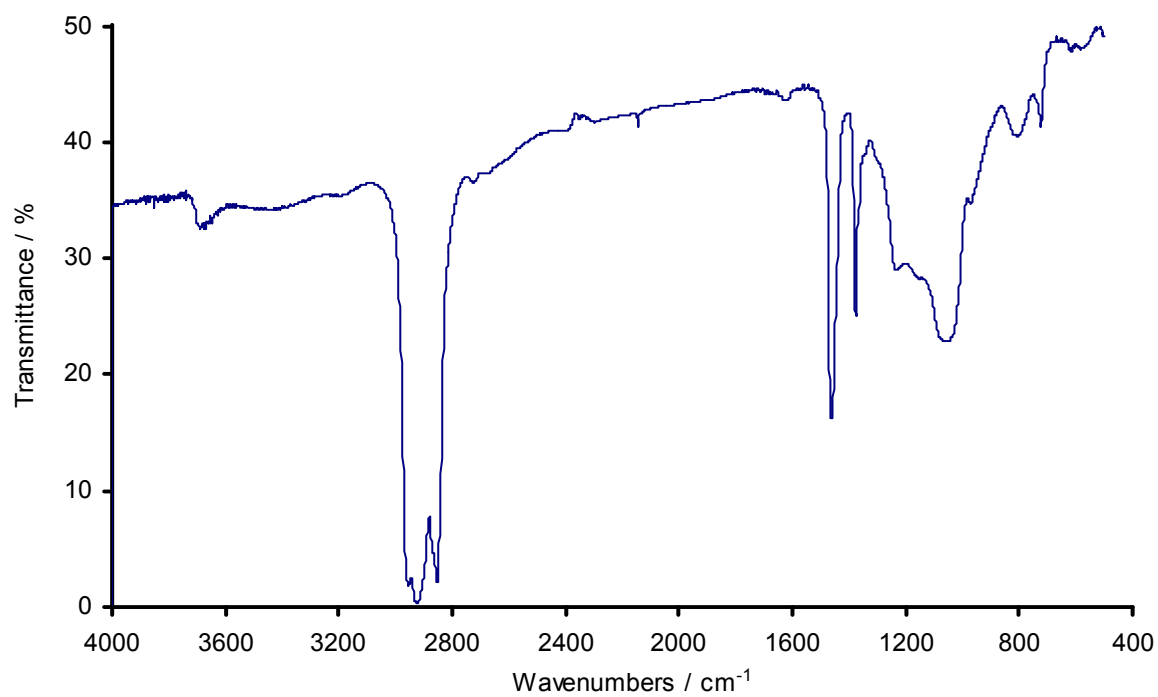
Wavenumber / cm^{-1}	Vibration
3695	O-H stretch
ca. 3000-2850	Nujol

Figure 6.28 FT-IR spectrum (Nujol mull) of SBA-1 1
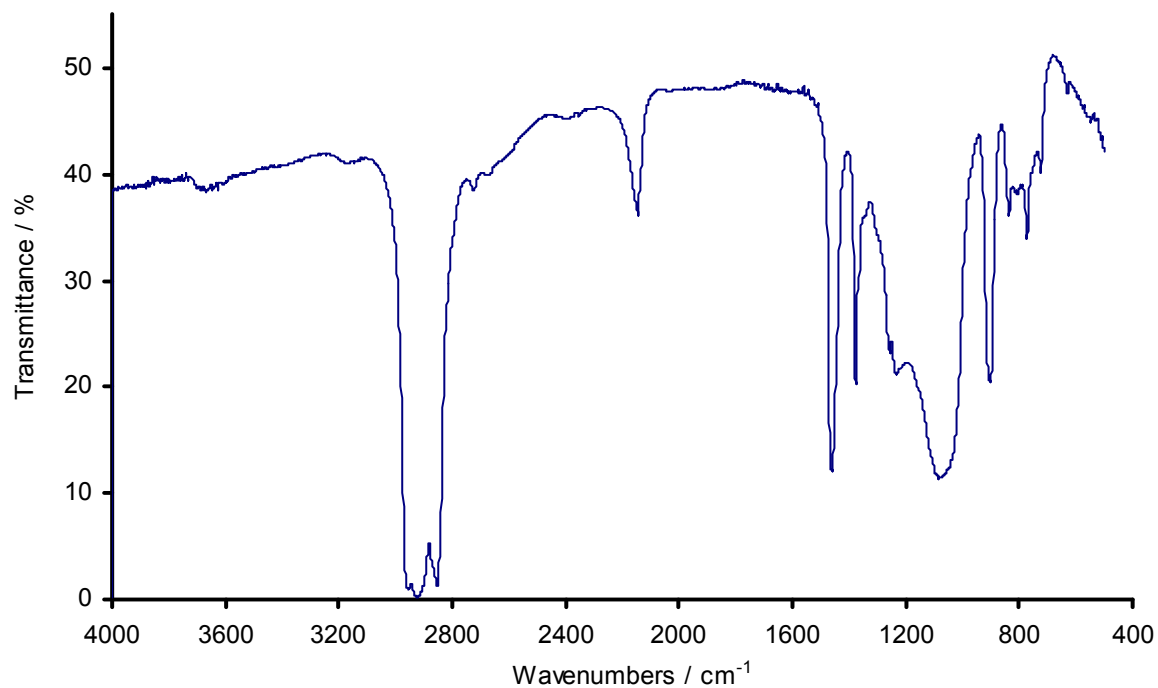
Wavenumber / cm^{-1}	Vibration
ca. 3000-2850	Nujol
2145	Si-H stretch

Figure 6.29 FT-IR spectrum (Nujol mull) of SiHMe$_2$@SBA-1 1a
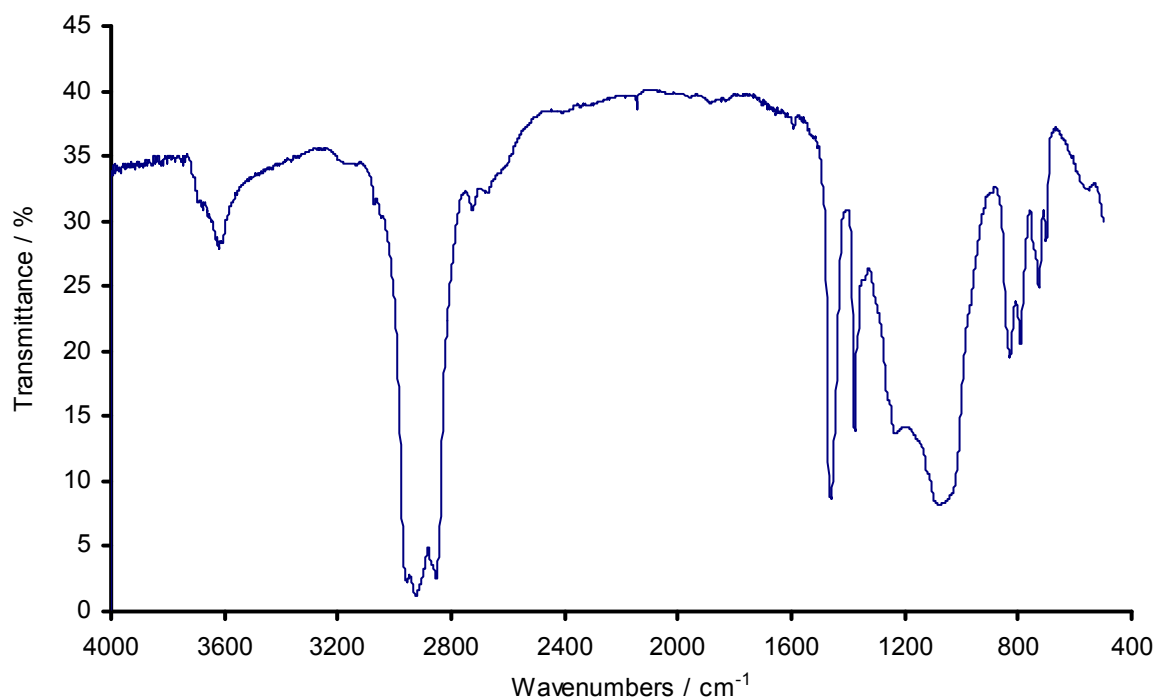
Wavenumber / cm^{-1}	Vibration
3675	O-H stretch
3620	O-H stretch
3075	C-H stretch aromatic
ca. 3000-2850	Nujol

Figure 6.30 FT-IR spectrum (Nujol mull) of SiMe$_2$Ph@SBA-1 1b
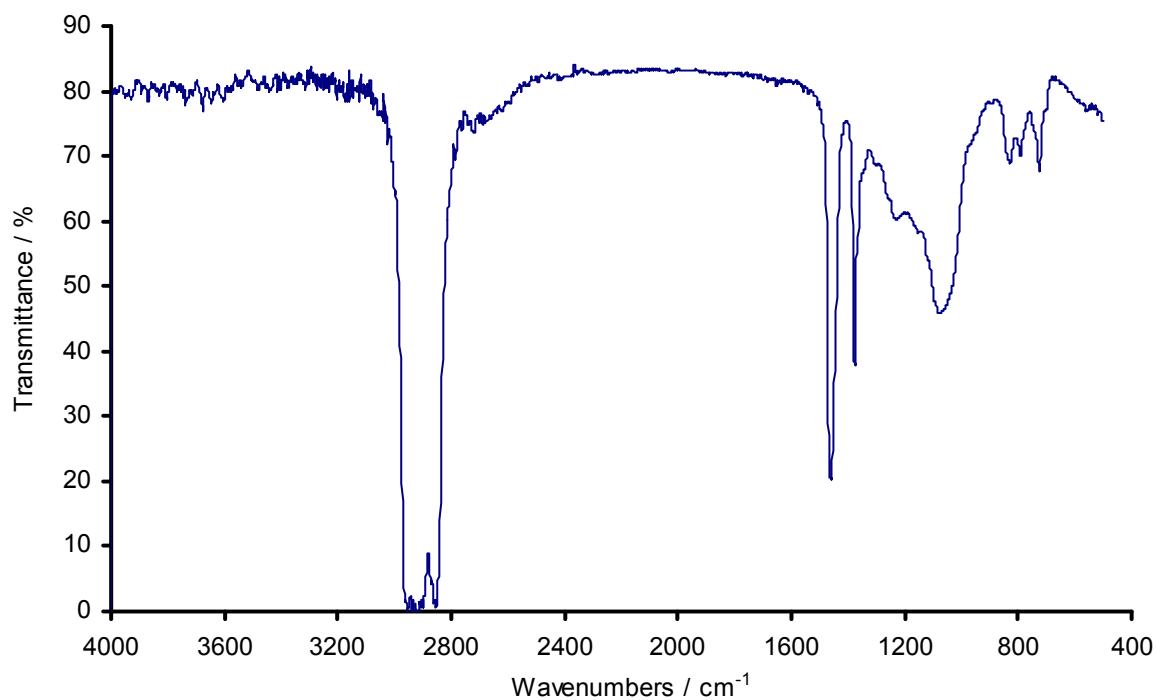
Wavenumber / cm⁻¹	Vibration
ca. 3000-2850	Nujol

Figure 6.31 FT-IR spectrum (Nujol mull) of Ti(NMe₂)ₓ@SiMe₂Ph@SBA-1 1be
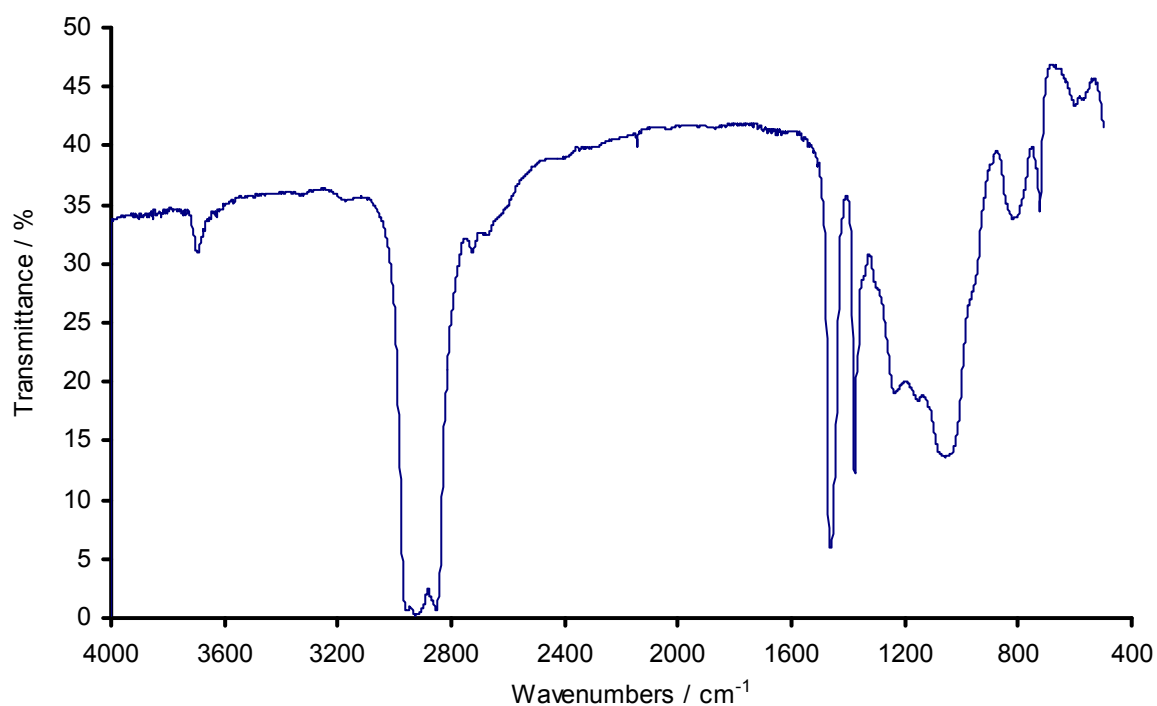
Wavenumber / cm⁻¹	Vibration
3695	O-H stretch
ca. 3000-2850	Nujol

Figure 6.32 FT-IR spectrum (Nujol mull) of Ti(NMe₂)ₓ@SBA-1 1e
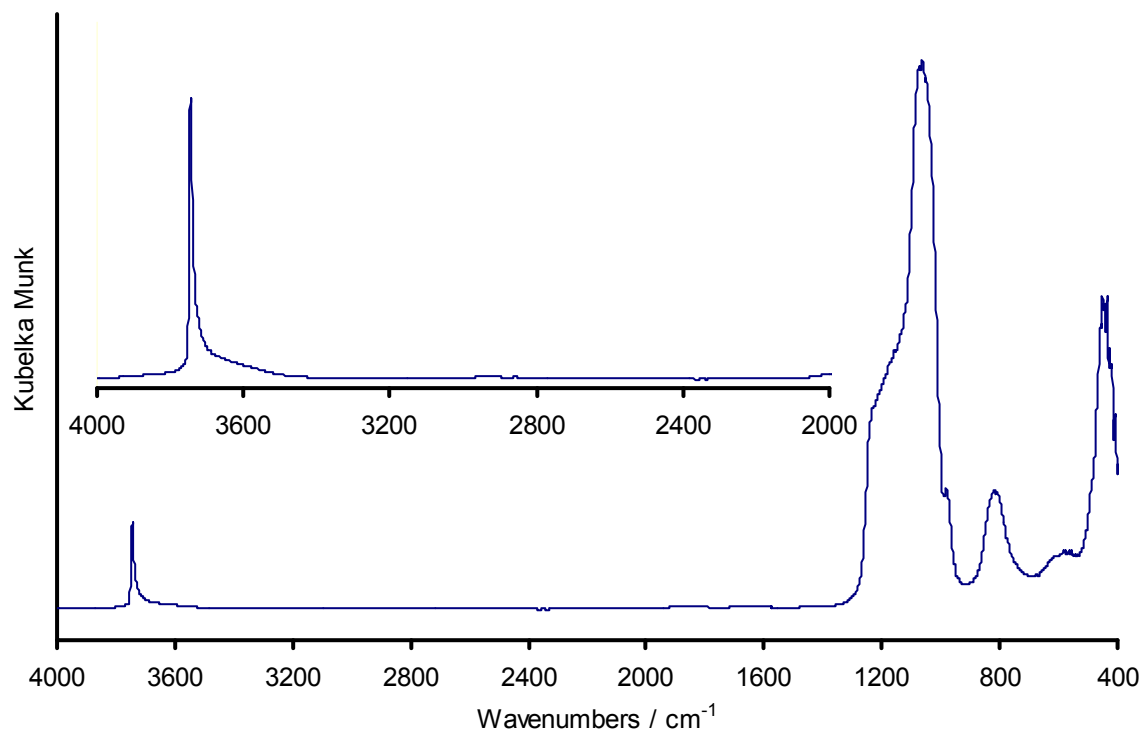
Wavenumber / cm⁻¹	Vibration
3745	O-H stretch

Figure 6.33 DRIFT spectrum of SBA-1 2

Wavenumber / cm^{-1}	Vibration
2970, 2900	C-H stretch
2150	Si-H stretch
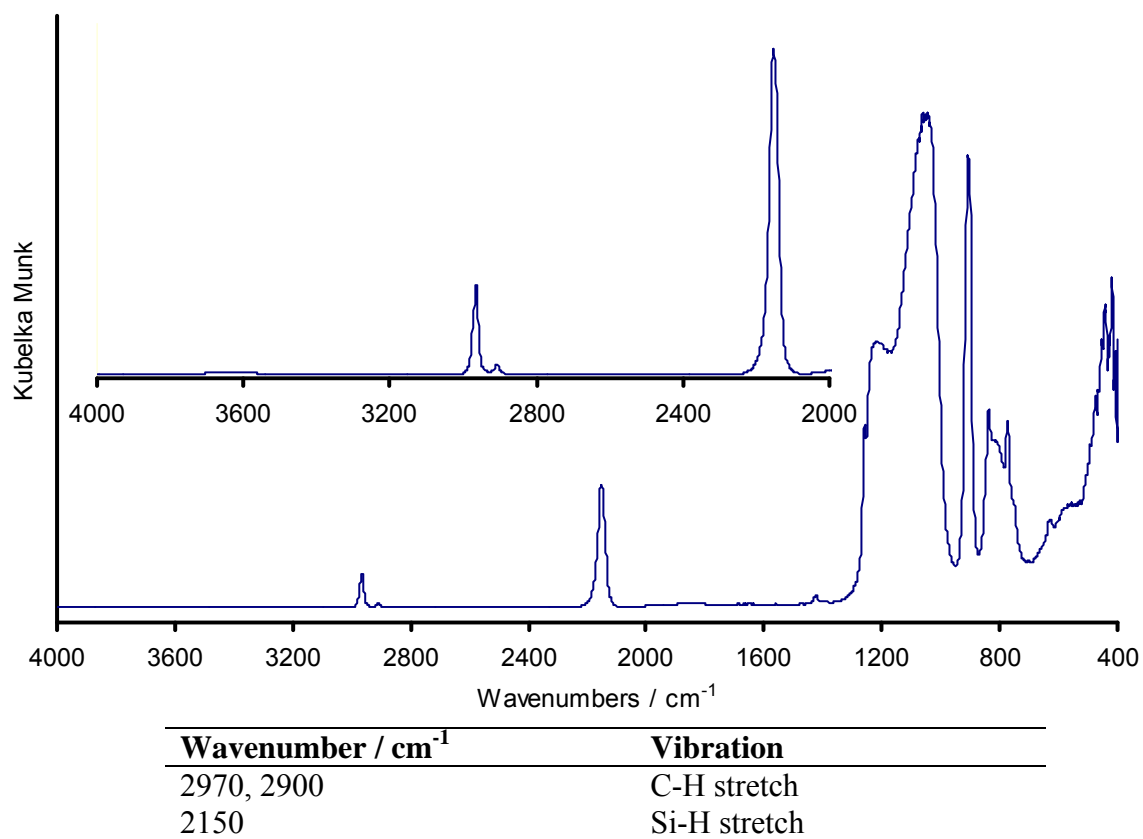
Figure 6.34 DRIFT spectrum of SiHMe$_2$@SBA-1 2a
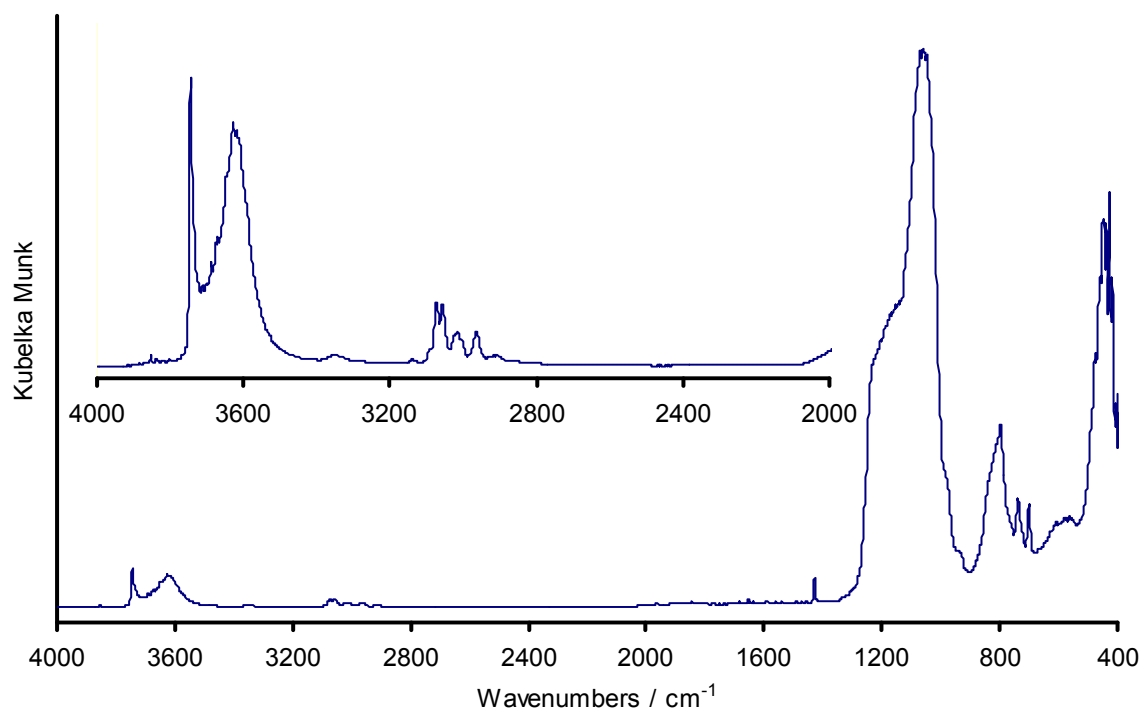
Wavenumber / cm^{-1}	Vibration
3740	O-H stretch
3620	O-H stretch
3069, 3050	C-H stretch aromatic
3000, 2955	C-H stretch aliphatic

Figure 6.35 DRIFT spectrum of SiMePh$_2$@SBA-1 2c
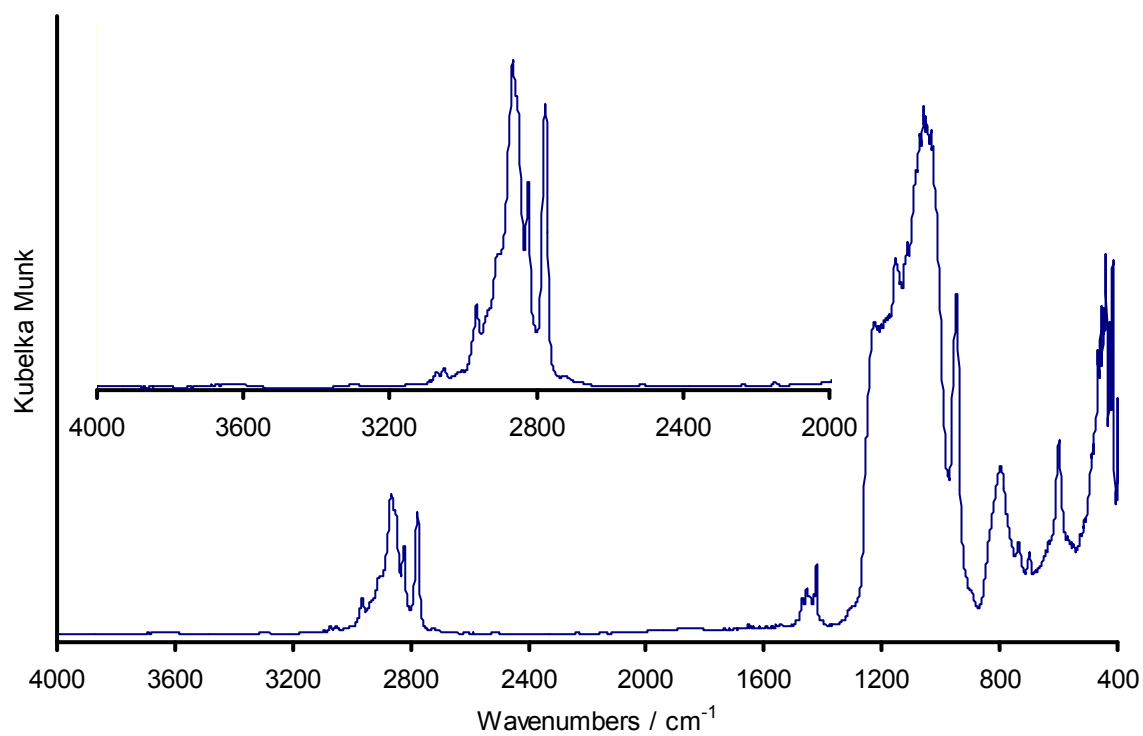
Wavenumber / cm^{-1}	Vibration
3620	O-H stretch
3075, 3050	C-H stretch aromatic
2970, 2860, 2760	C-H stretch aliphatic

Figure 6.36 DRIFT spectrum of Ti(NMe$_2$)$_x$@SiMePh$_2$@SBA-1 2ce
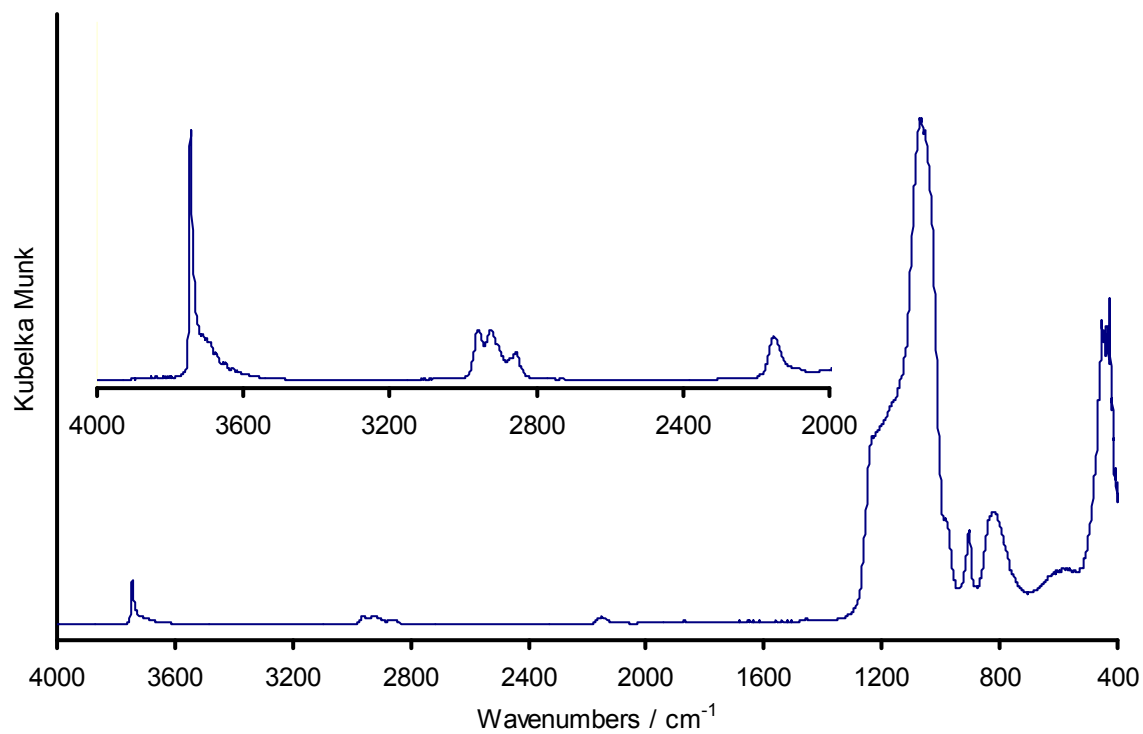
Wavenumber / cm^{-1}	Vibration
3740	O-H stretch
2955, 2915, 2845	C-H stretch, aliphatic
2150	Si-H stretch

Figure 6.37 DRIFT spectrum of Mg[N(SiHMe$_2$)$_2$]$_x$@SBA-1 2d

Wavenumber / cm^{-1}	Vibration
2960, 2870, 2770	C-H stretch, aliphatic
2145	Si-H stretch
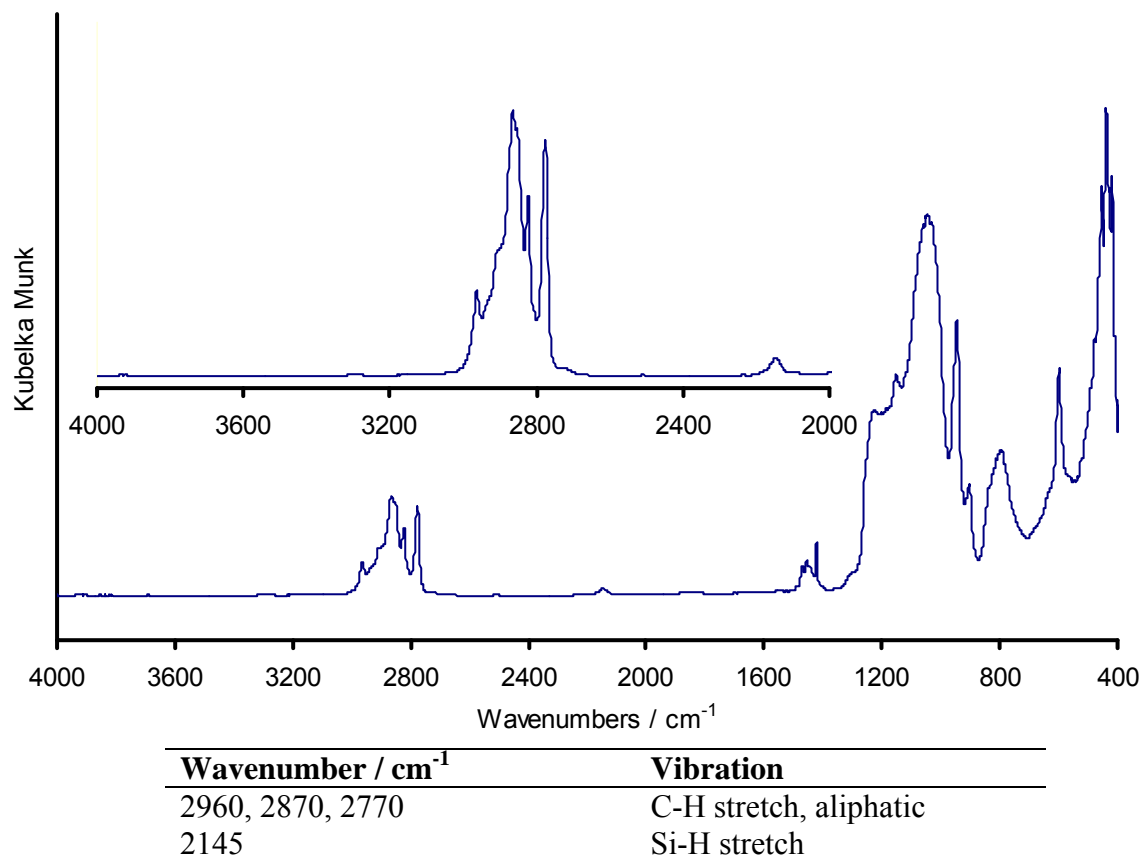
Figure 6.38 DRIFT spectrum of Ti(NMe$_2$)$_x$@Mg[N(SiHMe$_2$)$_2$]$_y$@SBA-1 2de

Wavenumber / cm^{-1}	Vibration
2955, 2860, 2770	C-H stretch, aliphatic
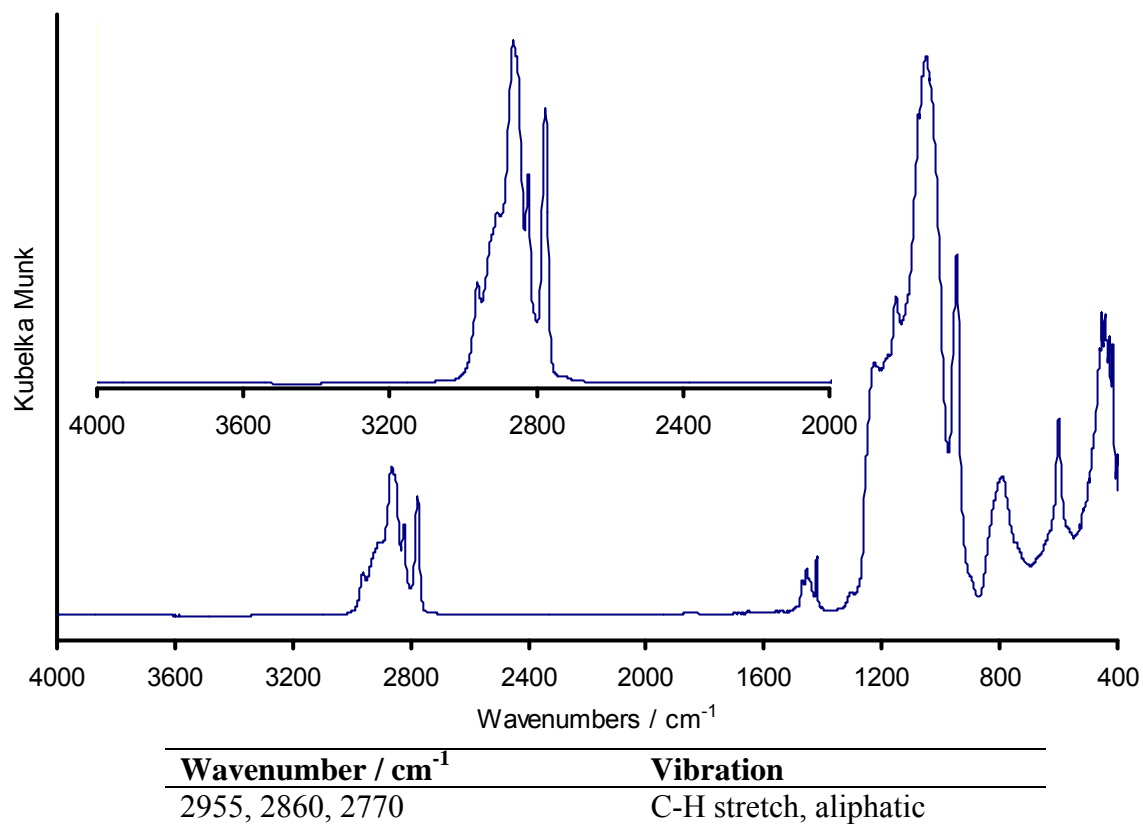
Figure 6.39 DRIFT spectrum of Ti(NMe$_2$)$_x$@SBA-1 2e
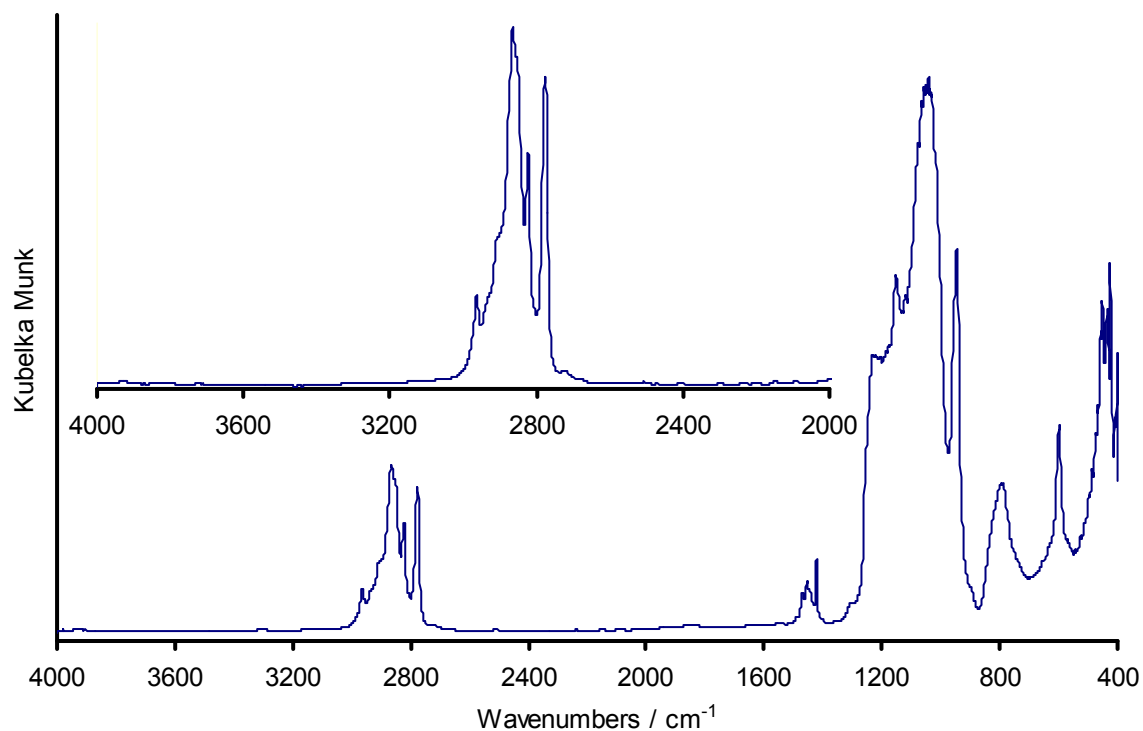
Wavenumber / cm^{-1}	Vibration
2960, 2870, 2770	C-H stretch, aliphatic

Figure 6.5.13 DRIFT spectrum of Ti(NMe$_2$)$_x$SBA-1 **2e2**
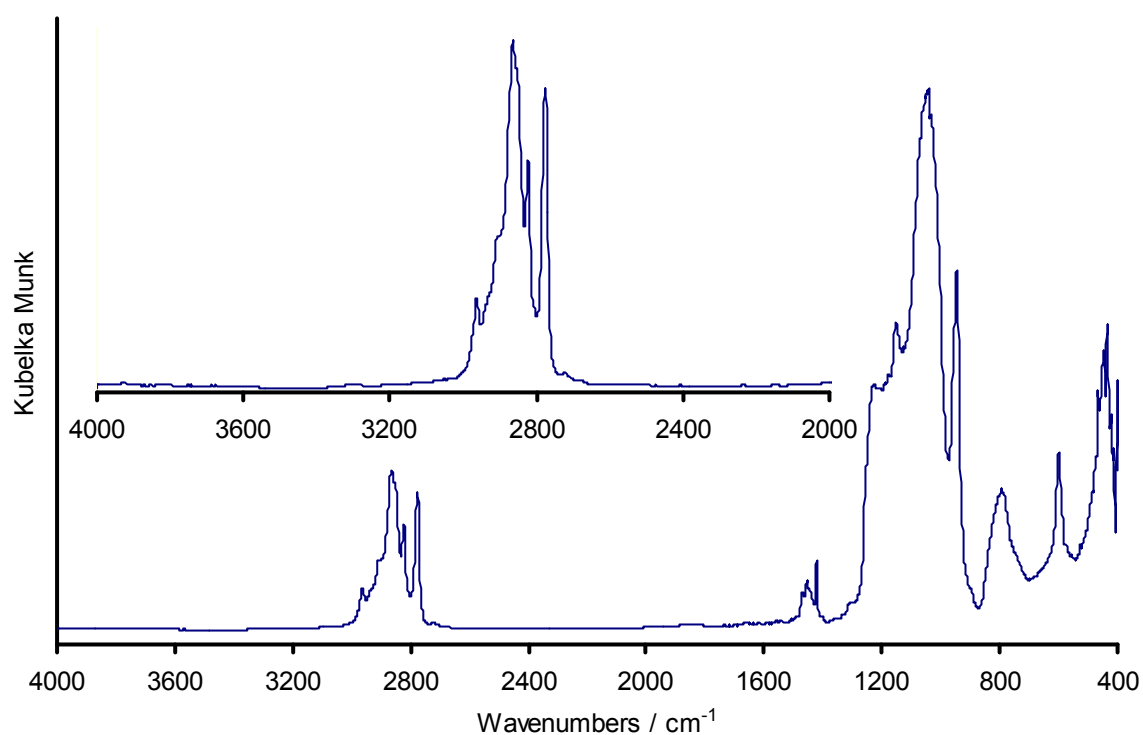
Wavenumber / cm^{-1}	Vibration
2960, 2870, 2770	C-H stretch, aliphatic

Figure 6.40 DRIFT spectrum of Ti(NMe$_2$)$_x$(BINOL)@SBA-1 2eB
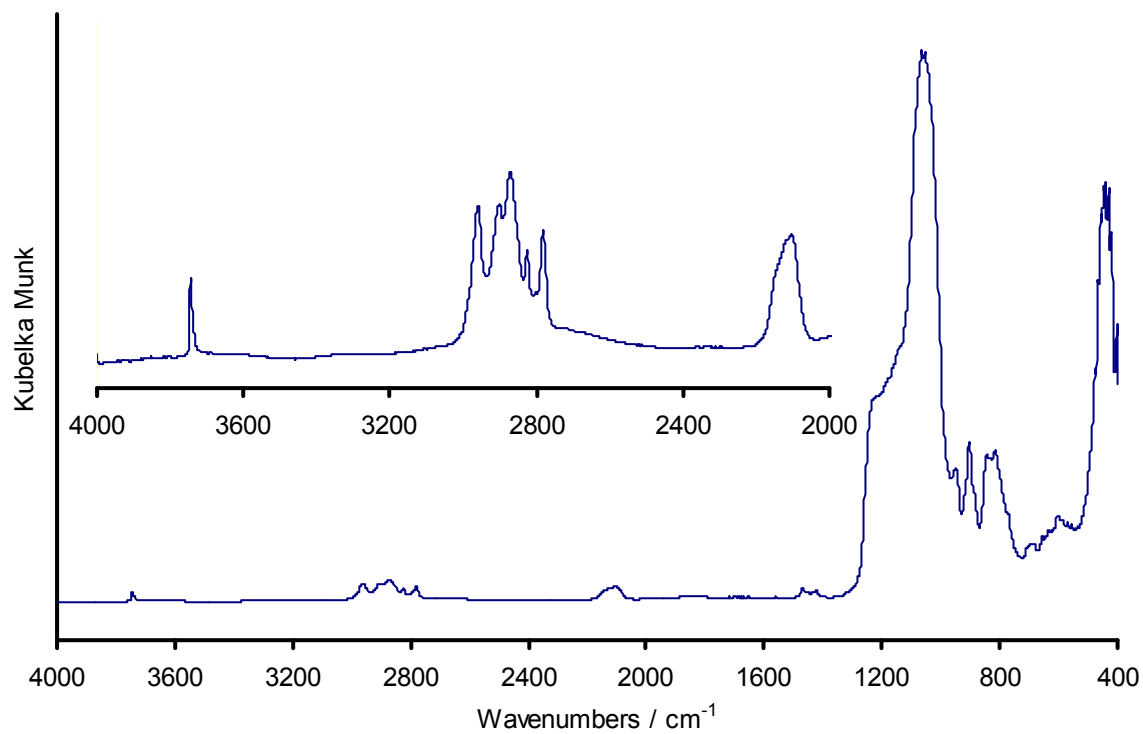
Wavenumber / cm^{-1}	Vibration
3740	O-H stretch
2960, 2870, 2780	C-H stretch, aliphatic
ca. 2150-2100	Si-H stretch

Figure 6.41 DRIFT spectrum of Ti(NMe$_2$)$_x$[N(SiHMe$_2$)$_2$]@SBA-1 2f

Wavenumber / cm⁻¹	Vibration
2960, 2860, 2770	C-H stretch, aliphatic
2140, 2080	Si-H stretch
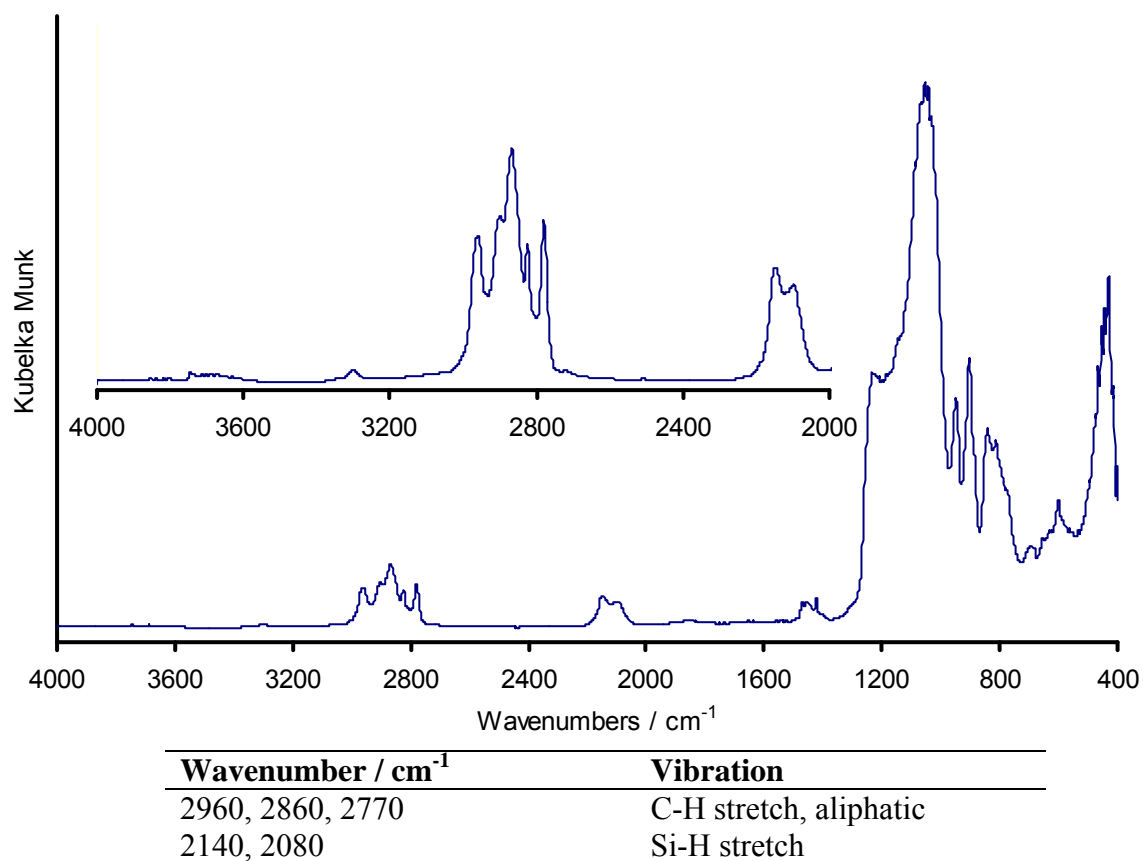
Figure 6.42 DRIFT spectrum of Ti(NMe$_2$)$_x$[N(SiHMe$_2$)$_2$]@SBA-1 2f2

Wavenumber / cm⁻¹	Vibration
3290	N-H stretch, residual NH$_3$
2970, 2855, 2770	C-H stretch, aliphatic
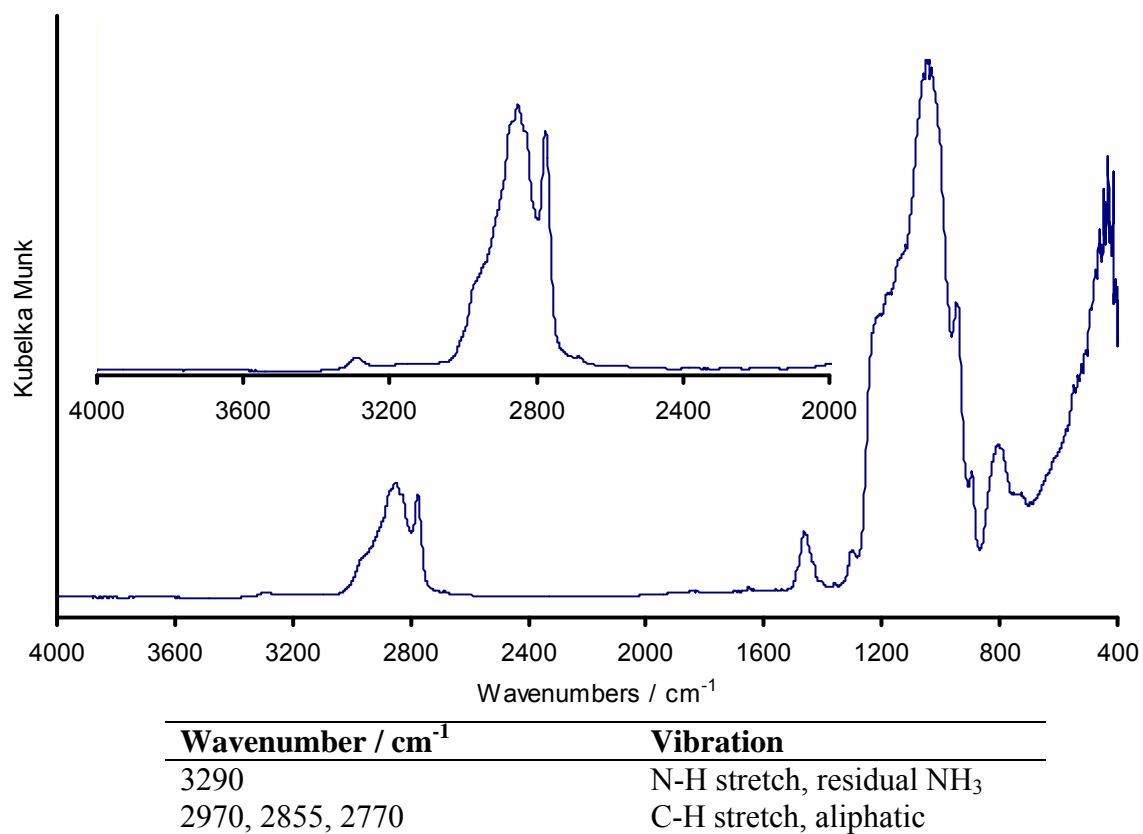
Figure 6.43 DRIFT spectrum of Zr(NMe$_2$)$_x$@SBA-1 2g
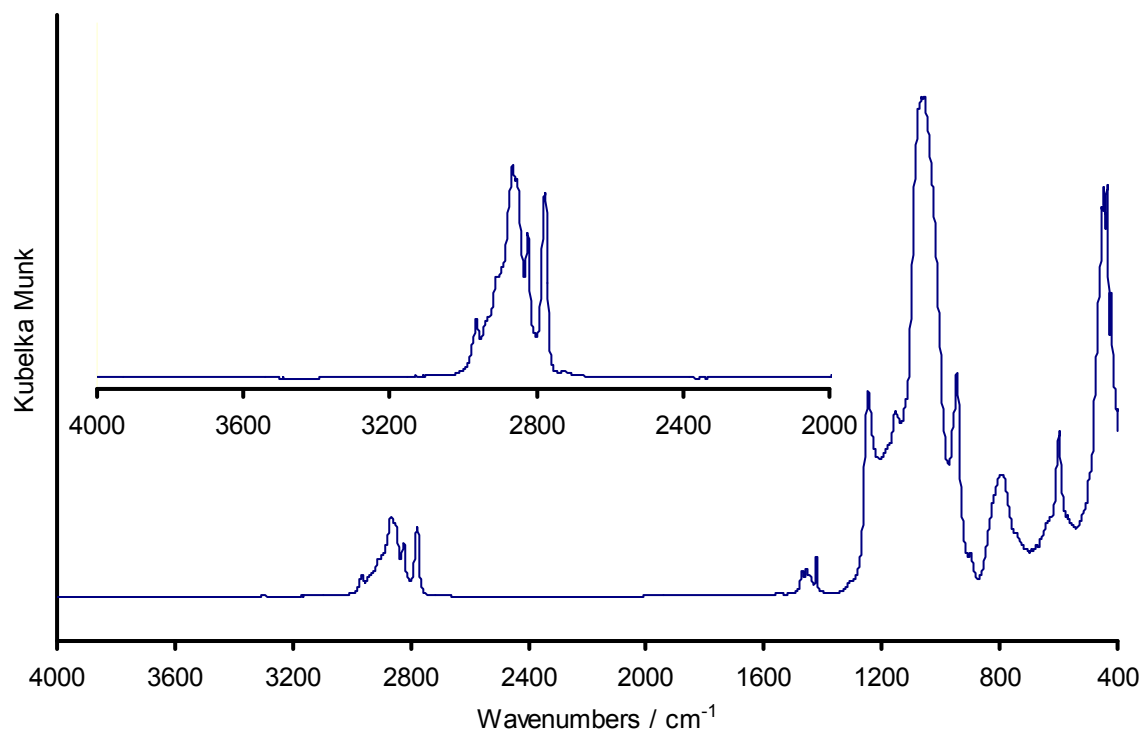
Wavenumber / cm^{-1}	Vibration
2960, 2860, 2775	C-H stretch, aliphatic

Figure 6.44 DRIFT spectrum of Ti(NMe$_2$)$_x$@MCM-41 3e
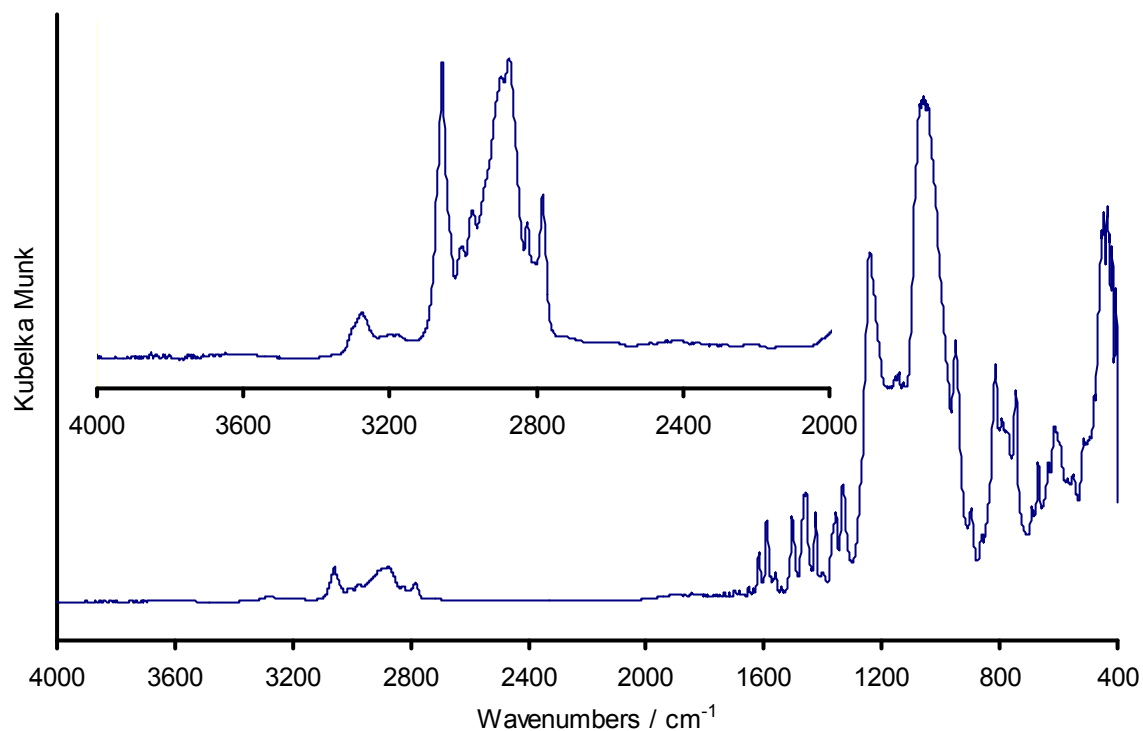
Wavenumber / cm^{-1}	Vibration
2960, 2860, 2775	C-H stretch, aliphatic

Figure 6.45 DRIFT spectrum of Ti(NMe$_2$)$_x$(BINOL)@MCM-41 4eB
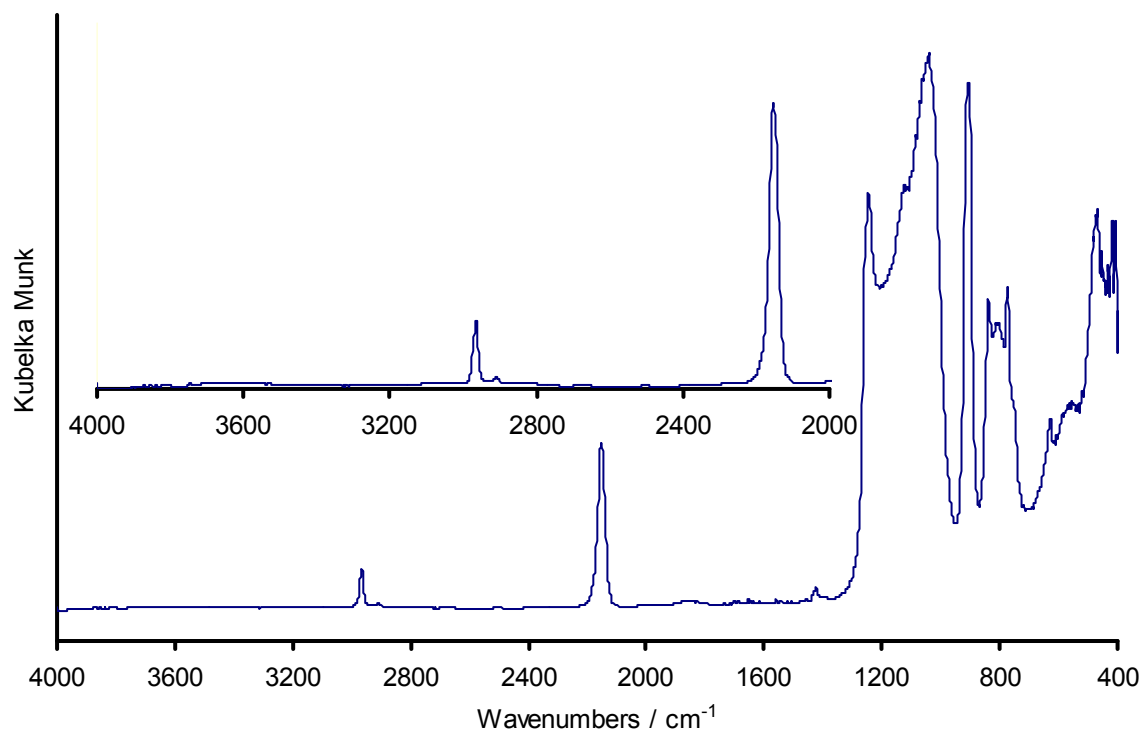
Wavenumber / cm^{-1}	Vibration
2970, 2900	C-H stretch
2150	Si-H stretch

Figure 6.46 DRIFT spectrum of SiHMe$_2$@MCM-41 4a
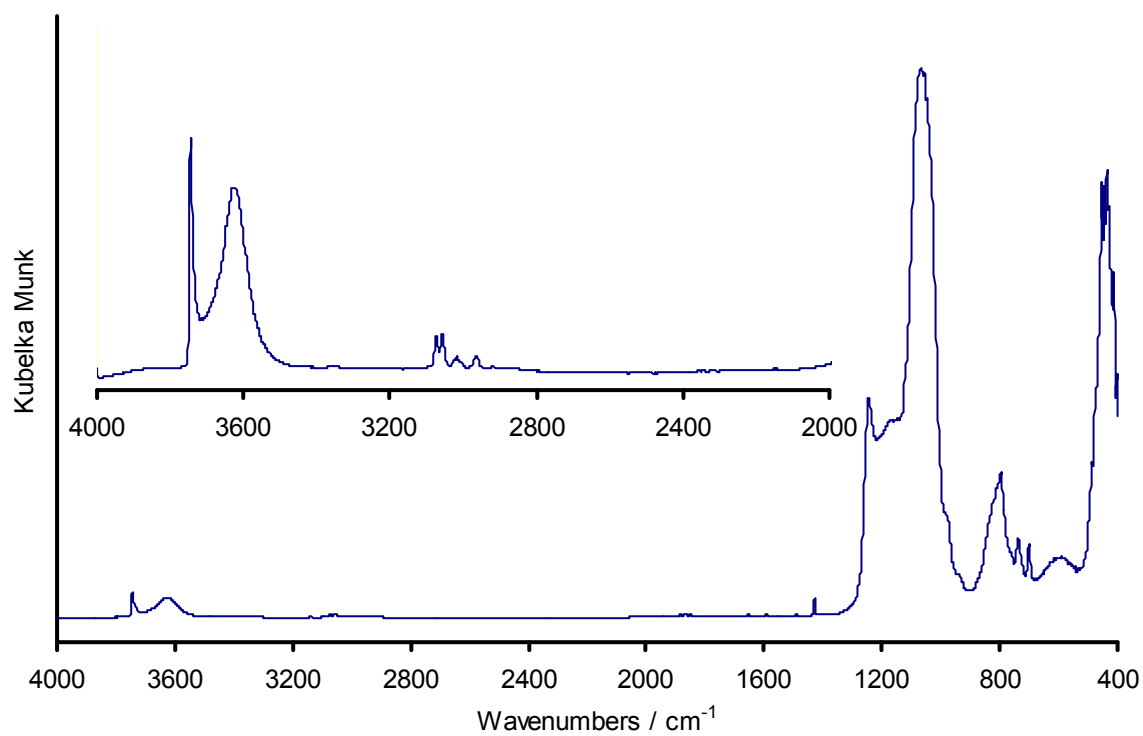
Wavenumber / cm^{-1}	Vibration
3775	O-H stretch
3620	O-H stretch
3075	C-H stretch, aromatic

Figure 6.47 DRIFT spectrum of SiMePh$_2$@MCM-41 4c
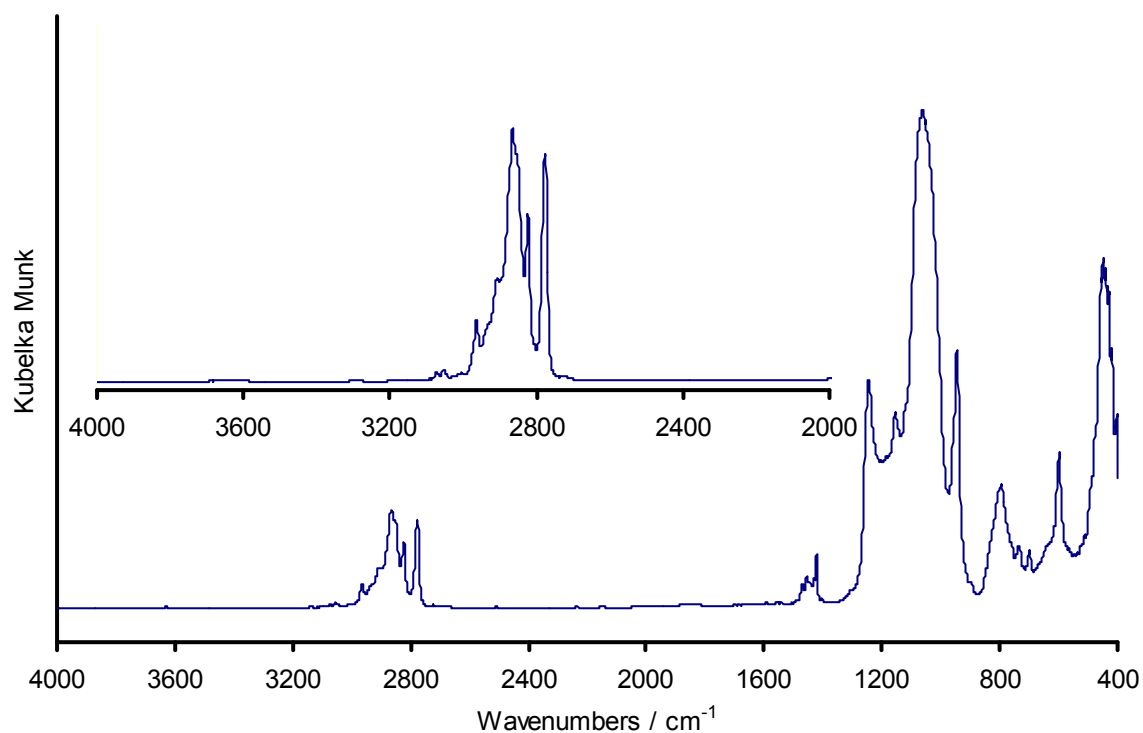
Wavenumber / cm^{-1}	Vibration
3050	C-H stretch, aromatic
2965, 2860, 2775	C-H stretch, aliphatic

Figure 6.48 DRIFT spectrum of Ti(NMe$_2$)$_x$@SiMePh$_2$@MCM-41 4ce
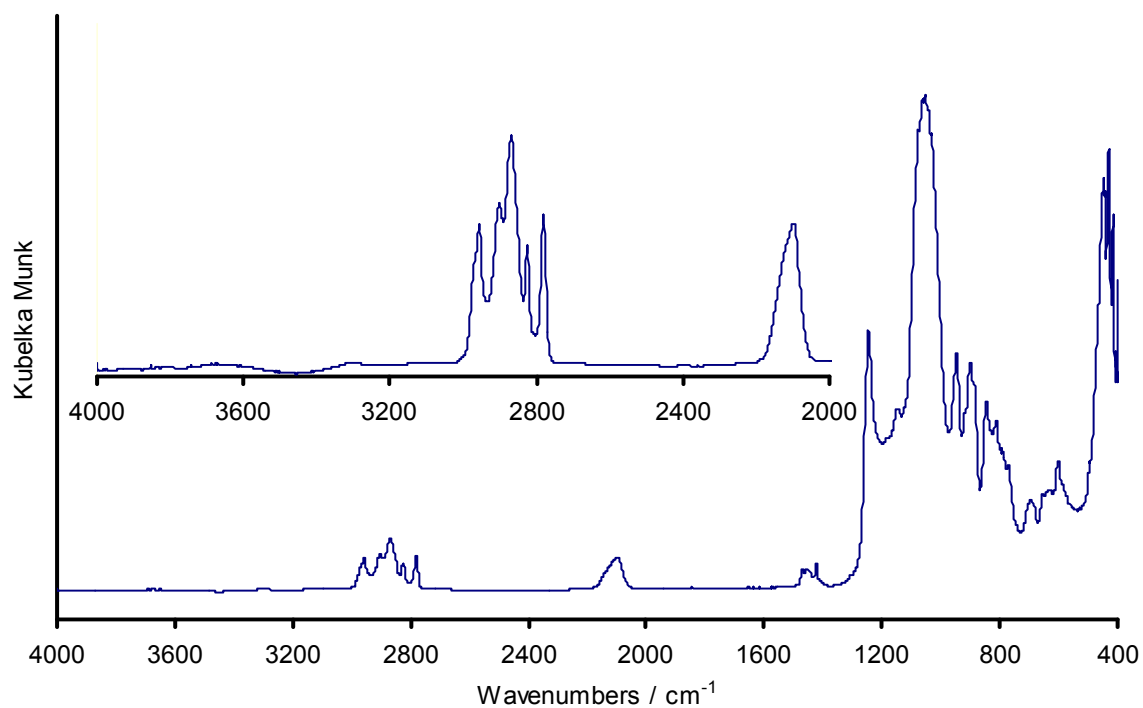
Wavenumber / cm^{-1}	Vibration
2960, 2885, 2780	C-H stretch, aliphatic
ca. 2140-2070	Si-H stretch

Figure 6.49 DRIFT spectrum of Ti(NMe$_2$)$_x$[N(SiHMe$_2$)$_2$]@MCM-41 4f
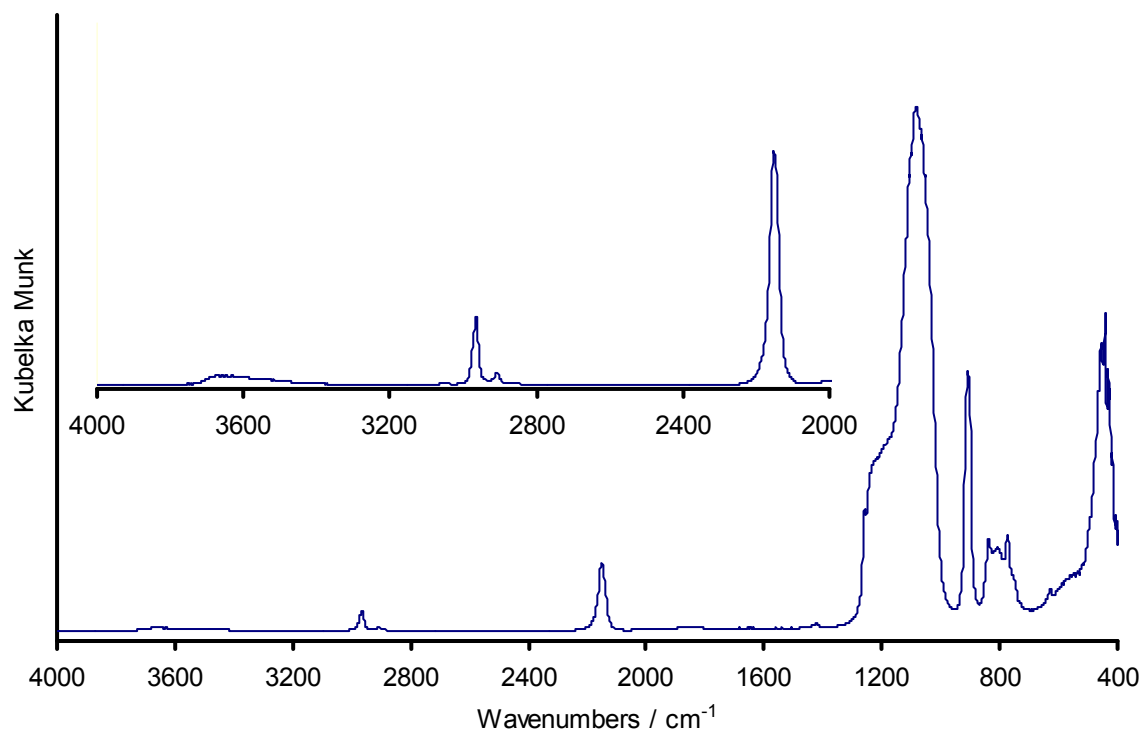
Figure 6.50 DRIFT spectrum of SiHMe$_2$@SBA-1 LP 6a

Wavenumber / cm^{-1}	Vibration
2970, 2900	C-H stretch
2150	Si-H stretch

6.7 N₂- physisorption data
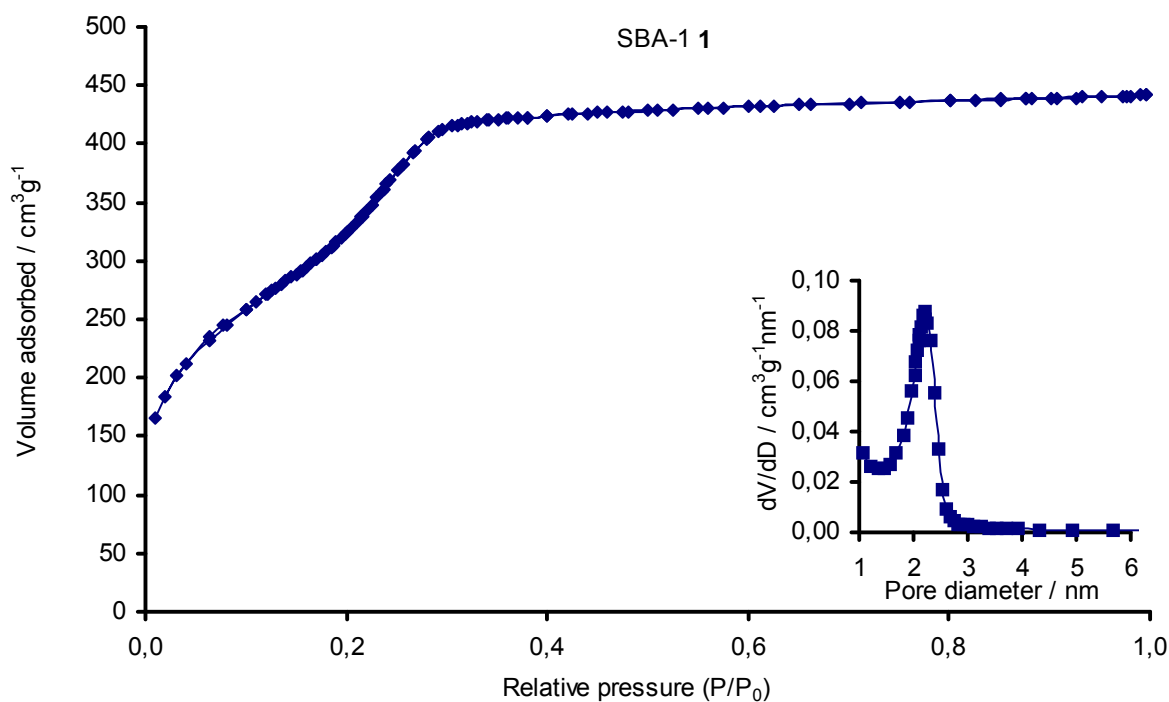
Figure 6.51 Nitrogen physisorption isotherm and BJH pore size distribution of SBA-1 1.
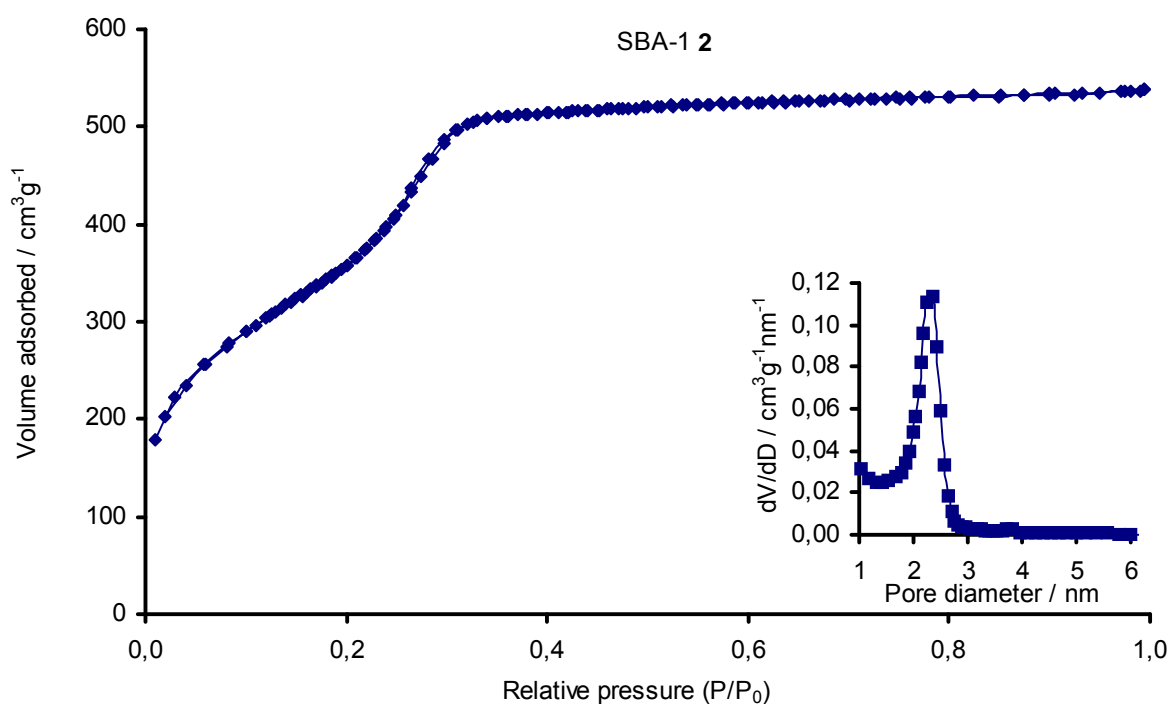
Figure 6.52 Nitrogen physisorption isotherm and BJH pore size distribution of SBA-1 2
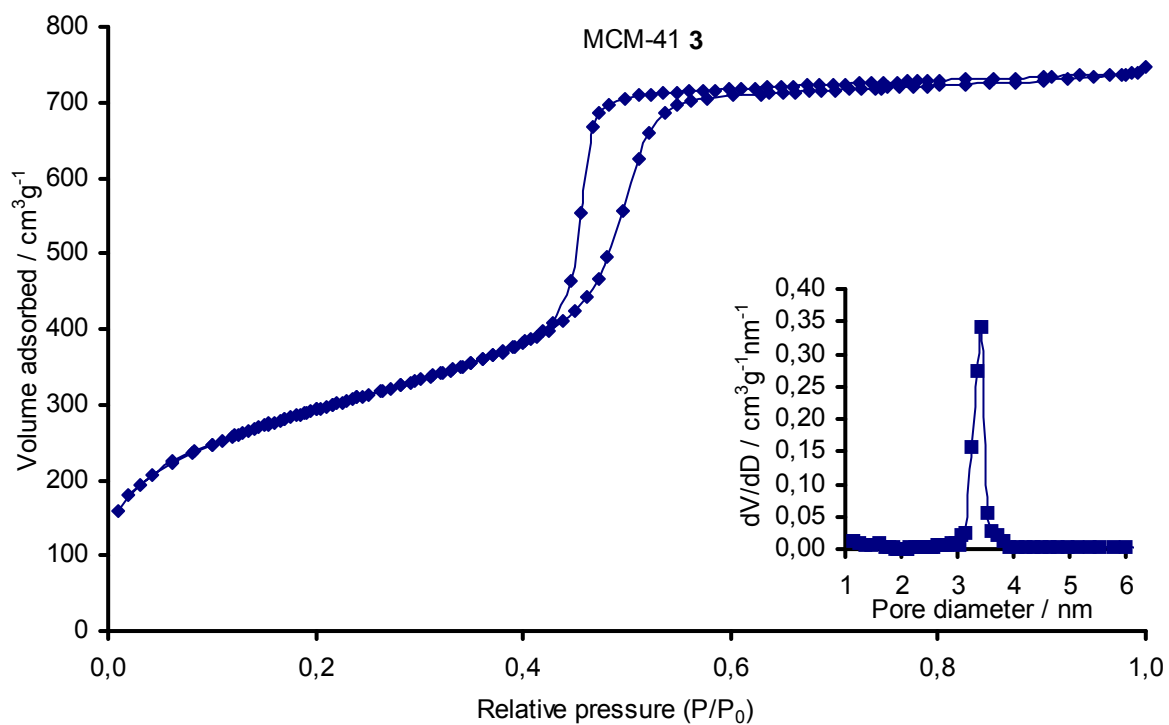
Figure 6.53 Nitrogen physisorption isotherm and BJH pore size distribution of MCM-41 3
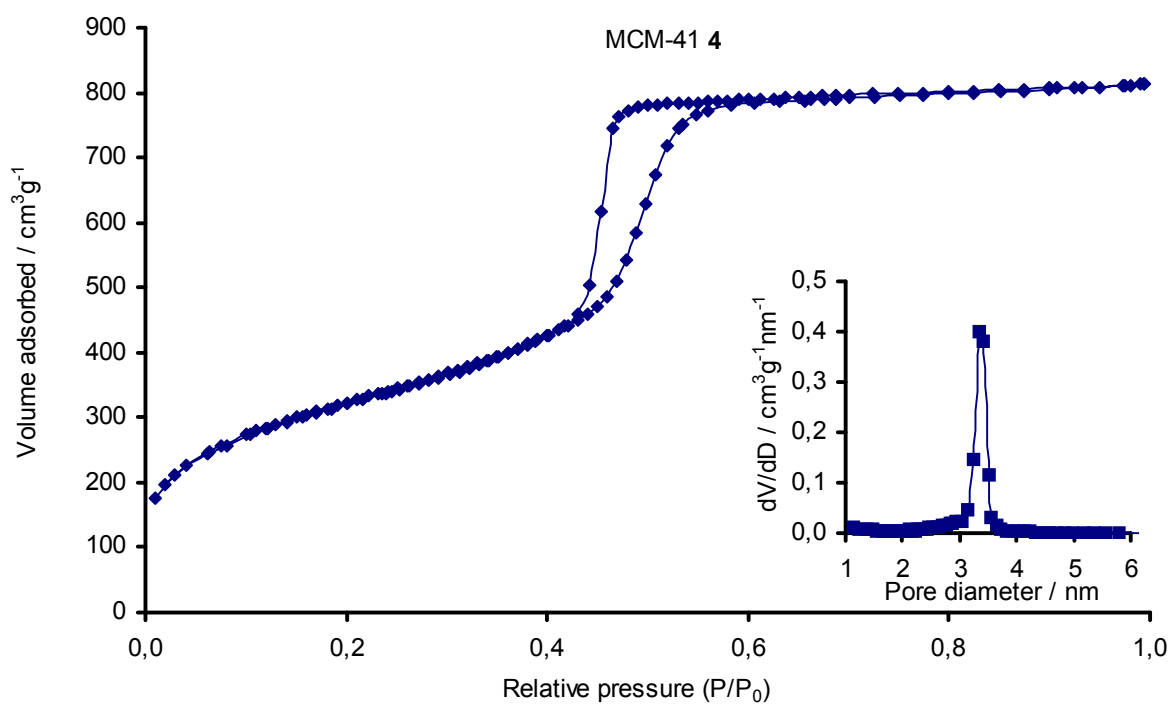
Figure 6.54 Nitrogen physisorption isotherm and BJH pore size distribution of MCM-41 4
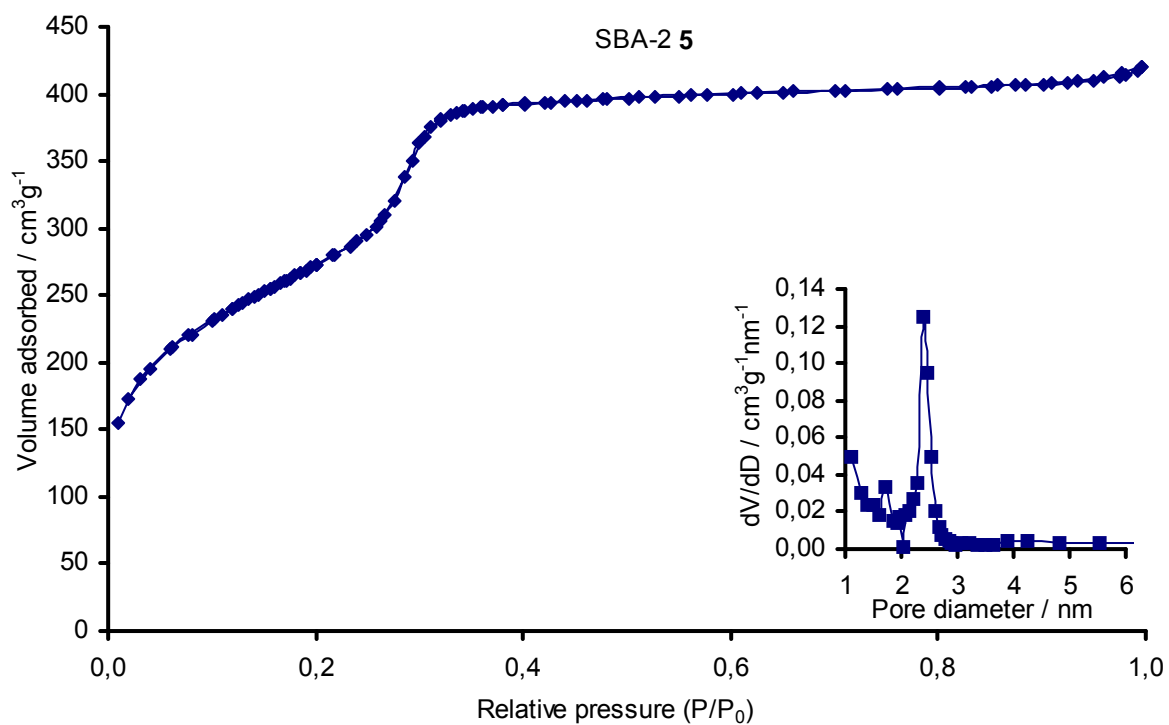
Figure 6.55 Nitrogen physisorption isotherm and BJH pore size distribution of SBA-2 5
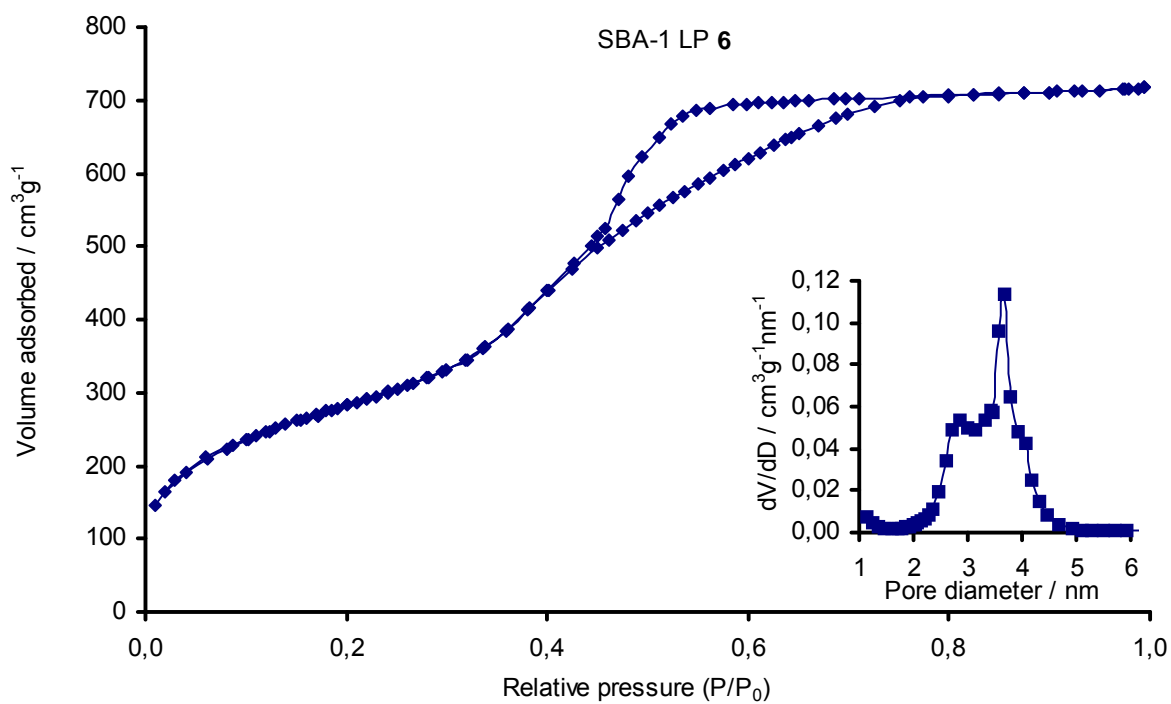
Figure 6.56 Nitrogen physisorption isotherm and BJH pore size distribution of SBA-1 LP 6
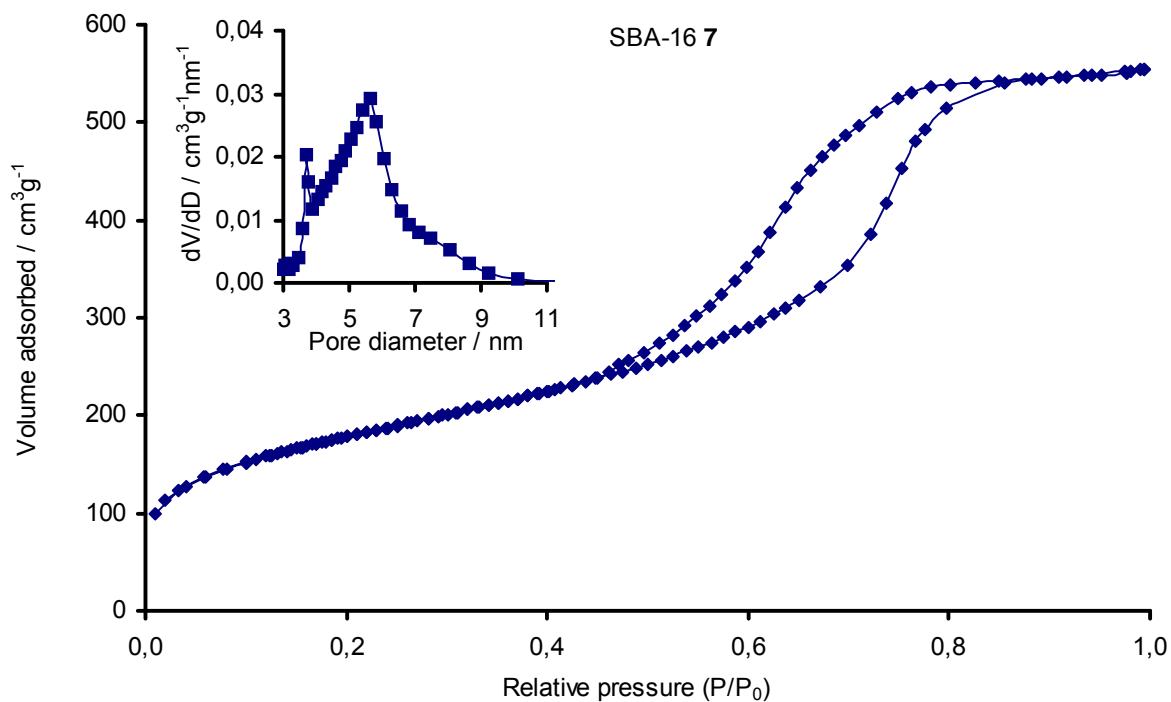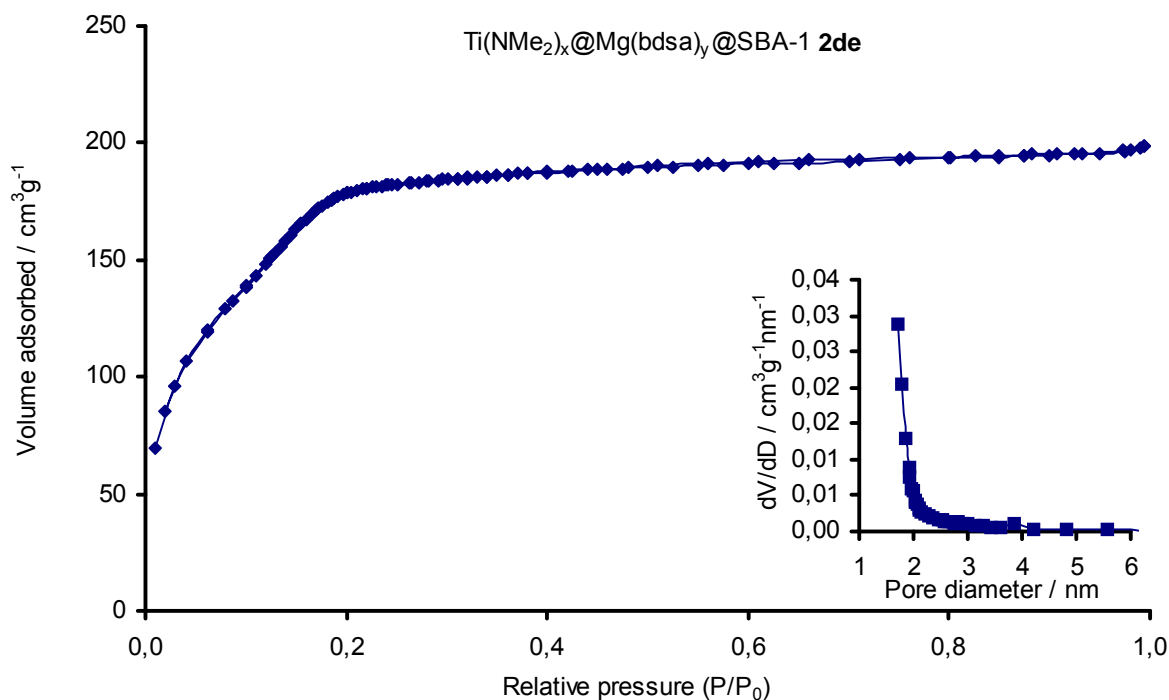
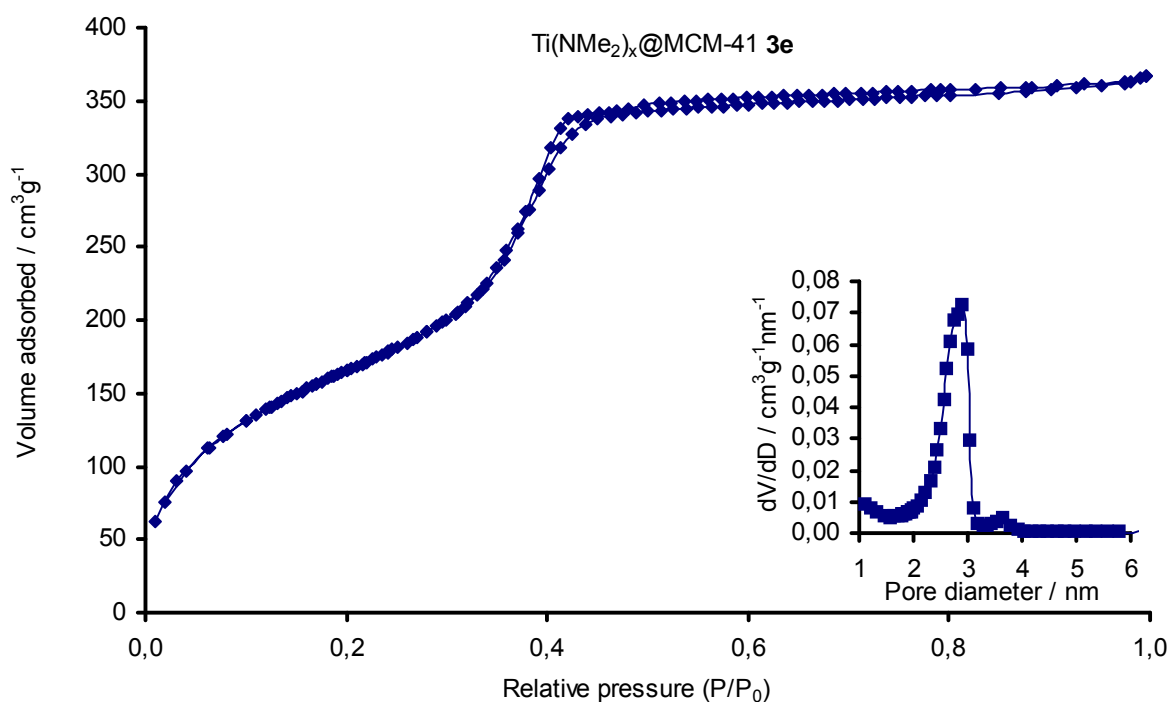Figure 6.57 Nitrogen physisorption isotherm and BJH pore size distribution of SBA-16 7
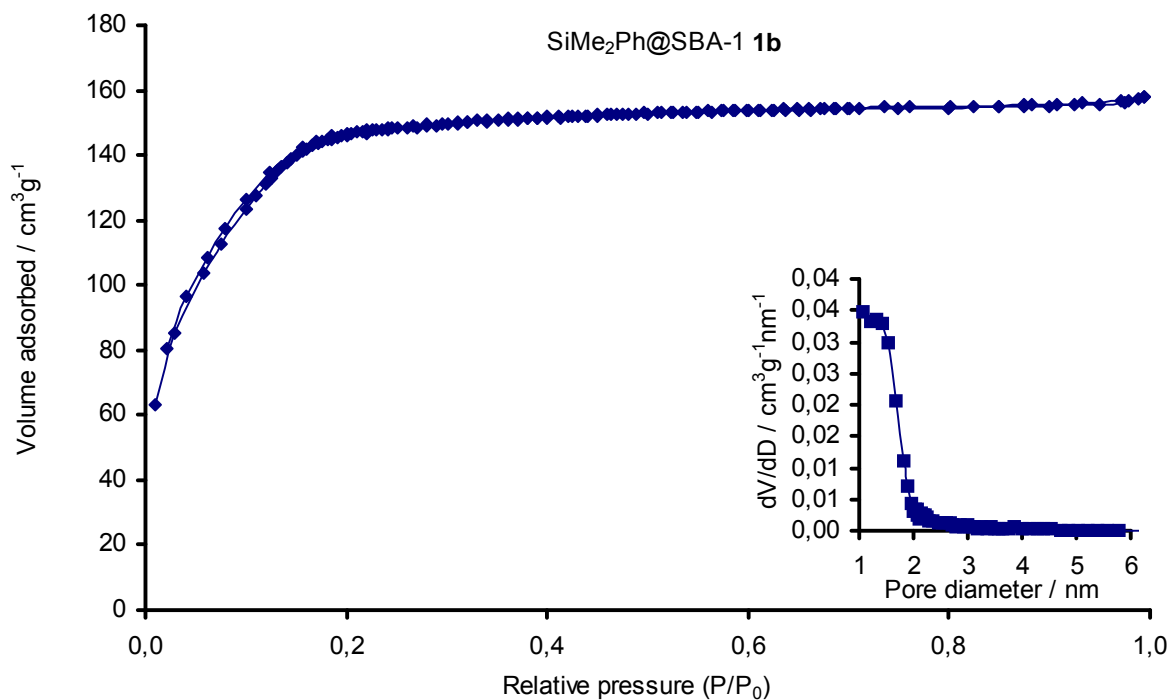
Figure 6.58 Nitrogen physisorption isotherm and BJH pore size distribution of SiMe$_2$Ph@SBA-1 1b
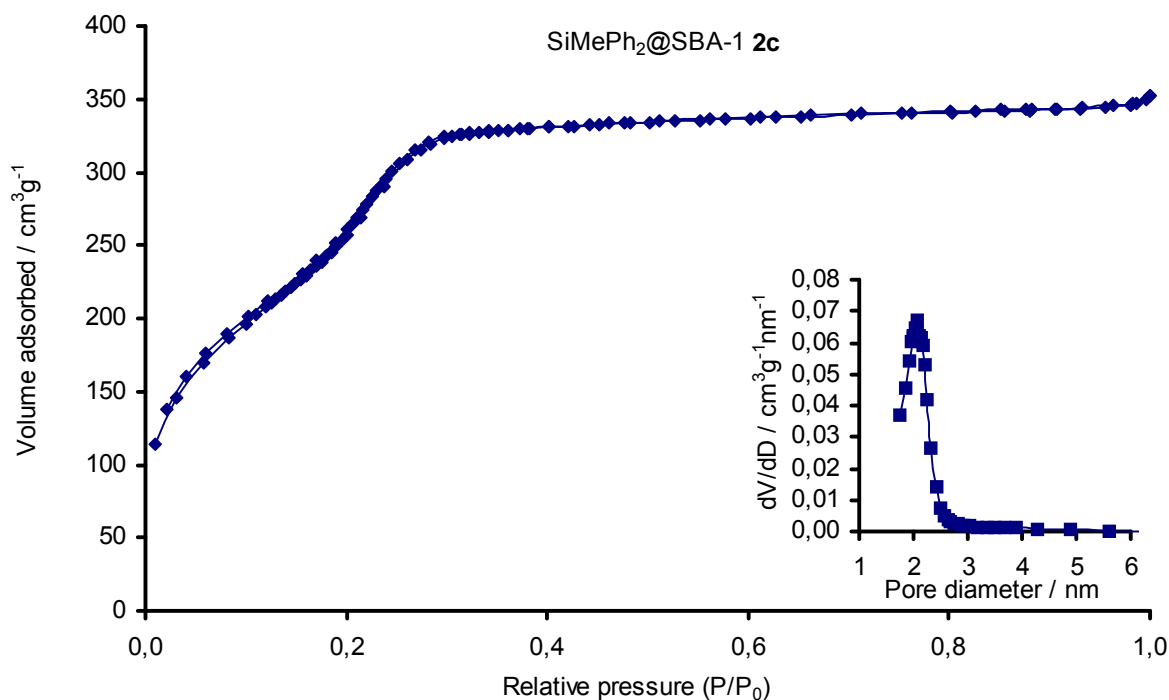
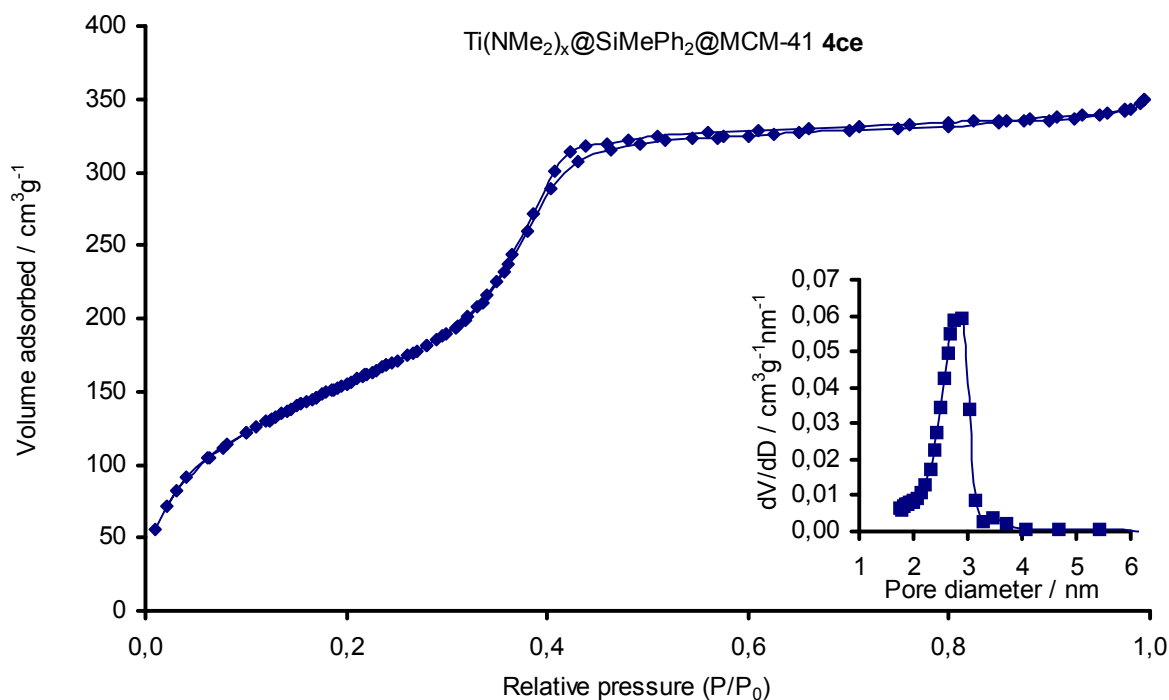Figure 6.59 Nitrogen physisorption isotherm and BJH pore size distribution of SiMePh$_2$@SBA-1 2c
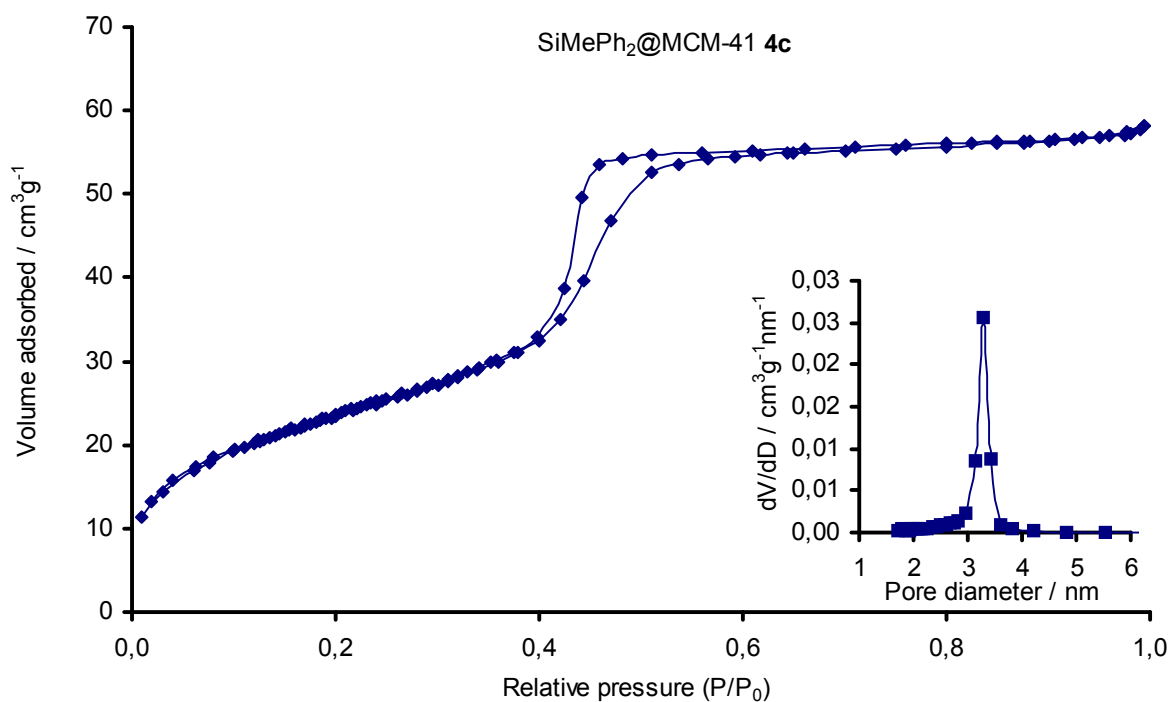
Figure 6.60 Nitrogen physisorption isotherm and BJH pore size distribution of SiMePh$_2$@MCM-41 4c
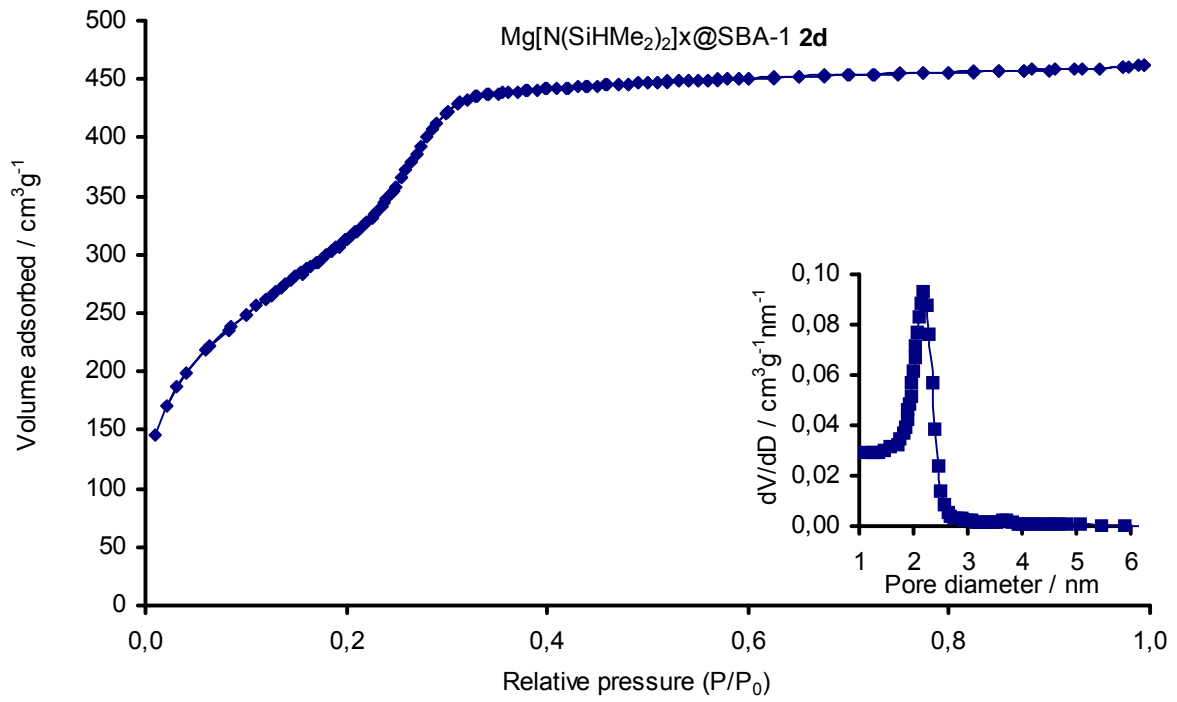
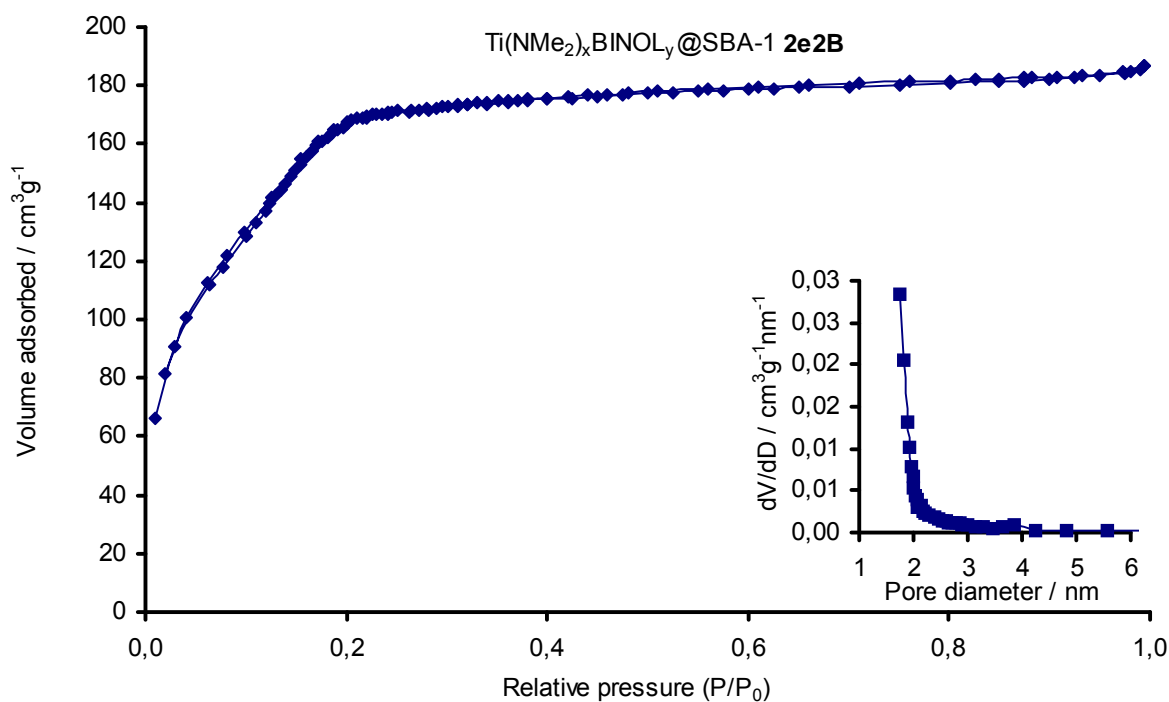Figure 6.61 Nitrogen physisorption isotherm and BJH pore size distribution of Mg[N(SiHMe$_2$)$_2$]$_x$SBA-1 2d
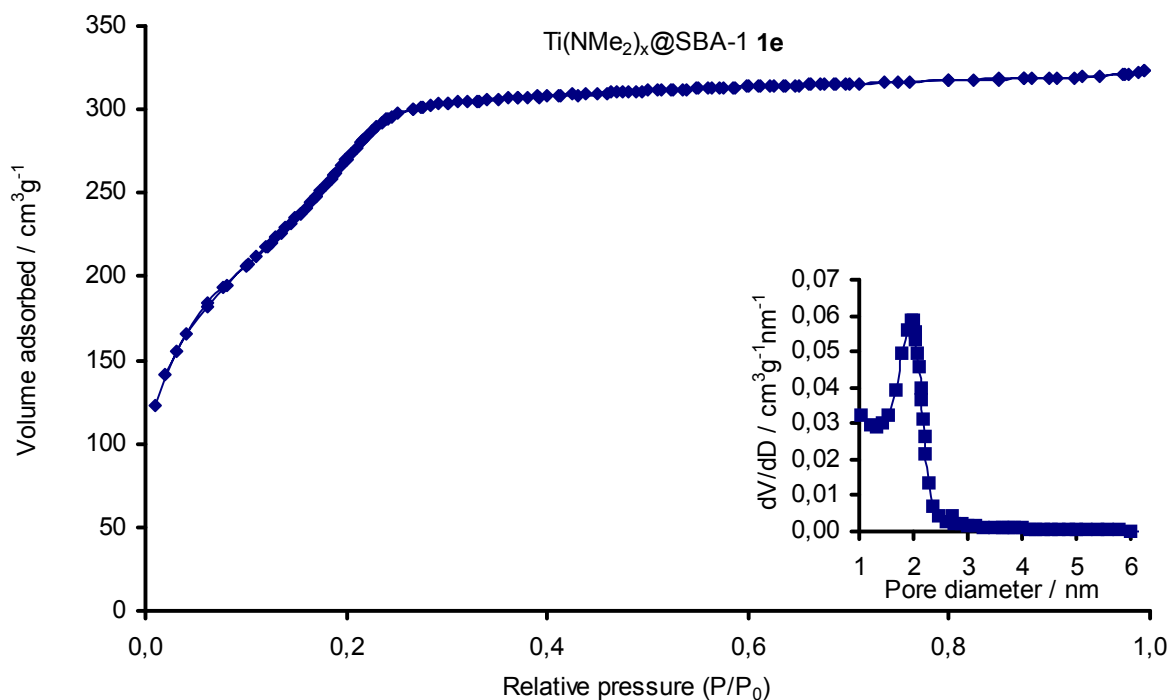
Figure 6.62 Nitrogen physisorption isotherm and BJH pore size distribution of Ti(NMe$_2$)$_x$@SBA-1 1e
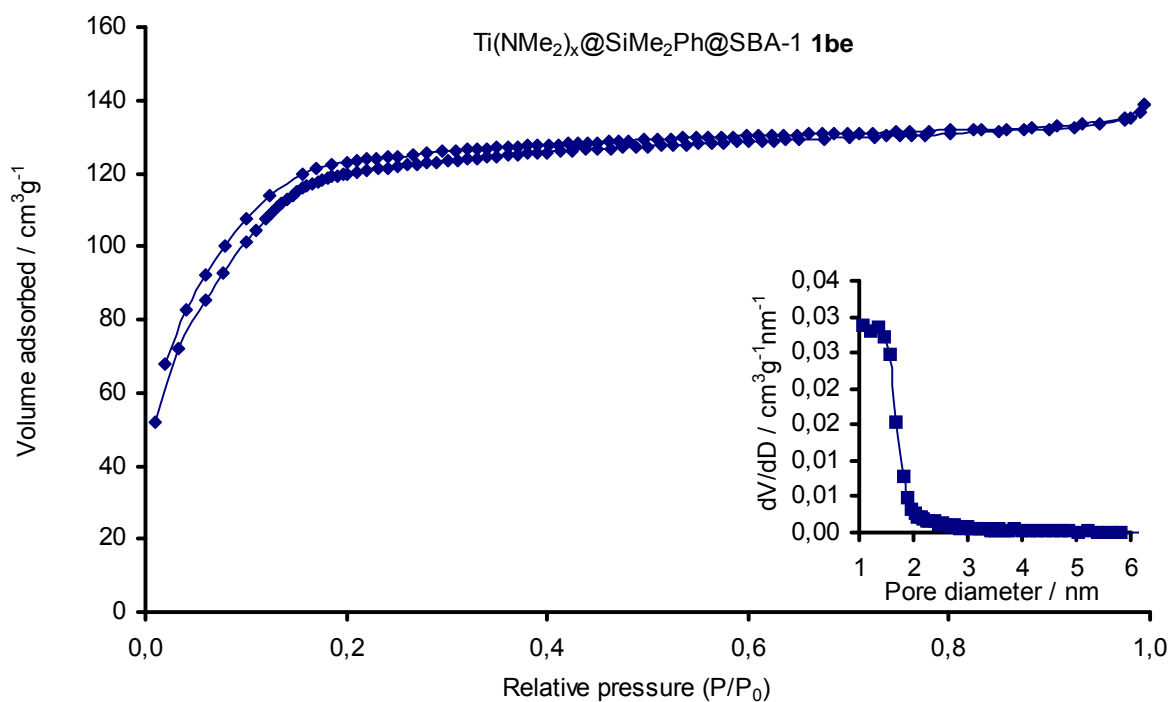
Figure 6.63 Nitrogen physisorption isotherm and BJH pore size distribution of Ti(NMe$_2$)$_x$@SiMe$_2$Ph@SBA-1 1be
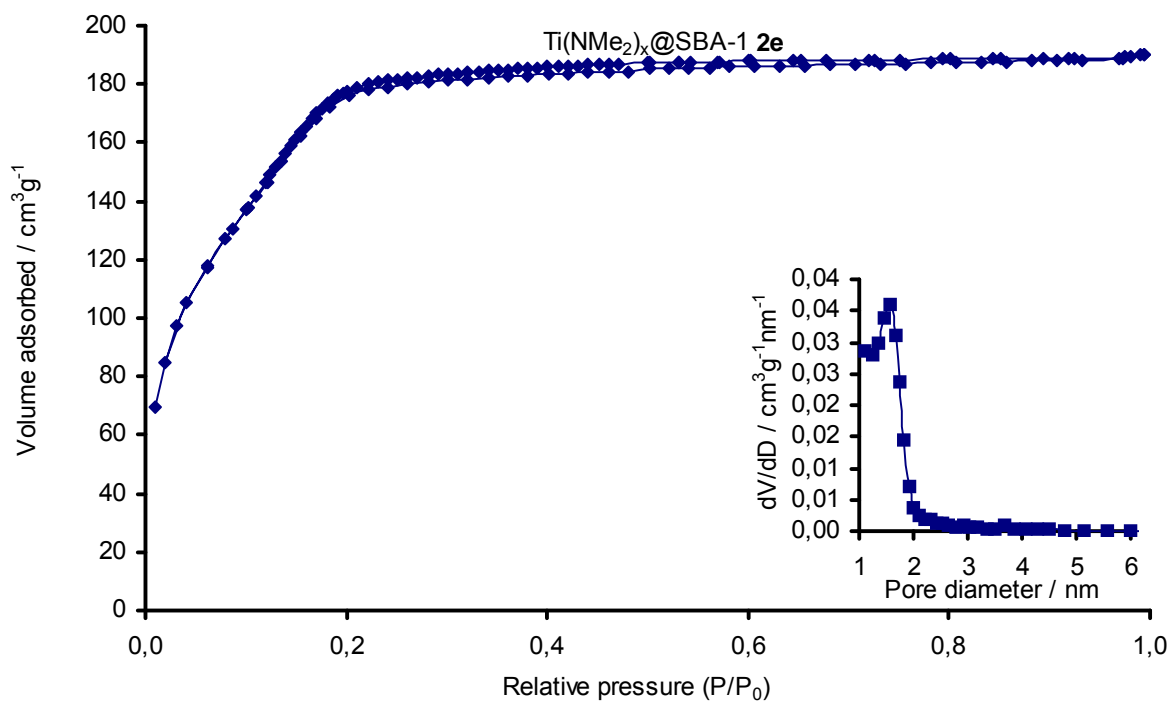
Figure 6.64 Nitrogen physisorption isotherm and BJH pore size distribution of Ti(NMe$_2$)$_x$@SBA-1 2e
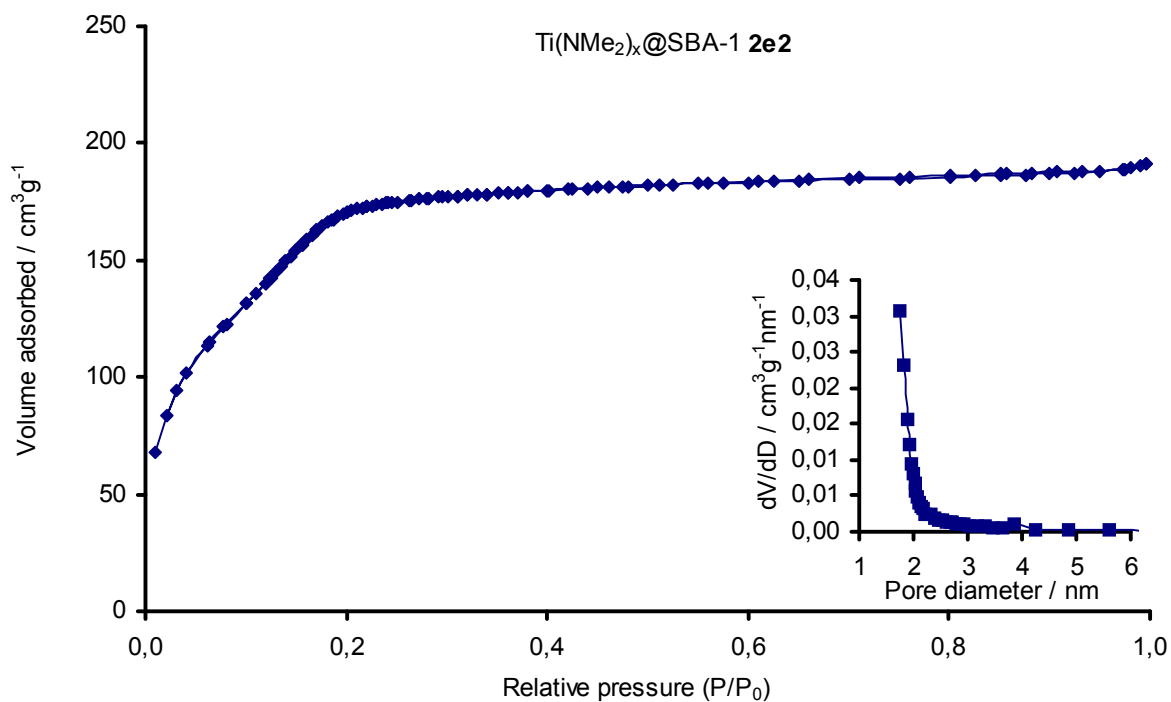
Figure 6.65 Nitrogen physisorption isotherm and BJH pore size distribution of Ti(NMe$_2$)$_x$@SBA-1 2e2
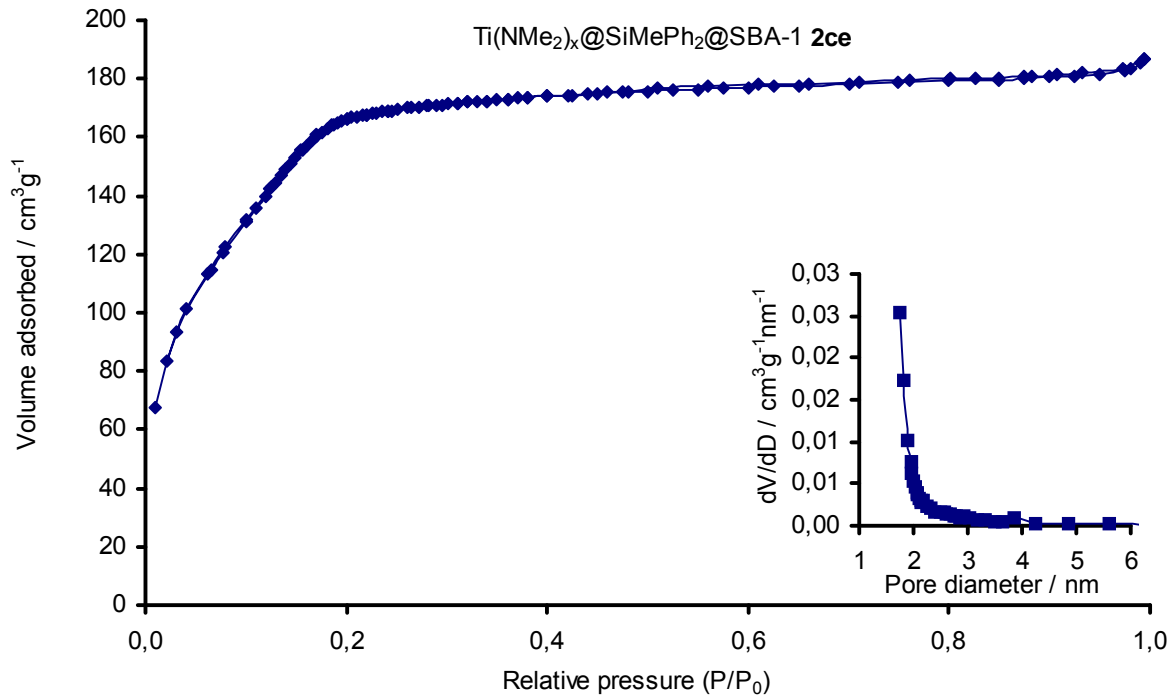
Figure 6.66 Nitrogen physisorption isotherm and BJH pore size distribution of Ti(NMe$_2$)$_x$@SiMePh$_2$@SBA-1 2ce

Figure 6.67 Nitrogen physisorption isotherm and BJH pore size distribution of Ti(NMe$_2$)$_x$@Mg[N(SiHMe$_2$)$_2$]$_y$@SBA-1 2de

Figure 6.68 Nitrogen physisorption isotherm and BJH pore size distribution of Ti(NMe$_2$)$_x$@MCM-41 3e

Figure 6.69 Nitrogen physisorption isotherm and BJH pore size distribution of Ti(NMe$_2$)$_x$@SiMePh$_2$@MCM-41 4ce

Figure 6.70 Nitrogen physisorption isotherm and BJH pore size distribution of Ti(NMe$_2$)$_x$(BINOL)$_y$@SBA-1 2e2B
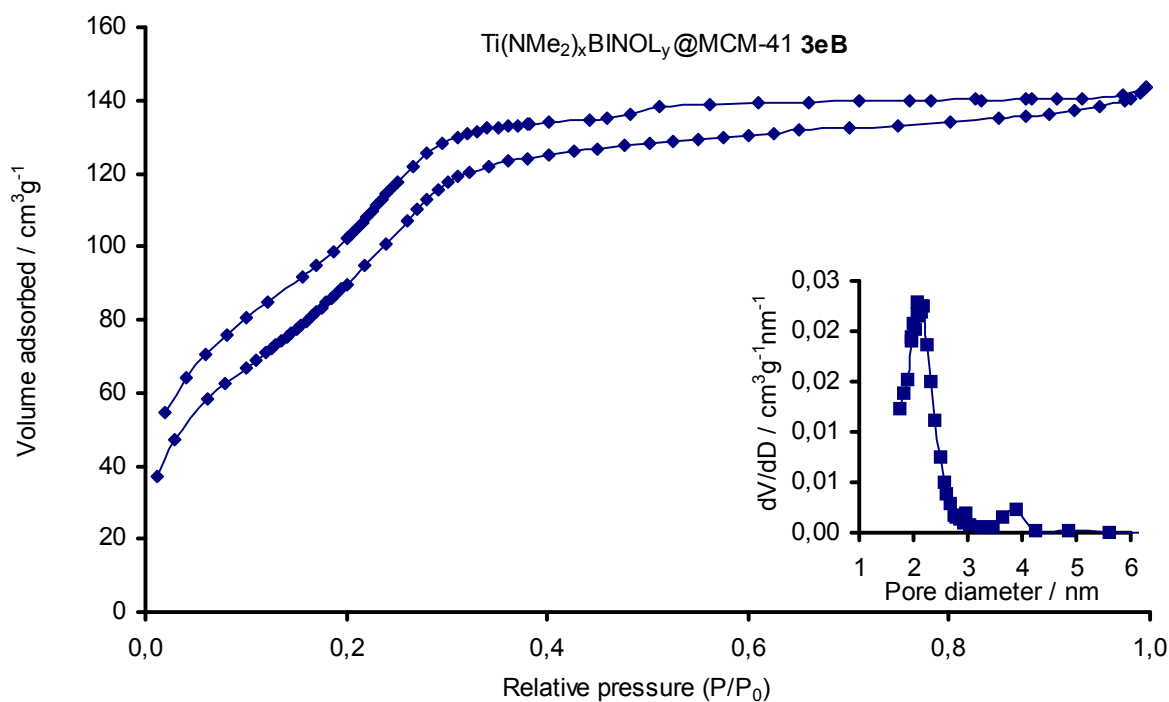
Figure 6.71 Nitrogen physisorption isotherm and BJH pore size distribution of Ti(NMe$_2$)$_x$(BINOL)$_y$@MCM-41 3eB
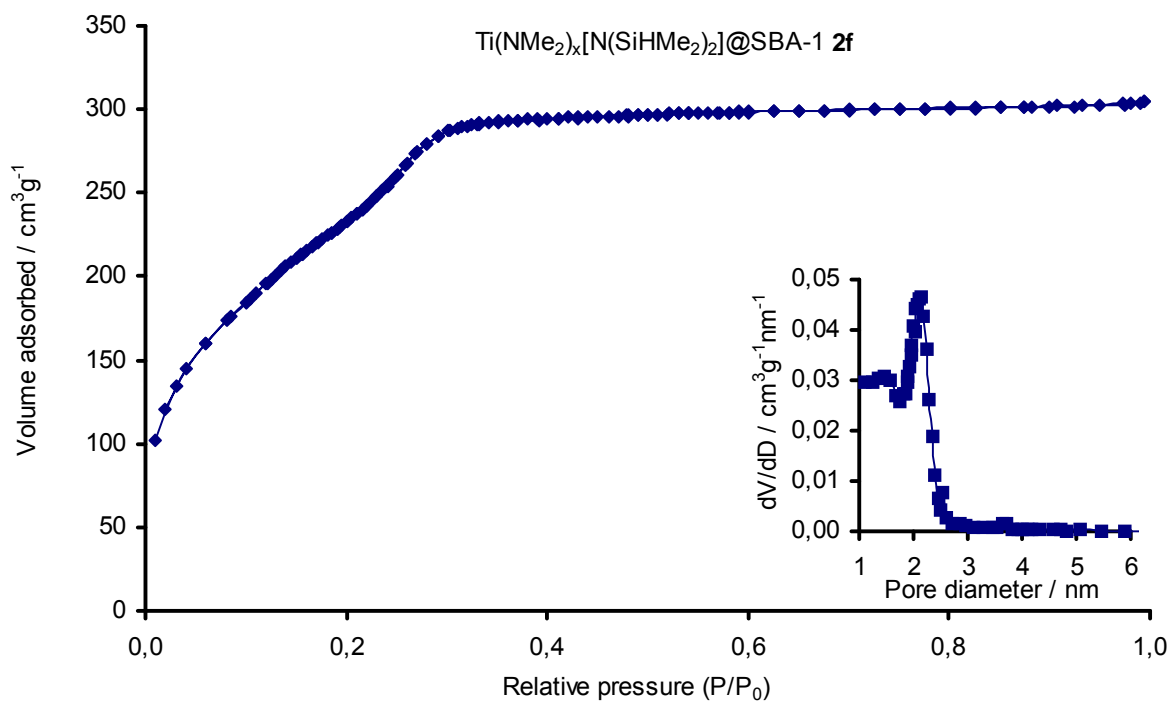
Figure 6.72 Nitrogen physisorption isotherm and BJH pore size distribution of Ti(NMe$_2$)$_x$[N(SiHMe$_2$)$_2$]@SBA-1 2f
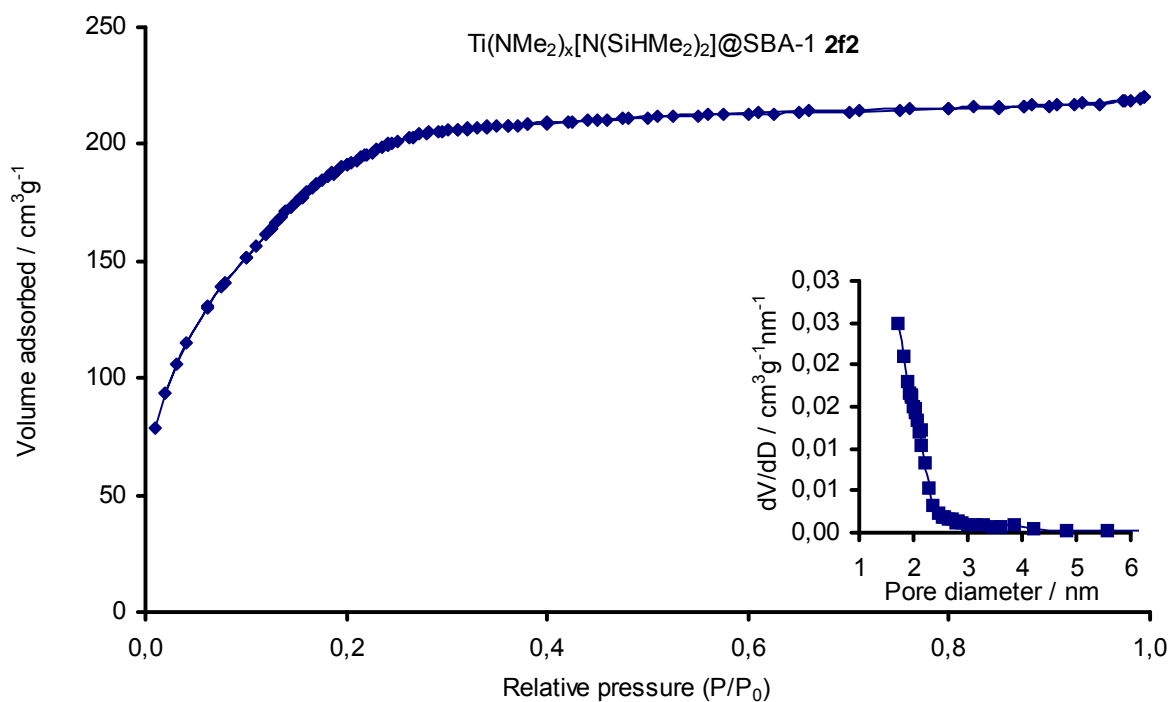
Figure 6.73 Nitrogen physisorption isotherm and BJH pore size distribution of Ti(NMe$_2$)$_x$[N(SiHMe$_2$)$_2$]@SBA-1 2f2
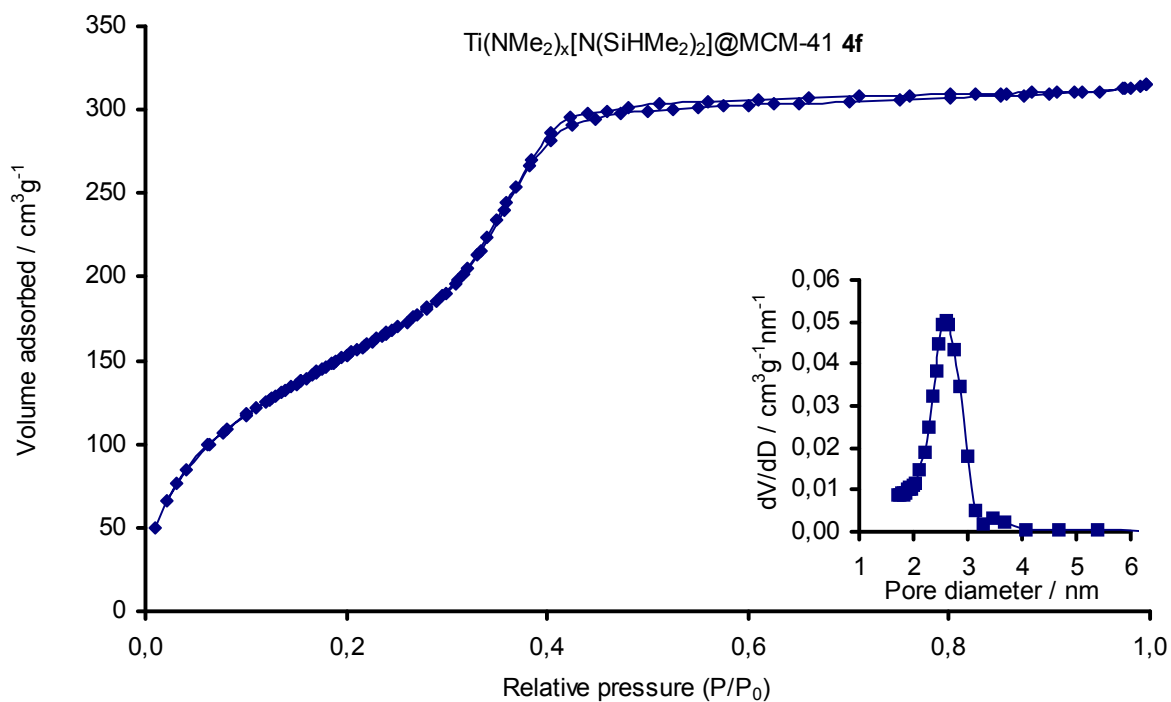
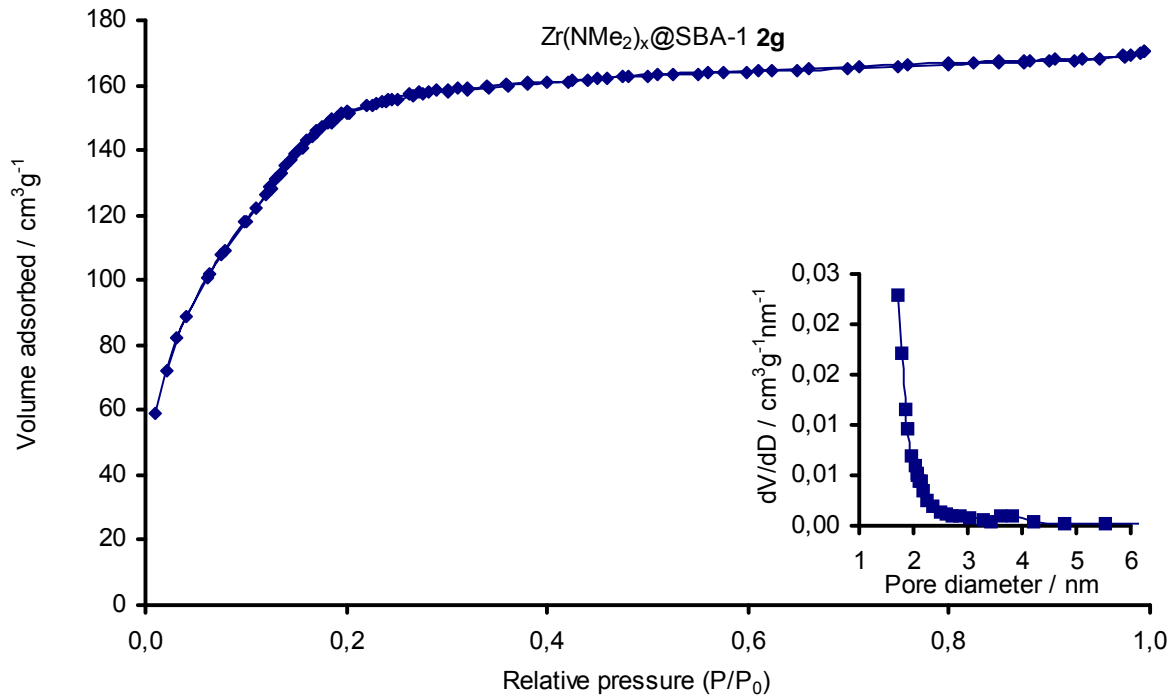Figure 6.74 Nitrogen physisorption isotherm and BJH pore size distribution of Ti(NMe$_2$)$_x$[N(SiHMe$_2$)$_2$]@MCM-41 4f

Figure 6.75 Nitrogen physisorption isotherm and BJH pore size distribution of Zr(NMe$_2$)$_x$@SBA-1 2g